The Effect of Chloride and Sulfate Ions on the Resistivity of Concrete

by

Omar Shaikhon

Department of Civil Engineering and Applied Mechanics

McGill University, Montréal

July 2015

A thesis submitted to McGill University in partial fulfillment of the requirements of the degree of Master of Engineering

Abstract

Electrical resistivity measurement is proving to be an essential tool for the durability assessment of concrete. It was mainly developed to assess reinforcement corrosion since moisture and chloride ingress are both factors that affect resistivity. The current method in use, the rapid chloride permeability (RCP) test, is outdated as specimen preparation is labor-intensive and the test is time-consuming. Resistivity measurement is the better alternative as it is non-destructive and comparatively faster, cheaper, and easier to use, as well as being more reliable. Due to the electrical nature of resistivity measurements, the presence of ions in contaminated concrete can alter resistivity measurements. The primary objective of this thesis was to study the effect of chloride and sulfate ions on the resistivity of concrete. Sodium chloride (NaCl) and anhydrous sodium sulfate ($\mathrm{Na_2SO_4}$) were used to achieve the required concentration of chlorides or sulfates, respectively. Tests were conducted on specimens with increasing concentration, where each individual specimen had a constant concentration throughout, and on specimens with a concentration gradient. The resistivity measurement techniques utilized were surface resistivity using a Wenner array and bulk resistivity. Surface resistivity was performed on the cylinders as well as on the split faces after the cylinder has undergone a splitting tensile strength test. The effect of water-to-cement ratio (w/c) and the geometric proportions of the cylinder on the resistivity were also studied.

Sommaire

Il a été prouvé que la mesure de la résistivité électrique est un outil essentiel à l'évaluation de la durabilité du béton. Ceci a été développé pour adresser le problème de corrosion de l'armature de l'acier étant donné que l'humidité et le chlorure sont tous deux des facteurs qui influencent la résistivité. La méthode utilisée aujourd'hui, l'essai accéléré de perméabilité aux chlorures (RCP), est dépassée puisque la préparation de l'échantillonnage requiert une forte main d'œuvre et le test en soi nécessite beaucoup de temps. La mesure de la résistivité est une meilleure alternative étant donné qu'elle est non-destructive, plus rapide, moins couteuse, plus facile à utiliser et plus fiable. Dû à sa nature électrique, la mesure de la résistivité pourrait être altérée par la présence d'ions dans le béton contaminé. L'objectif primaire de cette présente thèse était d'étudier les effets du chlorure et des ions de soufre sur la résistivité du béton. Le chlorure de sodium (NaCl) et le sulfate de sodium à la forme anhydre ($\mathrm{Na_2SO_4}$) ont été utilisés respectivement afin d'atteindre les concentrations requises de chlorures et sulfates. Les essais ont été faites sur des échantillons en augmentant les concentrations deux deux différentes façons : la première avec des échantillons individuels de concentration constante et la seconde avec des échantillons avec un gradient de concentration. La mesure de la résistivité de surface en utilisant la méthode de Wenner ainsi que la mesure de la résistivité volumique ont été les deux techniques de mesure utilisées. Pour la première technique citée précédemment, les mesures ont été prises sur des cylindres ainsi que sur des faces intérieures de cylindres après que ceux-ci aient été fractionnés avec l'essai de fendage. Les effets du rapport ciment à eau et des proportions géométriques du cylindre sur la résistivité ont aussi été étudiés.

Acknowledgements

First and foremost, I wish to express my sincere thanks to Prof. Andrew J. Boyd for his supervision and guidance throughout the program. His patience and invaluable knowledge proved essential for the completion of this thesis. I would also like to thank Jon Bartczak for his help around the lab from dealing with small problems to machining and helping set up the permeability apparatus. To everyone that contributed to the research and the completion of this thesis I offer my profound gratitude. Last but not least, I am especially grateful to my parents for their financial and emotional support and my friends who were always there for me when I needed it most.

Table of Contents

List of Figures

List of Tables

Introduction

Concrete is the most commonly used construction material in the world. It is a highly versatile and relatively inexpensive building material that can be formed into a variety of shapes and sizes. The majority of our infrastructure is comprised of reinforced concrete structures, with applications including buildings, bridges, highways, water and sewer systems, and many more. However, concrete is far from perfect and will deteriorate over time under certain conditions. Design codes in practice focus on the minimum requirements for a structure to be able to withstand the forces acting on it, but much less emphasis is placed on durability characteristics. Poor construction quality or designing without proper consideration of durability can lead to accelerated deterioration of a structure, incurring additional expenses to repair the damage. Thus, the durability of concrete is vital for cost effectiveness and long term performance to uphold or even exceed the design service life. When it comes to assessing the durability of concrete, the rapid chloride permeability (RCP) test is usually conducted in accordance with the ASTM C 1202 or AASHTO T 277 standards. The test, however, is far from rapid and requires significant specimen preparation beforehand. Furthermore, if the test is to be conducted on an existing structure, then a sample needs to be cored from the structure. There is a need for a quick, easy and reliable method of assessing durability that does not induce further damage to the structure in the process.

Electrical resistivity is a geometry independent and intrinsic material property that quantifies the ability of the material to resist electrical current flow. Electrical resistivity measurement techniques have been adopted from the field of geophysics where it was used to study and classify different soils and minerals. The four-probe Wenner array is the most commonly used configuration to measure the surface resistivity of concrete. The current from the resistivity device flows through the ionic solution within the concrete’s pore network and can consequently be used as a measure of the concrete’s transfer properties. Concrete with a higher resistivity will generally have a finer pore structure with less pore connectivity and lower permeability. This is of utmost importance when dealing with durability since the ingress of deleterious substances is the main cause of deterioration in reinforced concrete structures.

Electrical resistivity measurement can be particularly useful in assessing steel reinforcement corrosion. For corrosion to initiate, chloride ions and moisture need to penetrate through the concrete to the reinforcement, both of which have a measureable effect on the electrical resistivity. Resistivity measurements can also be used for quality control of concrete during construction. This is achieved by comparing the resistivity of concrete on site at different time intervals with lab produced specimens having an identical mixture design. Furthermore, resistivity measurements can be used to indicate members or sections within a structure that have higher moisture content.

Electrical resistivity measurement is slowly gaining acceptance in the construction industry as a quick and reliable method for quality control and durability assessment of concrete. The current standards available are the AASHTO TP 95 for measuring surface resistivity of a concrete cylinder and the ASTM C 1760 for measuring bulk resistivity of a concrete cylinder. ASTM is currently working on a standard for surface resistivity measurement using the Wenner four-probe array (ASTM WK37880).

There are many factors that can affect the electrical resistivity of concrete (Section 1.2.2). To avoid variability caused by these factors, it is important to control them, keep them constant, or develop correction factors to account for them. The main focus of the experimental section of this thesis is to study the effect of chloride and sulfate ions on the electrical resistivity of concrete. Chlorides have no known reaction with concrete but are a major concern for durability of reinforced concrete structures as they lead to corrosion of the steel reinforcement. Sulfates, on the other hand, chemically react with components of the hydrated cement paste to produce ettringite and gypsum, causing concrete to expand and crack.

1 Literature Review

1.1 Concrete Components

In order to fully grasp the theory behind the electrical conductance of concrete, and its subsequent resistance, it is essential to review the components that make up concrete. The basic raw materials required to produce concrete are water, cement and aggregates. The two constituents that make up hardened concrete, namely aggregates and hydrated cement paste, are what remain after the raw materials are mixed and the concrete is left to set and harden.

1.1.1 Aggregates

Aggregate is a solid mineral material used in concrete as a filler that also aids in structural resistance. Aggregates are classified by size into two categories: fine and coarse. Fine aggregate sizes range from 75 µm to 4.75 mm, while coarse aggregate sizes range from 4.75 mm to 50 mm. Sand is the most commonly used fine aggregate. As for coarse aggregates, gravel and crushed stone are the most common. Aggregates are generally non-conductive and therefore do not contribute to the electrical resistivity of concrete.

1.1.2 Hydrated Cement Paste

Concrete is a composite material and hydrated cement paste is the main constituent of its matrix. Hydrated cement paste is formed through several chemical reactions that take place between cement and water. Under a scanning electron microscope the various final products of the hydration reactions that collectively make up the hydrated cement paste can be seen as shown in Figure 1.

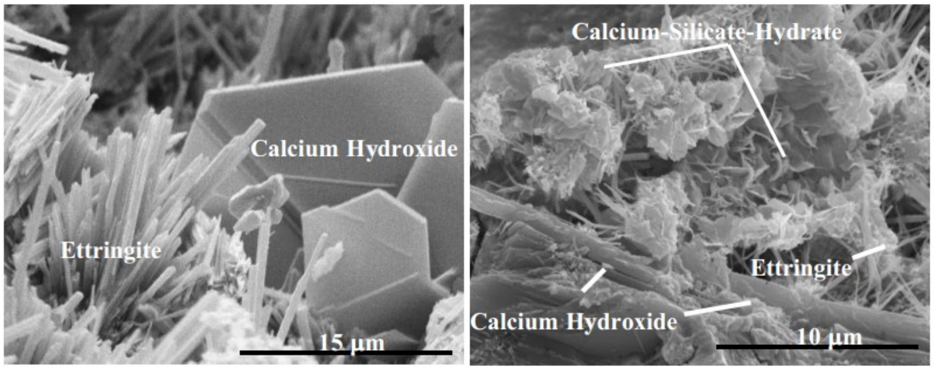

Figure 1: Scanning electron microscope image of hydrated cement paste (Stutzman, 2000).

Calcium silicate hydrate (C-S-H) makes up the majority of the hydrated cement paste, occupying approximately 50% of the paste's volume (Bye, 1999). C-S-H contributes to the overall strength of concrete by acting as the primary binding phase in the hydrated cement paste. Due to its variable composition, amorphous nature and morphology that isn't full resolved, C-S-H is still poorly understood (Mindess, et al., 2003, Yu, et al., 1999) and is typically represented by models and theoretical relations (Brandt, 2009). The microstructure of C-S-H is similar to that of a poorly crystallized clay mineral. C-S-H is built up of layers of warped and arbitrarily arranged calcium silicate sheets. As a result, it is intrinsically porous with calcium and water contained within its pores (Mindess, et al., 2003).

Calcium hydroxide (CH) is another product of hydration that occupies approximately 15% of the volume of the paste (Bye, 1999). It is a well crystallized material that usually forms flat hexagonal prisms that can be seen with an optical microscope (Mindess, et al., 2003). Calcium hydroxide contributes to the strength of the paste but works hand in hand with the binding ability of C-S-H and lowers the paste's permeability by growing in voids. However, calcium hydroxide is water soluble and can leech out of concrete, increasing porosity and causing further durability concerns.

Similar to calcium hydroxide, ettringite forms crystals with a hexagonal morphology but, unlike CH, grows into long slender needles. Ettringite usually occupies around 10 – 15% of the volume of the paste (Brandt, 2009). It contributes slightly to strength and fills in voids much like calcium hydroxide, but it is not water soluble. If the cement used to produce concrete contains excessive amounts of calcium sulfate, then the formation of ettringite in hardened concrete can be expansive and damaging (see Section 1.3.2.1).

Most of the water is used up in the hydration reactions but, depending on the water to cement ration, what is leftover eventually evaporates to form voids in the hydrated cement paste. These voids can become interconnected, allowing the concrete to exhibit transport properties. The water inside these voids is not pure; it contains Ca^{2+}, OH^-, Na^+, K^+ and SO_4^{2-} ions dissolved readily in it (Maierhofer, et al., 2010). Therefore, concrete can be conductive through the ionic solution contained within its pores. It is important to note, however, that concrete that has been sufficiently dried, such as being placed in an oven, will not conduct electricity.

1.2 Electrical Resistivity

Electrical resistance is opposition to the flow of electrical current through a conductor. By applying an electrical current (I) through a conductor and measuring the potential difference (V), the resistance (R) can be calculated using Ohm's law as follows:

$$R = \frac{V}{I}$$

Electrical resistivity is defined as the ability of a material to oppose or impede the flow of current. The resistivity (ρ) of a material is directly proportional to the resistance and there are various equations that demonstrate this relationship depending on the equipment and method used for measurement. The different methods for measuring resistivity that will be discussed in this section are single probe, two probe, four probe, and bulk arrangements.

When measuring resistance, an alternating current should be applied and not a direct current. This is due to electrochemical processes that occur at the electrode-concrete surface, called polarization, which can distort the measurement and lead to errors (McCarter and Brousseau, 1990). Using an alternating current helps minimize this effect.

It is recommended to keep the concrete sample or surface saturated with water before measuring resistivity. This is done to achieve consistency and to avoid variations in results due to different moisture contents in the concrete. The effect of moisture content is discussed in Section 1.2.2.2.

1.2.1 Methods of Measuring Electrical Resistivity of Concrete

1.2.1.1 Single Probe

The single probe method is best suited for measuring the resistivity of concrete cover in a reinforced concrete structure. Contrary to what the method's name suggests, this technique technically utilizes two probes. A direct connection from device to the embedded steel reinforcement is required, forming what is called the counter electrode. This can be achieved by exposing the rebar through drilling or similar. A metallic disc probe is then placed on the concrete surface as shown in Figure 2. It is recommended that the disc probe be placed on the surface between rebars connected in the reinforcement mesh instead of directly above them (Broomfield, 2002, Polder, et al., 2000).

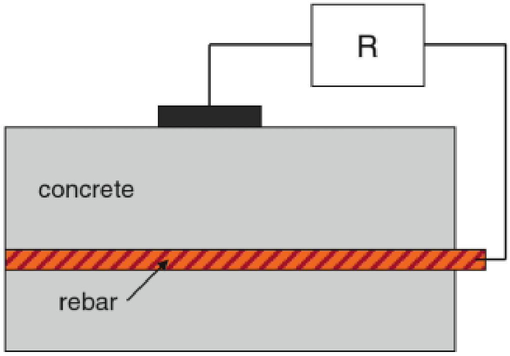

Figure 2: Schematic of single probe method (Breysse, 2012).

This single probe's configuration allows the electrical current to flow through the concrete between the probe at the surface and the connected rebar. The resistivity (ρ) of the concrete cover can then be calculated from the resistance (R) and the diameter of the circular probe (D) using the following equation:

$$\rho = 2RD$$

The main disadvantage of this method is the high sensitivity to variation in contact resistance (Broomfield, 2002, Maierhofer, et al., 2010).

1.2.1.2 Two Probe

The two probe method utilizes two electrodes where an alternating current is applied from one electrode to the other and the potential difference is measured between the same two electrodes (Figure 3). This method only measures resistance without any means of converting these values into resistivity. Therefore, the spacing of the probes should be kept constant if this method is to be used to compare resistance measurements. The two probe device is sensitive to electrical properties close to the probes and can be used to detect surface irregularities (Maierhofer, et al., 2010).

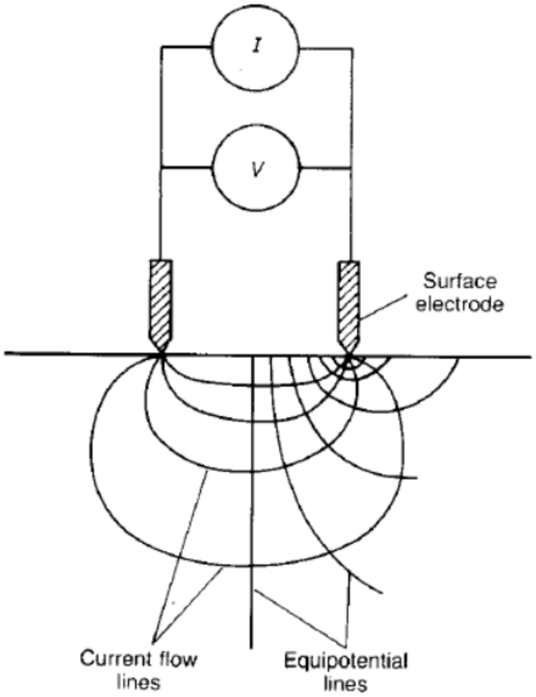

Figure 3: Schematic of two probe method (Millard, 1991).

The measured resistance is also dependent on the contact area between the concrete and the electrode. The greater the contact area, the larger the volume represented in the resistance measurement (Millard, 1991). To keep the contact areas relatively constant throughout measurements, some devices require two holes of the same size to be drilled onto the concrete surface. The holes are then filled with a conductive fluid into which the electrodes are inserted.

1.2.1.3 Four Probe

In the four probe method an electrical current is applied between the outer electrodes while the potential difference is measured between the two inner electrodes. The resistivity of all the concrete between the potential (inner) electrodes is measured, as opposed to the two probe method where measurement of resistance is influenced by concrete in close proximity to the electrodes (Millard, 1991).

Initially developed for use on soils for geophysical applications, devices utilizing four probes have been designed and calibrated for use on concrete. The two most commonly used arrays in the four probe method are the Schlumberger and Wenner arrays (Figure 4), the latter is almost exclusively used in measuring resistivity of concrete.

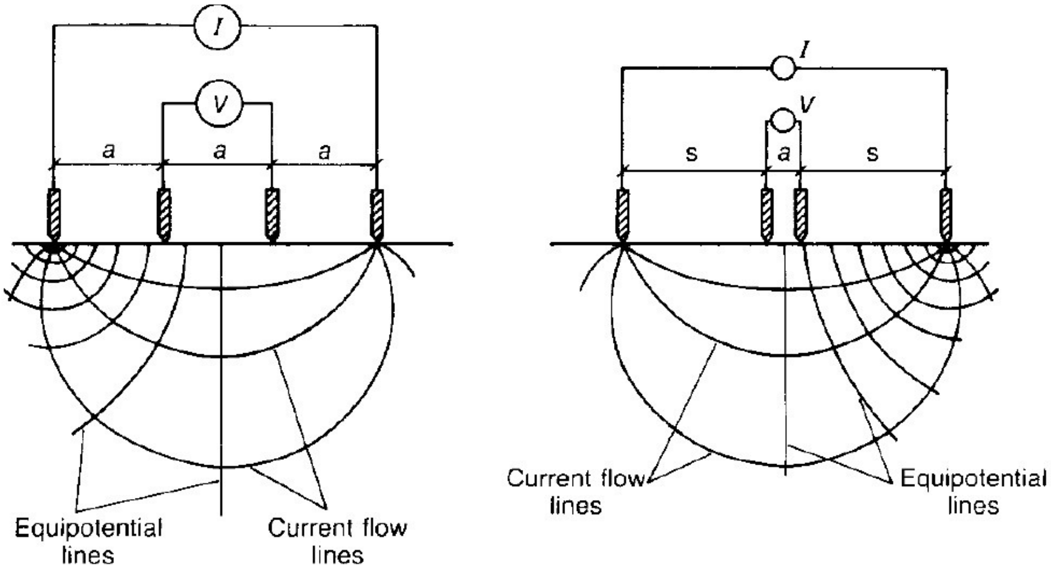

(a) (b)

Figure 4: Schematic of four probe method (a) Wenner Array (b) Schlumberger Array (Millard, 1991)

The equations derived for calculating the resistivity using the four probe method assume the material is homogenous and semi-infinite. Since concrete is heterogeneous and of finite size, an “apparent” resistivity is measured instead. The apparent resistivity is the average of the resistivity over the volume covered by the device.

When using the Schlumberger array, the apparent resistivity (ρ_a) can be calculated from the outer electrode spacing (s), the inner electrode spacing (a) and the resistance measured (R) using the equation:

$$\rho_a = \pi \frac{s(s+a)}{a} R \qquad IF \qquad s > 2a$$

When using the Wenner array, the apparent resistivity (ρ_a) can be calculated using the electrode spacing (a) and the resistance (R) using the equation:

$$\rho_a = 2\pi a \cdot R$$

1.2.1.4 Bulk

The bulk method for measuring resistivity utilizes two flat circular electrodes that are placed on the ends of a concrete cylinder that is usually the standard 100 mm x 200 mm (4” x 8”). The concrete cylinders could either be produced in a lab using the appropriate mold or cored from an existing structure. Similar to the other methods of measuring resistivity, a current is applied from one of the electrodes to the other while simultaneously measuring the potential difference between them.

To improve the electrical contact between the electrodes and the concrete surface, thin sponges that are saturated in water are usually inserted between the probes and the concrete. The resistance of the sponges (R_s) must be measured with the device to be later subtracted from the total resistance (R_T) of the concrete cylinder and the two sponges. Knowing the area of the electrodes (A) and the length of the cylinder (L), the bulk resistivity (ρ) can be calculated using the equation:

$$\rho = \frac{A}{L}(R_T - R_s)$$

Improving contact resistance and ensuring consistency throughout testing is of major importance in reducing the variability of test results. Saturating the sponges in an electrolyte solution, such as NaCl or $\mathrm{Ca(OH)_2}$ solutions, has been shown to reduce contact resistance (Newlands, et al., 2008). Caution should be taken when doing so since the solution in the sponges may seep into the concrete cylinder being tested and affect the test results. Applying pressure to the electrodes has also been shown to reduce the contact resistance (Newlands, et al., 2008). It is recommended, however, that the pressure remain constant throughout the testing.

1.2.2 Factors Affecting the Electrical Resistivity of Concrete

1.2.2.1 Intrinsic Factors

Porosity

The degree of porosity in concrete can have a major effect on its electrical resistivity. The higher the porosity within the concrete the lower the measured resistivity. This is because concrete gains its electrical conductivity properties through the ionic solution contained within its pores, the solid components do not conduct electricity. Only the interconnected pores have an effect on the resistivity, as the electrical current flows through them. Sealed pores cannot carry current and will have no effect on resistivity. Therefore, resistivity measurements of water saturated concrete can be used as an indicator of pore connectivity (Andrade, 2009). This is particularly advantageous in durability assessment since the interconnected pore system is what allows concrete to exhibit transport properties.

The water-to-cement ratio that is selected during the design of the concrete mixture has a direct effect on the porosity of the concrete produced. Excess water that is not used up in the hydration reactions with cement will eventually evaporate leaving voids behind in its place. For this reason, a higher water-to-cement ratio will result in a concrete that is more porous and will consequently yield a lower resistivity. Gjørv et al. (1977) found that reducing the water-to-cement ratio from 0.7 to 0.5 for mortar specimens increased the electrical resistivity by a factor of 2, and for the same water-to-cement ratio of 0.5 the mortar specimen's resistivity was more than 3 times that of concrete. This goes to prove that electrical resistivity is greatly affected by the porosity, pore structure and pore size distribution of the hydrated cement paste.

Cement Type

There are several different types of cement that can produce concrete with characteristics better suited for its application. The cement types used in Canada and their acronyms are: General use cement (GU), high sulfate resistance cement (HS), moderate sulfate resistance cement (MS), moderate heat of hydration cement (MH), low heat of hydration cement (LH), and high early strength cement (HE). They differ from one another in their chemical composition. The ions present in the pore water and their relative concentration is then understandably linked to what type of cement was used. This can affect resistivity as one cement type may produce concrete with a more conductive pore water solution than another.

Aggregates

The resistivity of the aggregates used in concrete is usually much higher than that of the surrounding cement paste and thus can be considered to be non-conductive (Maierhofer, et al., 2010). They can, however, still affect the resistivity of the concrete in which they are used in three ways: volume proportion, particle size distribution, and type of aggregate.

Due to aggregates having a high resistivity, an increase in total aggregate volume used for the same volume of concrete will increase the resistivity of the hardened concrete (Sengul, 2013, Wei and Xiao, 2011). To avoid variability in results, a continuous particle size distribution of aggregates is required. Using larger aggregate sizes can also lead to greater variability (Morris, et al., 1996). Some resistivity measurement devices even recommend that the maximum aggregate size be less than the spacing between the probes.

Different types of aggregates will have a different effect on the resistivity of the concrete. An aggregate with a relatively lower resistivity, compared to one with a higher resistivity, will produce concrete with a lower resistivity, keeping all other factors constant. The aggregate type can also cause variability in test results. For instance, concrete using siliceous aggregates will show less variability in results as opposed to a concrete using calcareous aggregate (Maierhofer, et al., 2010).

Chemical and Mineral Admixtures

Chemical admixtures are used to improve certain fresh properties of a concrete mixture, or the durability of the hardened concrete. Ions present in these admixtures, such as chlorides and nitrates, can remain in the pore solution once the concrete sets, potentially reducing the resistivity. Calcium chloride, for example, is a chloride-bearing admixture that was commonly used as an accelerator to speed up the setting of concrete.

Mineral admixtures, also known as supplementary cementing materials (SCM), are used to improve the strength and durability of the hardened concrete. Most SCMs are byproducts of manufacturing industries, which makes their use in concrete highly sustainable in addition to being beneficial. The three most commonly used SCMs are: fly ash (byproduct of burning coal in thermal power plants), ground granulated blast-furnace slag (byproduct of iron manufacturing), and silica fume (byproduct of silicone and ferrosilicon alloy production). They are often used in various combinations with one another as a replacement for part of the cement content. SCM's pozzolanic or hydraulic properties improve concrete's durability by decreasing transport properties through refining the pore structure (Hooton, 1986). They may also lower the ionic concentration within the pore water solution (Whiting and Nagi, 2003). Using SCMs will therefore increase the resistivity of the resulting concrete. When taking resistivity measurements in the field, the mixture design should be consulted, as the quality of the concrete tested may be overestimated without previous knowledge of which SCMs were used.

Hussain and Rasheeduzzafar (1994) conducted tests on concrete specimens made with fly ash blended cement replacing 30% of the cement by mass. Results of the pore solution test showed a decrease in the hydroxyl ion (OH^-) concentration as well as the unbound chlorides (Cl^-). The authors also found that concrete made from the fly ash blended cement had "significant pore refinement" as it showed reduced permeability to water and chlorides.

Wolsiefer (1991) studied the effect of silica fume on the electrical resistivity of concretes made with cement contents of 100, 250, and 400 kg/m^3. Replacing 20% of the cement by mass with silica fume increased the resistivity of the 100 kg /m^3 mixture from approximately 4 to 16 kΩ·cm, the 250 kg /m^3 mixture from 8 to 45 kΩ·cm, and the 450 kg /m^3 mixture from 4 to 130 kΩ·cm. Silica fume seems to have a more pronounced effect on resistivity at lower water-to-cement ratio.

1.2.2.2 Extrinsic Factors

Temperature

Fluctuations in temperature can cause variability in resistivity measurement results. A rise in temperature will increase the average kinetic energy of the molecules within the concrete pores, increasing ion mobility. Furthermore, a higher concentration of ions may be present with increasing temperature as solubility increases as well (Barron and Ashton, 2005). Those two factors will increase the conductivity of the pore water solution and lower the resistivity of the concrete measured.

Moisture Content

Moisture within concrete's pores is essential for the passage of electrical current, through which resistivity can be determined. Lowering the moisture content will restrict the current flow and will consequently increase the measured resistivity. One advantage to this relationship is that resistivity measurements can be used to identify sections of a structure with different moisture contents. However, the disadvantage is that it can cause variability in resistivity measurements. An oven-dried concrete specimen will have resistivity values that are several orders of magnitude higher than one that is moist (Monfore, 1968). To circumvent this issue, concrete specimens are usually tested in a saturated surface dry (SSD) condition.

Presence of Ions

Concrete, being a porous material, can become contaminated with ions such as chlorides or sulfates when exposed and the solution containing the ions slowly permeates inward. This is a cause for concern from a durability perspective since chlorides cause corrosion of the steel reinforcement and sulfates cause sulfate attack of the hydrated cement paste (see Section 1.3). The ingress of ions will increase their concentration within the pore network and facilitate the flow of current from the electrical resistivity device, subsequently lowering the measured resistivity.

Saleem et al. (1996) studied the effect of chlorides, sulfates, and the combination of both, on the electrical resistivity of concrete. Results showed that when the chloride concentration increased, the electrical resistivity decreased. At a moisture content of 1.5%, the resistivity decreased from 76 kΩ·cm to 5 kΩ·cm when the chloride concentration increased from 0 to 19.2 kg/m^3. Similar to the chlorides, the results indicated a decrease in resistivity as the concentration of sulfates increased. An increase in sulfate concentration from 7.2 to 43.2 kg/m^3 at a moisture content of 1.5% decreased the resistivity measured from 40 to 10 kΩ·cm. It was interesting to note however that when the concrete specimens contained both sulfates and chlorides, the reduction in resistivity was not equal to the sum of each individual effect. At a moisture content of 2%, the concrete specimens with a chloride concentration of 2.4 kg/m^3 and a sulfate concentration of 7.2 kg/m^3 had a resistivity of 19 kΩ·cm, which was close to the 20.5 kΩ·cm resistivity of the concrete specimens containing only chlorides at a concentration of 2.4 kg/m^3. In addition, the decrease in resistivity between subsequent intervals of increasing chloride or sulfate concentration decreased as the moisture content increased. The results of the sulfate contaminated specimens were contrary to the findings of the experimental section of this thesis. This is possibly due to the concrete specimens being exposed to a sulfate solution as opposed to having the sulfates within the mixing water itself. However, the authors did not mention how the concentration of the ions within the concrete was achieved.

Presence of Steel Rebar

Steel reinforcement has long been used in reinforced concrete structures to strengthen the concrete's relatively low tensile strength. The presence of steel rebar, or any electrically conductive material, in close proximity to the surface where a resistivity measurement is being taken will alter the readings. The electrical current will favorably flow through the rebar instead of the concrete pores, as steel is highly conductive relative to concrete, which will lower the measured resistivity. To circumvent this, the locations of the rebar should first be located with a magnetic inductance device or similar. Then the resistivity device should be placed as far away from the rebars as possible as shown in Figure 5(a) or perpendicular to the rebars if they are closely spaced as shown in Figure 5(b).

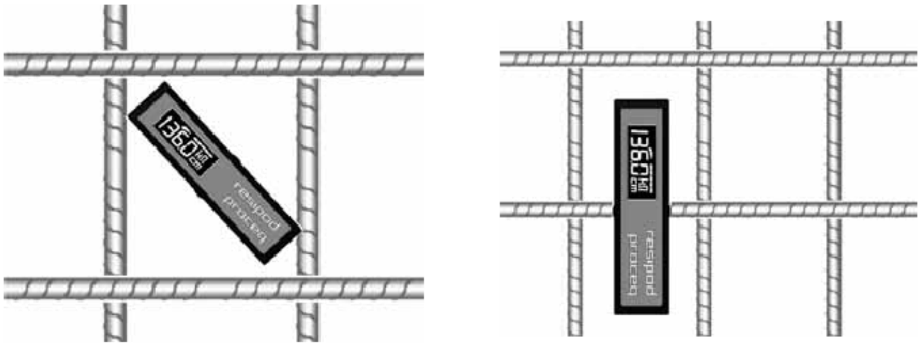

(a)

(b)

Figure 5: Placement of the resistivity measurement device if (a) rebars are far apart enough to avoid (b) rebars are closely spaced

Carbonation

Carbonation of concrete occurs when carbon dioxide (CO_2) from the air reacts with calcium hydroxide [$Ca(OH)_2$] in the cement paste to form calcium carbonate ($CaCO_3$). Concrete exposed to carbon dioxide daily, such as bridges, will experience carbonation. The calcium carbonate forms within the concrete's pores which leads to a measureable reduction in permeability as well as pore volume (Claisse, et al., 1999). Furthermore, the concentration of calcium (Ca^{2+}) and hydroxyl (OH^-) ions decreases as the carbonation chemical reactions continue (Claisse, et al., 1999). Both these factors will cause a reduction in electrical resistivity.

Geometry and Edge Closeness

The geometry of the concrete specimen has an effect on its electrical resistivity. The Wenner method of measuring resistivity is based on the assumption that the current and potential fields flow through a semi-infinite volume of the material (Whiting and Nagi, 2003). A geometrical correction factor is required when that assumption does not hold true. Therefore, comparing resistivity measurements for specimens of different geometries requires the use of correction factors. If the comparison is between specimens of the same geometry then a correction factor is not necessary as the error is constant for all specimens (Maierhofer, et al., 2010).

Taking resistivity measurements close to an edge also introduces errors. The edge causes a concentration of the current density due to the limited volume available, which overestimates the resistivity measured (Maierhofer, et al., 2010). As with geometrical errors, a correction factor can be applied which requires finite element modelling and conduction equation calculations (Maierhofer, et al., 2010).

Presence of Cracks

Cracks are almost always present in concrete and their presence can affect the measured surface resistivity. Cracks disrupt the flow of electrical current which travels through the ionic solution contained within the concrete's pore network. Lataste et al. (2003) conducted experiments to investigate the effects of different cracks on the surface resistivity. The surface resistivity device utilized four probes in a square arrangement with a 5 and 10 cm spacing between the probes. The device also contained a switch allowing the device to measure surface resistivity in two orthogonal directions by changing the probe’s role. The device was successful in detecting a delamination crack in a slab when used in a 5 cm step to form an isoresistivity map. The average resistivity increased from around 800 Ω·m in “healthy” concrete zones up to 1700 Ω·m in the delamination zone. The crack had a resistivity of 200 Ω·m while the area surrounding the crack had a resistivity of 400 Ω·m.

To study the effect of different crack parameters on surface resistivity, Lataste et al. (2003) conducted experiments on a 35 x 35 x 15 cm^3 prism with a 0.2 mm wide crack. The crack was considered either conductive, such as a water saturated crack, or non-conductive, such as an air filled crack. Results show that in a non-conductive crack, apparent resistivity increases when the current applied is perpendicular to the crack and decreases when it’s parallel. For a conductive crack, the apparent resistivity was unaffected when the crack was perpendicular to the current application but decreased when the crack was parallel. Increasing the depth of the crack seemed to exacerbate its effect on the measured resistivity.

1.3 Sulfate Attack

Sulfate attack of concrete occurs when sulfate ions chemically react with components of the hydrated cement paste. Sulfates can be present in soils or dissolved in groundwater. Some naturally occurring minerals contain sulfates of sodium, magnesium, calcium and potassium. Ammonium sulfate is commonly used as a fertilizer and can be found in the soil and water in agricultural regions. Structures in contact with seawater or built on coastal soil and pipes carrying waste water are also exposed to sulfates. The damage caused by the sulfate anion is independent of the source of sulfate, but the associated cation may aggravate the deleterious effects through chemical reactions of its own (Mehta and Monteiro, 2013). The rate of deterioration and its processes are governed by the environmental and physical conditions present with the sulfates (Marchand, et al., 2003).

Sulfate attack follows a complex chemical process, but the two products that are generally associated with it are the formation of ettringite and gypsum (Mehta, 1983). The chemical reactions that lead to the formation of ettringite have a net increase in solid volume which causes expansion within the concrete which consequently causes cracking. The formation of gypsum on the other hand can cause softening of the hydrated cement paste and loss of cohesiveness which leads to a progressive loss in strength. If magnesium sulfate is the cause of sulfate attack, brucite will be formed in addition to ettringite and gypsum (Bonen and Cohen, 1992). Sulfate attack occurring at colder temperatures, below 5 °C to 10 °C, may form thaumasite, which is arguably more damaging to concrete than ettringite formation (Marchand, et al., 2003).

1.3.1 Consequences of Sulfate Attack

The damage caused to concrete through sulfate attack can be classified as either chemical or physical. Chemical damage will involve the various chemical reactions that occur between sulfate ions and certain products of the hydrated cement paste. Physical damage occurs as a result of crystallization of the sulfate salts.

1.3.1.1 Chemical

The molecular formulas of certain reactants and products of sulfate attack are long and complex. Abbreviations of the Cement Chemist Notation (CCN) are commonly used for simplification, namely: $\mathbf{C}$ for CaO, $\mathbf{S}$ for $\mathrm{SiO_2}$, $\mathbf{A}$ for $\mathrm{AL_2O_3}$, $\bar{\mathbf{S}}$ for $\mathrm{SO_3}$, and $\mathbf{H}$ for $\mathrm{H_2O}$.

1.3.1.1.1 Gypsum Formation

In the presence of sulfate ions [$\mathrm{SO_4^{2-}}$], calcium hydroxide [$\mathrm{Ca(OH)_2}$ or $\mathbf{CH}$], a constituent of the hydrated cement paste, reacts chemically to form gypsum [$\mathrm{CaSO_4 \cdot 2H_2O}$ or $\mathbf{C\bar{S}H_2}$] according to the following reaction:

$$SO_4^{2-} + \boldsymbol{CH} + 2\boldsymbol{H} \longrightarrow \boldsymbol{C\bar{S}H_2} + 2OH^-$$

Calcium Hydroxide is a component of the hydrated cement paste that contributes to stiffness and strength. $\mathbf{CH}$ is formed when alite ($\mathbf{C_3S}$) and belite ($\mathbf{C_2S}$) in cement reacts with water (Marchand, et al., 2001). It’s conversion to gypsum will lead to a loss in strength over time, as well as a loss of cohesion between the components of the hydrated cement paste. The formation of gypsum is also believed to cause expansion, but research on the subject matter is limited (Tian and Cohen, 2000).

Quantifying the expansion caused solely by gypsum formation is challenging as ettringite formation also causes expansion during sulfate attack (Santhanam, et al., 2003). One method of isolating the expansion caused by gypsum is to use cements with a low tricalcium aluminate ($\mathbf{C_3A}$) content to limit ettringite. González and Irassar (1997) performed experiments on mortar bars produced using four ASTM Type V cements with very low $\mathbf{C_3A}$ content (0 – 1%) and varying $\mathbf{C_3S}$ content (40 – 74%) immersed in 5% $\mathrm{Na_2SO_4}$ solutions. Results showed that all the mortar bars experienced expansion, the most being that with the highest $\mathbf{C_3S}$ content expanding 0.117% in 180 days. X-Ray diffraction (XRD) analysis detected gypsum formation at 90 days for all four cements, whereas at 720 days the cement with the highest $\mathbf{C_3S}$ content had the highest peak for gypsum. This shows the importance of limiting $\mathbf{C_3S}$ content in cements, as limiting $\mathbf{C_3A}$ content alone may not be sufficient in prevent sulfate attack.

Tian and Cohen (2000) also investigated whether gypsum formation causes expansion. Two different sources of $\mathbf{C_3S}$ were used: a white powder $\mathbf{C_3S}$ and a grey powdered alite with impurities such as MgO, $\mathrm{Al_2O_3}$, $\mathrm{Fe_2O_3}$, and alkalies. Paste specimens were made from the alite while mortar bars were made from the $\mathbf{C_3S}$. When exposed to a 5% $\mathrm{Na_2SO_4}$, the alite specimens did not show any expansion for 360 days, but then expanded rapidly reaching 0.10% at 480 days. The $\mathbf{C_3S}$ specimens on the other hand began expanding after only 40 days at a faster rate reaching an expansion of 1.05% at 230 days. Replacing 10% of the alite or $\mathbf{C_3S}$ with silica fume prevented any considerable expansion. When alite specimens were exposed to a 4.65% $\mathrm{(NH_4)_2SO_4}$ solution, they expanded rapidly without a dormant period, reaching an expansion of 1.28% after only 60 days. The effect of silica fume was not tested on $\mathrm{(NH_4)_2SO_4}$ exposure. XRD analysis indicated that gypsum formed in all specimens with higher peaks when silica fume was not used. The alite specimens exposed to $\mathrm{(NH_4)_2SO_4}$ showed the highest peaks for gypsum while still showing the highest peak for $\mathbf{CH}$. The authors explain that $\mathrm{(NH_4)_2SO_4}$ may attack calcium silicate hydrate ($\mathbf{CSH}$), without any further explanation, and that the high amounts of $\mathbf{CH}$ will later cause further gypsum formation leading to more expansion.

Sulfate attack of cements low in $\mathbf{C_3A}$ content will predominately form gypsum which leads to softening and a loss of cohesion in the hydrated cement paste (Rasheeduzzafar, et al., 1994). Standards that quantify the effects of surface softening and mass loss due to spalling should be developed (Santhanam, et al., 2001) since current standards, such as the ASTM C452 and ASTM C1012, mainly focus on expansion. Mehta et al. (1979) conducted tests on mortar prisms made using alite cements ground to a Blaine fineness of 3300 $\mathrm{cm^3/g}$ and 4500 $\mathrm{cm^3/g}$. The prisms were exposed to a 10% sulfate solution comprising of 5% $\mathrm{Na_2SO_4}$ and 5% $\mathrm{MgSO_4}$. Compressive strength tests performed at 90 days on the alite prisms containing added gypsum showed a reduction in strength from 36.9 MPa to 22.8 MPa in the 3300 $\mathrm{cm^3/g}$ alite and from 44.8 MPa to 33.8 MPa in the 4500 $\mathrm{cm^3/g}$ alite when added gypsum was increased from 0% to 6%. Both alite cements were below the ASTM C452 limit, expanding only 0.006% at 14 days. Alite concrete cylinders stored for 5 years in the sulfate solution had an average compressive strength of 23.9 MPa which was less than half that of the reference cylinders stored in water averaging 48.3 MPa. Visual evaluation of the damage after 6 years showed severe spalling in the alite concrete prism as compared to concrete prism formed from ASTM Type V cement. The authors go on to state that ASTM C452 is not sufficient in predicting spalling and loss of cohesion due to sulfate attack.

Sulfate attack seems to favor the formation of gypsum over ettringite at high sulfate concentrations of 5,000 ppm or more (Santhanam, et al., 2003). Raising the pH of the pore solution increases the sulfate concentration required for the reaction forming gypsum to proceed (Bellmann, et al., 2006). Standardized tests for sulfate attack utilize high sulfate concentration, which is rarely seen in the field, to accelerate the test and therefore is not an accurate representation.

1.3.1.1.2 Ettringite Formation

Ettringite [$\mathrm{Ca_6Al_2(SO_4)_3(OH)_{12} \cdot 26H_2O}$ or $\mathbf{C_6A\overline{S}_3H_{32}}$] is a product of sulfate attack that forms when sulfates attack calcium hydroxide and alumina-bearing phases of the hydrated cement paste. Most of the alumina is found as $\mathbf{C_3A}$ in the form of monosulfate hydrate ($\mathbf{C_3A \cdot C\overline{S} \cdot H_{18}}$) if the $\mathbf{C_3A}$ content is greater than 5%. If the $\mathbf{C_3A}$ content is greater than 8% then it will also be found in the form of tetracalcium aluminate hydrate ($\mathbf{C_3A \cdot CH \cdot H_{18}}$) (Mehta and Monteiro, 2013). Ettringite is then formed by the following chemical reactions:

$$\boldsymbol{C_3A \cdot C\overline{S} \cdot H_{18}} + 2\boldsymbol{CH} + 2\boldsymbol{\overline{S}} + 12\boldsymbol{H} \longrightarrow \boldsymbol{C_6A\overline{S}_3H_{32}}$$

$$\boldsymbol{C_3A \cdot CH \cdot H_{18}} + 2\boldsymbol{CH} + 3\boldsymbol{\overline{S}} + 11\boldsymbol{H} \longrightarrow \boldsymbol{C_6A\overline{S}_3H_{32}}$$

Ettringite also forms when gypsum ($\mathbf{C\overline{S}H_2}$) reacts with monosulphoaluminate ($\mathbf{C_3A \cdot C\overline{S} \cdot H_{12}}$) found in the hydrated cement paste (Marchand, et al., 2003) through the following chemical reaction:

$$\boldsymbol{C_3A \cdot C\overline{S} \cdot H_{12}} + 2\mathbf{C\overline{S}H_2} + 16\boldsymbol{H} \longrightarrow \boldsymbol{C_6A\overline{S}_3H_{32}}$$

However, under conditions of low alkalinity, such as when the pH drops below 12, ettringite becomes unstable and could decompose to gypsum (Santhanam, et al., 2001).

Detection of ettringite within concrete is not always synonymous with sulfate attack. Ettringite is usually formed within hours of hydrating cement as a result of gypsum and $\mathbf{C_3A}$ within the cement reacting in the presence of moisture (Collepardi, 2003). This reaction, named Early Ettringite Formation (EEF), is not detrimental as the cement paste is still in a plastic phase and unrestrained. EEF has been attributed to set retardation of Portland cement, high early strength of supersulfated cements, and prestressing of restrained expansive cements (Mehta, 1976).

Expansion of concrete suffering from sulfate attack has generally been attributed to the formation of ettringite. There are various hypotheses on the mechanism through which ettringite formation causes expansion but the subject matter remains controversial (Mehta and Monteiro, 2013). One hypothesis suggests that the pressure exerted by the ettringite crystals as they grow creates tensile stresses within hardened concrete that exceeds its weak tensile strength resulting in cracking and expansion (Mehta, 1973). Another proposed hypothesis is that ettringite with weak crystalline structure will adsorb water, more so under alkaline conditions, causing the crystals to swell (Mehta and Hu, 1978, Mehta and Monteiro, 2013).

Min and Mingshu (1994) conducted experiments to investigate the effect alkalis have on the expansion caused by ettringite formation. The authors discussed the nature of their experimentation with minimal details but results indicated that expansion of supersulfated cement pastes increased with increasing added $\mathrm{Na_2O}$ concentration. Increasing added $\mathrm{K_2O}$ concentration in sulfoaluminate cement pastes also increased the measured expansion. The authors conclude by attributing the expansion to both the crystallization pressure of forming ettringite and swelling due to adsorption, the former being more dominant.

Odler and Colán-Subauste (1999) studied the effect of different alumina bearing materials on the expansion caused by ettringite formation during sulfate attack. The materials used were: monocalcium aluminate ($\mathbf{CA}$), $\mathbf{C_3A}$, tetracalcium aluminate sulfate ($\mathbf{C_4A_3S}$), tetracalcium aluminate ferrite ($\mathbf{C_4AF}$), $\mathbf{C_3A \cdot C\overline{S} \cdot H_{12}}$, and $\mathbf{CAS}$-glass. Specimens containing $\mathbf{CA}$, $\mathbf{C_4A_3S}$, and $\mathbf{C_3A \cdot C\overline{S} \cdot H_{12}}$ expanded rapidly and disintegrated in less than a month's time. The $\mathbf{C_3A}$ specimens, according to the authors, expanded significantly but at a slower rate due to the relatively lower dissolution and solubility rates. The $\mathbf{C_4AF}$ specimens expanded even slower but the $\mathbf{CAS}$-glass showed no measurable expansion. Specimens cured in water expanded more than when cured in humid air. However the results of specimens cured in dry air revealed that moisture is not required for ettringite formation to cause expansion but seems to exacerbate its effect. The authors also studied the relationship between the amount of ettringite formed and the expansion measured and reported that it was not uniform.

Ettringite crystals can be found in a couple of different forms. It's morphology depends on the total available space or the water to solids ratio (Mehta, 1976). The crystals formed are thin and needle-like if adequate space is available (high water-solid ratio), growing up to 100 µm long. Otherwise they form 1 µm short prismatic crystals if the water-solid ratio is low (Mehta, 1976). The morphology of the crystals also depends on the concentration of hydroxyl ions (Mehta, 1983). Under conditions where the concentration is low, the crystals grow large and "lath-like" ranging in size from 10 – 100 µm, named Type 1 ettringite crystals. If the hydroxyl concentration is high, the crystals are small and rod shaped ranging in size from 1 - 2 µm, named Type 2 ettringite crystals (Mehta, 1983).

1.3.1.2 Physical

Damage to concrete due to sulfate attack can manifest itself physically in the form of surface scaling. This occurs as a result of salt crystallization, or salt weathering, taking place at or near the concrete surface. The effects of salt weathering are exacerbated under conditions of partial immersion. The moisture gradient draws the solution to the dryer section which then evaporates at the surface (Hartell, et al., 2010, Scherer, 2004). Salt weathering is not limited to concrete alone; in fact it can cause deterioration to other porous materials such as stone and masonry (Liu, et al., 2012). Two different hypotheses are proposed to explain the mechanism through which salt weathering causes damage: salt hydration pressure and salt crystallization pressure (Tsui, et al., 2003).

Salt hydration occurs when a salt is converted from its anhydrous form to a hydrous one, which is believed to cause damage due to a solid volume increase as the hydrous form has a larger volume (Tsui, et al., 2003). A well-known example is the transformation of anhydrous sodium sulfate ($\mathrm{Na_2SO_4}$), known as thenardite, to its hydrous form sodium sulfate decahydrate

($\mathrm{Na_2SO_4 \cdot 10H_2O}$), known as mirabilite. First, mirabilite precipitates from a solution containing sodium and sulfate ions, followed by a temperature dependent process of repeated crystallization as shown in the equations below (Marchand, et al., 2003):

$$\underbrace{2Na^{+} + SO_4^{2-}}_{Solution} \xrightarrow[Evaporation]{} \underbrace{Na_2SO_4 \cdot 10H_2O}_{Solid}$$

$$\underbrace{Na_2SO_4 \cdot 10H_2O}_{Mirabilite} \xLeftrightarrow[\substack{Repeated\\Crystallization}]{} \underbrace{Na_2SO_4}_{Thenardite}$$

When thenardite is converted to mirabilite, it is accompanied by a 315% volume expansion (Thaulow and Sahu, 2004, Tsui, et al., 2003) which under repeated crystallization can cause fatigue of the hydrated cement paste (Marchand, et al., 2003). However, Thaulow and Sahu (2004) argue that if the volume of water was accounted for in the net calculation, then there would be a volume decrease of 5.6%. Using an environmental scanning electron microscope (ESEM), Rodriguez-Navarro and Doehne (1999) deduced that physical damage from sodium sulfate did not occur due to hydration, but due to crystallization pressure from the rapid dissolution and subsequent precipitation of mirabilite. The authors also state that the formation of either the anhydrous or hydrous form of a salt is a through-solution process. This is in accordance with the views of Folliard and Sandberg (1994) that hydration of thenardite to mirabilite is not a solid-state phenomenon. Furthermore, the crystal structure of thenardite and mirabilite are different and transformation from one to the other cannot occur by solid-state hydration (Thaulow and Sahu, 2004).

The salt crystallization pressure theory suggests that salts crystallizing out of a supersaturated solution can exert high pressures when confined in a pore space (Flatt, 2002, Steiger and Asmussen, 2008, Thaulow and Sahu, 2004, Tsui, et al., 2003). This theory explains how salts without a hydrous form, such as halite (NaCl), still cause damage and surface scaling of porous materials (Winkler and Singer, 1972). It is imperative, however, that the solution be supersaturated for the crystallization to generate sufficient stress, owing to the higher potential energy a solute possesses in a supersaturated state as compared to a saturated one (Thaulow and Sahu, 2004). With sodium sulfate, supersaturation can occur without evaporation

(Rodriguez-Navarro and Doehne, 1999) making it one of the more destructive salts. The solubility of mirabilite decreases substantially when the temperature drops below 32 °C which is coupled with thenardite dissolution creating a supersaturated solution with respect to mirabilite, prompting crystallization (Chatterji and Jensen, 1989, Flatt, 2002). This process can develop tensile hoop stresses in the range of 10 – 20 MPa, which exceeds the tensile strength of most concretes and stones (Flatt, 2002).

1.3.2 Source of Sulfates

1.3.2.1 Internal

Internal sulfate attack occurs when the source of sulfates originates from the constituents used to make concrete. Cement contains calcium sulfate, in its various forms, as sulfates accelerate the hydration of the calcium silicates which contributes to early strength (Marchand, et al., 2003). The addition of calcium sulfates, such as gypsum, to clinker during cement grinding also controls the cement's setting characteristics (Marchand, et al., 2003). Other sulfates may be found incorporated in clinker from the raw materials used during manufacturing or from the by-products of fuel combustion (Marchand, et al., 2003). Aggregates, such as those containing gypsum or iron pyrite, may contain sufficient sulfates or sulfides to initiate internal sulfate attack (Marchand, et al., 2003). Sulfates may also originate from mixing water if used from an unverified source.

The main concern with internal sulfate attack of concrete is expansion caused by delayed ettringite formation (DEF) in hardened concrete. The occurrence of DEF has been associated with curing concrete at elevated temperatures such as steam curing (Diamond, 1996, Mehta and Monteiro, 2013), as well as mass concrete reaching high temperatures due to heat of hydration (Hobbs, 1999). At temperatures of 70 °C or more (Diamond, 1996, Taylor, et al., 2001), ettringite that is formed during hydration is no longer stable and decomposes to monosulfate hydrate (Mehta and Monteiro, 2013, Taylor, et al., 2001). The sulfate ions released as a result of ettringite decomposition are adsorbed by calcium silicate hydrate ($\mathbf{CSH}$) in the hydrated cement paste (Mehta and Monteiro, 2013, Taylor, et al., 2001). Subsequently, during the service life of the affected concrete, the sulfate ions are desorbed allowing for the reformation of ettringite in hardened concrete which causes expansion and subsequent cracking (Mehta and Monteiro, 2013).

The prerequisites for DEF to take effect are: an internal source of sulfates, curing at elevated temperatures, and the presence of moisture either by constant exposure or by drying and wetting cycles (Fu, et al., 1997, Taylor, et al., 2001). The rate and extent of damage caused by DEF is exacerbated in the presence of microstructural flaws such as those caused by alkali-silica reaction (ASR) or freeze-thaw (Yang, et al., 1999). Two hypotheses are proposed to explain the mechanism of expansion caused by DEF: the uniform paste expansion theory and the ettringite crystal growth pressure theory (Taylor, et al., 2001, Yang, et al., 1999).

The uniform paste expansion theory proposes that DEF causes expansion in the paste, but not the aggregates, which leaves a gap between the two. Ettringite then recrystallizes around the aggregates forming “bands” which can be seen under a scanning electron microscope (SEM). In this theory the observed expansion is associated with the paste expanding and not the ettringite reformation around the aggregates (Yang, et al., 1999). On the other hand, the ettringite crystal growth pressure theory suggests that ettringite crystals reforming within preexisting cracks in the paste or the interfacial transition zone (ITZ) can cause the cracks to propagate and widen, leading to expansion. For the ettringite crystal growth to exert enough pressure, it needs to form from a supersaturated solution. Taylor et al. (2001) and Johansen et al. (1993) argue that from a thermodynamics standpoint, the degree of supersaturation of ettringite is not sufficient to cause cracking and expansion. However, Diamond (1996) suggests that concrete is a “quasi-brittle” material and follows fracture mechanics principles, which implies that tensile stresses are magnified at the tip of the crack and a “modest” degree of saturation could produce the required stresses to cause crack propagation and expansion.

Findings by Diamond (1996) and Yang et al. (1999) seems to support the ettringite crystal growth pressure theory. Under an SEM they observed that the cracks formed did not go all the way around the aggregates and some aggregates had no rim cracks at all. Instead, they observed a network of partial rim cracks around the aggregates connected by cracks through the paste. The ettringite crystal growth pressure theory also helps explain why damage caused by DEF is amplified when coupled with ASR (Diamond, 1996, Shayan and Ivanusec, 1996), freeze-thaw and other microstructural flaws (Yang, et al., 1999).

1.3.2.2 External

Sulfate attack of concrete more commonly occurs due to sulfates that originate from an external source. Of the many external sources that contain sulfates, groundwater is the most common (Marchand, et al., 2003). Groundwater partially dissolves minerals containing sulfates from soils and rocks such as sodium, potassium and magnesium sulfates. Ammonium sulfate is found in some fertilizers and when used in large quantities, such as for agricultural purposes, it can contaminate the soil and underlying ground water and cause significant damage to concrete. Sewage water can be particularly deleterious to the concrete pipes that contain them due to the combined actions of sulfate attack and sulfuric acid attack which results indirectly from bacterial processes. Industrial waste waters can have varying amounts of sulfates depending on the industry and what is being processed. Seawater can contain high levels of sulfates but damage due to sulfate attack is mitigated due to the high chloride concentration (Santhanam, et al., 2006).

External sulfate attack begins at the surface of the concrete in contact with the sulfate source and gradually works its way inwards. The rate at which sulfates penetrate into the concrete and cause damage is dependent on the water to cement ratio and the subsequent porosity of the concrete. The higher the porosity of the concrete, the faster and deeper the sulfates will ingress and the more extensive the damage will be.

Damage due to external sulfate attack can be exacerbated under conditions of partial exposure. When part of a concrete member is saturated with a sulfate solution while other part is relatively dry, the moisture gradient induces a transport mechanism that draws the sulfate solution through the concrete to the dryer section where it evaporates and crystalizes at the surface (Boyd and Mindess, 2004). Salt scaling damage will then be evident at the evaporation front after prolonged exposure. The sulfate attack reactions are accelerated due to the higher influx of sulfates causing the concrete member to deteriorate at a more rapid rate (Boyd and Mindess, 2004).

1.3.2.2.1 Alkali Sulfates

External sulfate attack of concrete can be caused by alkali sulfates, namely sodium sulfate ($\mathrm{Na_2SO_4}$) and potassium sulfate ($\mathrm{K_2SO_4}$). The sulfate ions from water contaminated with alkali sulfates reacts with monosulfate in the hydrated cement paste to form ettringite according to the following chemical reaction (Marchand, et al., 2003):

$$2SO_4^{2-} + \boldsymbol{C_3A \cdot C\overline{S} \cdot H_{12}} + 2Ca^{2+} \longrightarrow \boldsymbol{C_6A\overline{S}H_{32}}$$

The calcium cation required in the chemical reaction is provided by the dissolution of the calcium hydroxide in the hydrated cement paste. Once that is depleted, then the decomposition of the **CSH** provides further calcium for the reaction (Marchand, et al., 2003). The decrease in calcium of the **CSH** phase will weaken its mechanical properties (Alexander, et al., 2012) and cause gradual loss in cohesion (Marchand, et al., 2003).

If the aluminum-bearing compounds needed to form ettringite are consumed while sulfate ions are still available, then gypsum is formed. As a result, gypsum can usually be detected closer to the concrete surface under attack than ettringite (Marchand, et al., 2003). According to Marchand et al. (2003), concrete exposed externally to alkali sulfates for an extended amount of time will exhibit 4 distinct zones. The first zone, which extends to the outermost surface of the concrete under attack, will be severely decalcified containing **CSH** with significantly reduced calcium content and “limited” amounts of sulfates adsorbed. The second zone will contain gypsum and partially decalcified **CSH** with an absence of calcium hydroxide. The following zone will contain ettringite and a decreased amount of calcium hydroxide. Finally, a zone containing hydrated cement paste that has not undergone sulfate attack.

The alkali cation can have adverse effects on concrete as well. As they penetrate into the concrete, they increase the alkalinity of the pore water solution in the hydrated cement paste increasing the pH. This is supplemented by the release of hydroxyl ions as calcium is consumed from the calcium hydroxide available, further increasing the alkalinity. If siliceous aggregates were used, it could result in alkali-silica reaction which, similar to sulfate attack, is expansive and damaging to concrete (Pettifer and Nixon, 1980).

Initially, when alkali sulfates attack concrete, ettringite forms in the pore spaces which consequently results in a temporary increase in compressive strength. Eventually it will reach a point where the availability of free pore space is low and additional formation of ettringite will exert pressure causing cracking and expansion (Marchand, et al., 2003). The cracking due to ettringite formation combined with the effects of gypsum and salt crystallization will cause observable surface scaling of the affected concrete member (Alexander, et al., 2012). Salt crystallization of sodium sulfate can be particularly damaging to concrete. At 32 °C, the solubility of the anhydrous form of sodium sulfate, thenardite, increases while simultaneously the solubility of its hydrous form, mirabilite, decreases considerably. This leads to a solution that is supersaturated with respect to mirabilite, and its precipitation can result in sufficiently high stresses to overcome the tensile strength of concrete. Salt weathering is discussed in further detail in section 1.3.1.2.

1.3.2.2.2 Calcium Sulfate

Environments containing the minerals anhydrite ($\mathrm{CaSO_4}$) or gypsum ($\mathrm{CaSO_4 \cdot 2H_2O}$) can cause external sulfate attack if they contaminate water in contact with concrete. Similar to the mechanism of alkali sulfates detailed in section 1.3.2.2.1, the sulfate ions in the solution react with monosulfate in the hydrated cement paste to form ettringite. The calcium cation needed for the reaction is almost exclusively provided by the calcium sulfate (Marchand, et al., 2003). Therefore, no leeching of calcium from calcium hydroxide and **CSH** of the hydrated cement paste occurs.

External sulfate attack caused by calcium sulfate can be distinguished from that of alkali sulfates due to the outer layers near the concrete surface not being decalcified. Furthermore, since the calcium content of the **CSH** phase isn’t reduced, its bonding and mechanical properties are not affected (Marchand, et al., 2003).

In the initial period, as concrete is being attacked by calcium sulfates, ettringite fills the empty pore spaces causing a temporary increase in strength. With time the empty pore spaces become less available and any additional ettringite that forms exerts pressure. With increasing pressure the concrete begins to crack and expand.

1.3.2.2.3 Magnesium Sulfate

If external sulfate attack is caused by magnesium sulfate ($\mathrm{MgSO_4}$), the sulfate ions react with the calcium cations of calcium hydroxide in the hydrated cement paste to form gypsum ($\mathrm{CaSO_4 \cdot 2H_2O}$), while the magnesium ions react with the remaining hydroxyl ions to form brucite [$\mathrm{Mg(OH)_2}$] according to the following chemical reaction (Marchand, et al., 2003):

$$Mg^{2+} + SO_4^{2-} + Ca(OH)_2 + 2H_2O \longrightarrow Mg(OH)_2 + CaSO_4 \cdot 2H_2O$$

As calcium hydroxide is consumed to produce the relatively insoluble brucite, the pH of the pore water solution decreases. Once all the available calcium hydroxide is consumed and the pH drops below the stability range of **CSH**, then calcium hydroxide is released from **CSH** in an attempt to restore its stability (Marchand, et al., 2003). However, if magnesium ions are still available then the released calcium hydroxide will react with it forming additional brucite and gypsum. This leads to the decomposition of the **CSH** phase and ultimately, its transformation to magnesium silicate hydrate (**MSH**) (Bonen and Cohen, 1992). In deeper sections where sulfates have penetrated but the pH still remains relatively high, ettringite can form though usually only in small amounts (Marchand, et al., 2003).

Magnesium sulfate induced sulfate attack drives the hydroxyl ions towards the surface to form brucite, while sulfate ions ingress inwards forming gypsum and small amounts of ettringite in deeper regions. This causes the formation of a surface double layer with brucite on the outer layer followed by a gypsum layer (Bonen and Cohen, 1992).

Magnesium sulfate will cause a more rapid deterioration of the **CSH** phase than with alkali or calcium sulfates (Marchand, et al., 2003). The consumption of calcium hydroxide followed by the decalcification of the **CSH** phase in the hydrated cement paste will result in gradual loss of strength and disintegration of the affected concrete. This is different from the surface scaling and expansion characterized by alkali or calcium sulfate attack.

1.3.2.2.4 Ammonium Sulfate

The deterioration of concrete by ammonium sulfate is arguably the most severe of the sulfate compounds (Mbessa and Péra, 2001, Miletić and Ilić, 1997, Xiong, et al., 2014). The sulfates from the solution containing ammonium sulfate in contact with the concrete surface will react with calcium hydroxide in the hydrated cement paste to form gypsum with the release of distinctive ammonia gas following the chemical reaction below (Marchand, et al., 2003):

$$Ca(OH)_2 + (NH_4)_2SO_4 \longrightarrow CaSO_4 \cdot 2H_2O + 2NH_3$$

Similar to sulfate attack by magnesium sulfate, the chemical reaction above proceeds until the calcium hydroxide in the affected area is depleted, lowering the pH. As the pH drops below the stability range of the **CSH** phase, calcium hydroxide is released from **CSH** which reacts with ammonium sulfate producing more gypsum and ammonia gas (Marchand, et al., 2003). The gradual drop in the calcium content of the CSH and its ultimate decomposition to amorphous hydrous silica is associated with strength loss and disintegration of the affected concrete. The drop in pH also causes the calcium sulfoaluminate hydrate phases in the hydrated cement paste to decompose to gypsum and aluminum sulfate (Marchand, et al., 2003).

As was the case with magnesium sulfates, the consumption of calcium hydroxide by ammonium sulfate followed by the decalcification and disintegration of the CSH phase leads to a loss in cohesion between the hydration products as well as a gradual loss in strength and disintegration of the concrete. However, the formation of a protective brucite outer layer in magnesium sulfate attack makes it less aggressive than ammonium sulfate attack (Mbessa and Péra, 2001).

2 Experimental

This chapter presents in detail the work involved in preparing the specimens and the procedure followed during the different experiments that were performed.

2.1 Concrete Specimen Preparation

2.1.1 Materials

2.1.1.1 Water

All of the water used in the mixture to make the specimens was taken from the city of Montréal drinking water supply.

2.1.1.2 Cement

Since the specimens were to represent concrete in the field, Type GU Portland cement was used. Type GU cement is the most commonly used type of Portland cement and is intended for general use, unless the special properties of a different type are required. The cement was produced by Lafarge Canada Inc. at the St. Constant cement plant.

2.1.1.3 Aggregates

Both the fine and coarse aggregates used in the mixture were crushed granite. Granite was selected as limestone aggregates are susceptible to sulfate attack and may form expansive thaumasite (Lacasse and Vanier, 1999). The gradation of the fine aggregate ranges from 0 mm to 5 mm whereas the coarse aggregate ranges from 5 mm to 10 mm. The maximum aggregate size was set at 10 mm so that the split faces are flat enough to perform surface resistivity testing on. The granite aggregates had a specific gravity of 2.68.

2.1.1.4 Admixtures

In order to facilitate the mixing and casting of the low water-to-cement ratio concrete batches, namely the 0.4 water-to-cement ratio, a high-range water reducer was added to the mixing water. The high-range water reducer used was ADVA Cast 575 produced by Grace Construction Products. According to the manufacturer’s product description “It is designed to impart extreme workability without segregation to the concrete”[*], it meets the specifications of ASTM C494 Type A/F and ASTM C1017 Type I, and does not contain chlorides.

2.1.2 Mixture Design

Three different mixture designs of varying water-to-cement ratio (w/c) were used throughout the research experimentation to attain a broader spectrum of results and to study the effect water-to-cement ratio has on surface resistivity (Table 1). The water-to-cement ratios selected for the purpose of this study were: 0.4, 0.5, and 0.6. The selection was done to cover water-to-cement ratios typically used in concrete construction.

Table 1: Concrete mixture designs

W/C		0.4		0.5		0.6	
Volume (m^3)		1	0.005931	1	0.005931	1	0.005931
Materials	Cement (kg)	517.5	3.069	414.0	2.455	400.0	2.372
	Water (kg)	207.0	1.228	207.0	1.228	240.0	1.423
	Fine Aggregate (kg)	641.8	3.807	677.0	4.016	646.4	3.834
	Coarse Aggregate (kg)	962.7	5.710	1015.6	6.023	969.6	5.751
	High-Range Water Reducer (mL)	1553	9.21	1242	7.37	1200	7.12

2.1.3 Mixing and Casting

To start, the insides of the 100 x 200 mm (4” x 8”) cylinder molds, in which the concrete was to be poured, were coated with form oil and placed upside down on a perforated table to attain a thin coat. All the required materials were then weighed and, where required, the sulfates, chlorides, or high-range water reducer were added directly to the mixing water.

The fine and coarse aggregates along with the cement were placed first in the mixer’s bowl and allowed to mix for 30 seconds to better distribute the contents. Water was then added and the mixer was run for 3 minutes followed by 3 minutes of no mixing. The mixer was run for an additional 2 minutes then switched off.

---

[*] Grace Concrete Products ADVA Cast 575 (https://grace.com/construction/en-us/Documents/DCAC-34D-ADVA%20Cast%20575.pdf)

The cylindrical molds were filled roughly halfway with the concrete mixture and placed on a vibrating table for consolidation. The process was repeated for the upper half of the mold. The surface was then smoothed with a trowel followed by placing a cap on the top of the mold to prevent evaporation. The specimens were demolded using pressurized air 24 hours after they were cast.

2.1.4 Curing

The specimens were labeled immediately after demolding to avoid confusion and placed in the moisture chamber for 28 days to cure. The moisture chamber method of curing is preferred over curing in a water/limewater tank as the latter will cause the ions to leech out of the concrete cylinders, lowering the concentration and affecting the resistivity results. It should be noted that when curing is done in a limewater tank, resistivity results should be multiplied by a correction factor of 1.1.

2.2 Testing Procedures

2.2.1 Surface Resistivity

Surface Resistivity testing was done in accordance with the AASHTO TP 95 standard. To achieve a saturated condition, the concrete cylinders were submerged in water with a chloride or sulfate concentration that was identical to that of the mixing water used to make them. A lid was placed on the buckets where the specimens were submerged to avoid evaporation. After 7 days, the specimens were removed from the water, one at a time, and 4 angle marks (0°, 90°, 180°, and 270°) were drawn on the top as shown in Figure 6(a). The height of the specimen was also measured, then it was placed halfway into the mold to draw the centerline mark as shown in Figure 6(b).

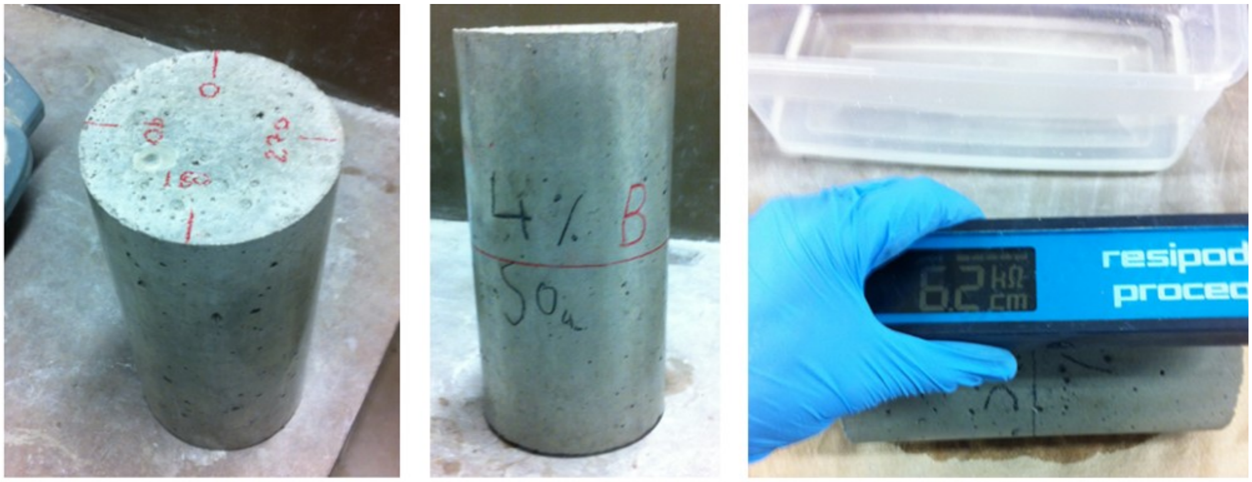

(a) (b) (c)

Figure 6: (a) Angle marks (b) Centerline mark (c) Surface resistivity measurement

Excess water on the surface of the concrete cylinder was blotted using a paper towel. The cylinder was placed on a non-conducting mount with the 0° at the top. The surface resistivity device, a Proceq Resipod, was then aligned with the 0° mark and having the centerline equidistant from each of the inner probes as shown in Figure 6(c). This specific device requires that the contacts be dipped in a shallow container of water and pressed several times to fill the reservoirs, which was done before every reading. The measurement was recorded once the reading stabilized. The specimen was then rotated having the 90° on top. This was repeated until two measurements were taken at each angle for a total of 8 measurements that were then averaged.

2.2.2 Bulk Resistivity

Specimens were submerged in water with a chloride or sulfate concentration that was equal to that of its mixing water for 7 days to induce saturation. Bulk resistivity measurements were done using the Proceq Resipod with the bulk resistivity accessory specifically designed for 100 x 200 mm (4” x 8”) cylinders. Before every measurement the foam inserts were rinsed with tap water and squeezed lightly by hand to drain excess water, such that the foam inserts were saturated but not dripping. The resistivity of the foam inserts were then measured. The resistivity of the top foam insert was measured by placing it between the two plates (electrodes) as shown in Figure 7(a). The resistivity of the bottom foam insert was measured by placing it between the two plates while having the concrete cylinder to be tested placed on the top plate as shown in Figure 7(b).

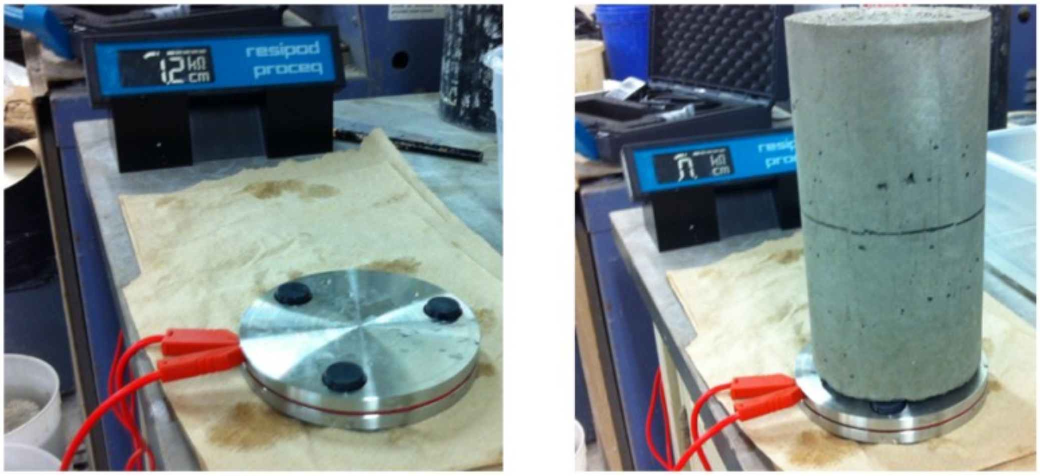

(a) (b)

Figure 7: Measuring resistivity of (a) top foam insert (b) bottom foam insert

The concrete cylinder to be tested was removed from the solution in which it was submerged and the surface was blotted with a paper towel to remove excess water. The cylinder was then placed between the two plates, with the wet foam inserts between each end of the cylinder and the adjacent plate to improve contact (Figure 8).

Figure 8: Measuring bulk resistivity

The bulk resistivity measurement was then recorded once the reading stabilized. The concrete cylinder was then flipped upside down and another measurement was taken. The two measurements per cylinder were averaged.

2.2.3 Effect of Change in Height on Surface Resistivity

The specimens were kept in a saturated condition by submerging them completely in water for 7 days. The height of the specimen was measured first. Then the steps outlined in section 2.2.1 were followed to measure the specimen's surface resistivity. Using a masonry saw, approximately equal sections of the specimen were sawed off and the debris washed off. The new height of the specimen was recorded and its surface resistivity was measured. This was done until the height of the specimen was around 11.4 cm, which was the maximum length the surface resistivity device with a spacing of 38 mm could measure.

2.2.4 Splitting Tension and Inner Resistivity

Splitting tension was performed mainly to obtain two halves of the concrete cylinder tested in order to measure the inner surface resistivity of each half. The specimen, kept in a moist condition, was placed in the splitting tension steel frame and centered. Plywood bearing strips were placed between the concrete cylinder and both the top and bottom of the steel frame to allow an even load distribution. Testing was done following the ASTM C 496 standard for splitting tension. Once the concrete cylinder had failed in tension, it was unloaded from the machine and lightly tapped on the table until the cylinder splits in halves. Before taking a measurement, the contacts of the surface resistivity device were pressed in a container of water to fill the reservoir, as per the instructions in the device's manual. The surface resistivity device was then placed on each of the halves and aligned to the drawn center line.

The inner surfaces of the halves obtained by splitting tension were jagged and rough which made it difficult to measure the surface resistivity. The maximum coarse aggregate size was limited to 6.35 mm (1/4") to help form a surface that was flat enough for all four steel probes of the surface resistivity device to come into contact with the surface. Although the steel probes were spring loaded, there were still some surfaces that were too jagged to allow all of them to make contact simultaneously. In that case, the steel probes were replaced with the large surface area foam contacts provided by Proceq. The foam contacts were moistened in a container of water before taking measurements.

Another issue faced with measuring inner resistivity was the formation of large cracks in the halves of some of the concrete cylinders due to the splitting tension loading. As outlined in Section 1.2.2.2, cracks can affect the resistivity measurement.

2.2.5 Achieving a Concentration Gradient

Concrete in the field that has become contaminated with chlorides or sulfates usually forms a concentration gradient with the highest concentration at the concrete surface in contact with the contaminated soil or water, followed by a gradually decrease with depth. Therefore, in addition to concrete cylinders with a constant concentration of chlorides or sulfates, experimentation was performed on cylinders with an induced concentration gradient. Two methods were explored in the attempt to induce a concentration gradient: using a pressure permeability apparatus and casting in layers.

2.2.5.1 Method 1: Using Pressure Permeability Apparatus

Concrete cylinders of the required water-to-cement ratio were cast and placed to cure in the moisture chamber for the standard 28 days. Once curing was completed, the concrete cylinder was inserted into a latex membrane that was cut to fit the cylinder and the two acrylic discs placed at each end. The acrylic discs were 100 mm (4”) in diameter and 25 mm (1”) thick with holes in their center and a 9.525 mm (3/8”) hydraulic connector attached to it. The surface of the acrylic disc in contact with the concrete cylinder was machined to be slightly concave to allow water and air to escape. A polyurethane adhesive sealant, Sikaflex-221, was applied to the surface of the acrylic disc to be in contact with the latex membrane to form an airtight seal. To ensure a tight seal, a hose clamp was used to hold the latex membrane firmly around the acrylic disc. The airtight latex sleeve containing the concrete cylinder and the two acrylic discs was then placed inside an aluminum tube and sealed with two aluminum plates. Rubber O-rings coated with silicon jelly were placed on grooves between the plates and each of the aluminum tube and acrylic discs. Finally, the system was bolted shut with six 25mm (1”) bolts. The system is shown in Figure 9.

Figure 9: Triaxial cell permeability apparatus

The triaxial cell permeability apparatus pressurized the system in two ways: driving pressure and confining pressure. Driving pressure was applied to a reservoir containing the solution to be driven into the concrete cylinder through the acrylic disc. Confining pressure was applied inside the cell between the aluminum tube and latex membrane and its purpose was to counteract the driving pressure within the sleeve and hold the membrane tightly around the concrete cylinder. This allowed the solution to move through the concrete cylinder and not between the cylinder and the membrane. Before applying the driving pressure, the cell was loaded with only the confining pressure and submerged under water to check for leaks. If no bubbles formed then the cell was considered airtight and the driving pressure was applied, otherwise the system was dismantled and adjusted. It was important to apply the confining pressure first before applying the driving pressure to force out any air trapped in the latex membrane. The triaxial cell utilized a driving pressure of 30 KPa and a confining pressure of 120 KPa. A test cell was set up in which it took 16 days for a 20,000 ppm chloride solution to permeate through a 100 x 200 mm (4” x 8”) concrete cylinder with a water-to-cement ratio of 0.5.

Setting up a cell and ensuring it was airtight proved to be an arduous task. Occasionally, overtightening the bolts caused the acrylic discs to crack and compromise the setup, while under-tightening caused leaks. That, along with the possibility of the chloride solution forming a concentration front as opposed to a gradient, led to the method of casting in layers to be favored.

2.2.5.2 Method 2: Casting in Layers

To achieve a concentration gradient, concrete cylinders where cast in equal layers where the concentration of chlorides or sulfates in the mixing water of each subsequent layer, from bottom to top, decreased. First, the materials required to cast a 100 x 200 mm (4” x 8”) concrete were split into 5 or 7 equivalent parts, depending on the concentration gradient required. A thin coat of oil was applied to the cylinder molds to be used. Then, layer by layer the materials were mixed in a bowl using an aluminum scoop. The cement, fine and coarse aggregates were mixed together for 30 seconds before the water was added. The concrete was mixed for three minutes and allowed to sit for another three minutes, followed by a final two minutes of mixing. Each subsequent layer decreased in concentration by equal intervals such that the first and last layers were the extremes of the concentration gradient’s range. A lid was placed on the mold after the last layer had been poured to avoid evaporation.

Following a 24 hour period, the cylinders were demolded using pressurized air and labelled. The cylinders were placed in a moisture chamber to cure. This was done as curing the cylinders in water or a lime water bath will affect the concentration of chlorides or sulfates in the concrete.

3 Results and Discussion

3.1 Effect on Surface Resistivity

3.1.1 Change in Height

The effect of reducing the height of a 100 x 200 mm (4”x8”) cylinder, by continually sawing sections off the ends, on the surface resistivity measurements was studied. It is important to note that the surface resistivity device used, the Proceq Resipod, was specifically designed to be used on concrete cylinders with the standard 100 x 200 mm (4”x8”) and 150 x 300 mm (6”x12”) sizes. Concrete cylinders with a water-to-cement ratio of 0.4 and 0.6 were used in the experimentation utilizing three cylinders per water-to-cement ratio.

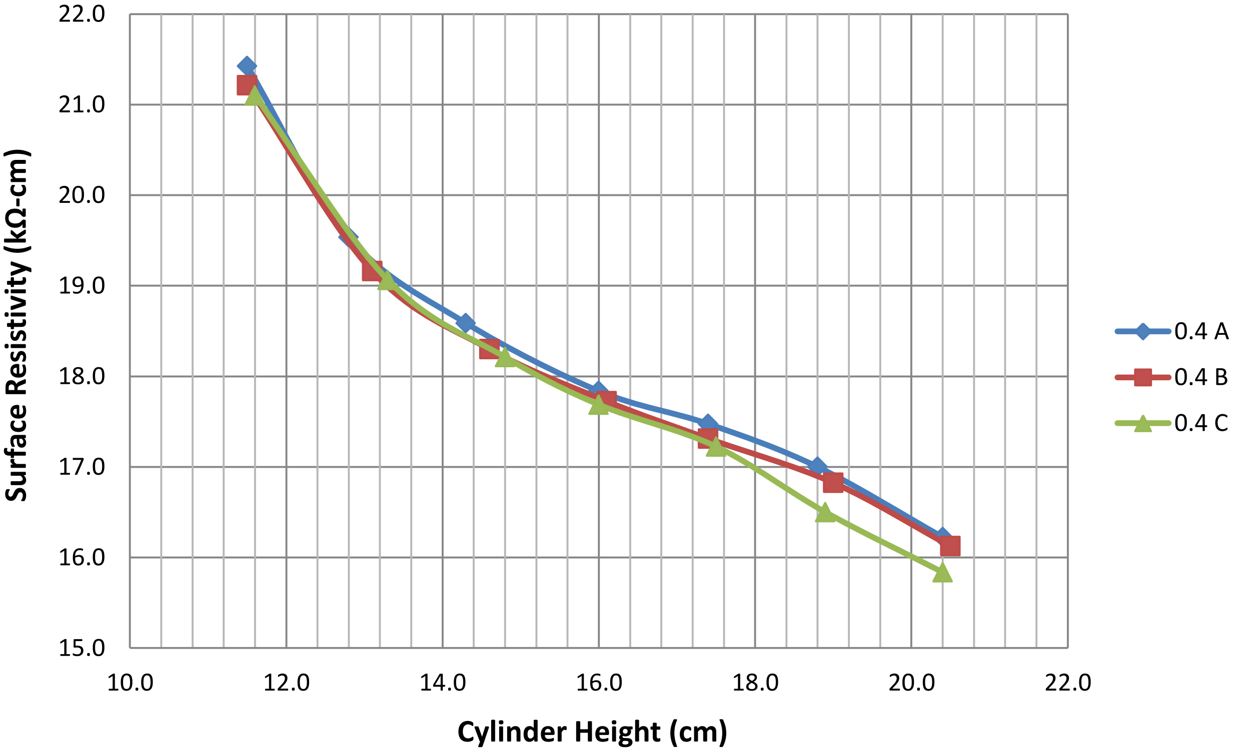

Figure 10: Change in surface resistivity as cylinder height is reduced (0.4 w/c)

Table 2: Trend-line equations and R^2 for 0.4 w/c specimens

Specimen	Trend-line Equation	Coefficient of Determination (R^2)
A	$y = -0.519x + 26.6$	0.922
B	$y = -0.505x + 26.2$	0.919
C	$y = -0.547x + 26.7$	0.945

For concrete cylinders having a water-to-cement ratio of 0.4, the surface resistivity increased as the cylinder height decreased (Figure 10). Specimens A, B and C experienced an increase in surface resistivity of 32.0%, 31.6% and 33.2% respectively as the height was reduced from approximately 20.4 to 11.5 cm. The rates at which the surface resistivity of Specimens A, B and C increased were 0.519, 0.505 and 0.547 kΩ·cm/cm respectively (Table 2).

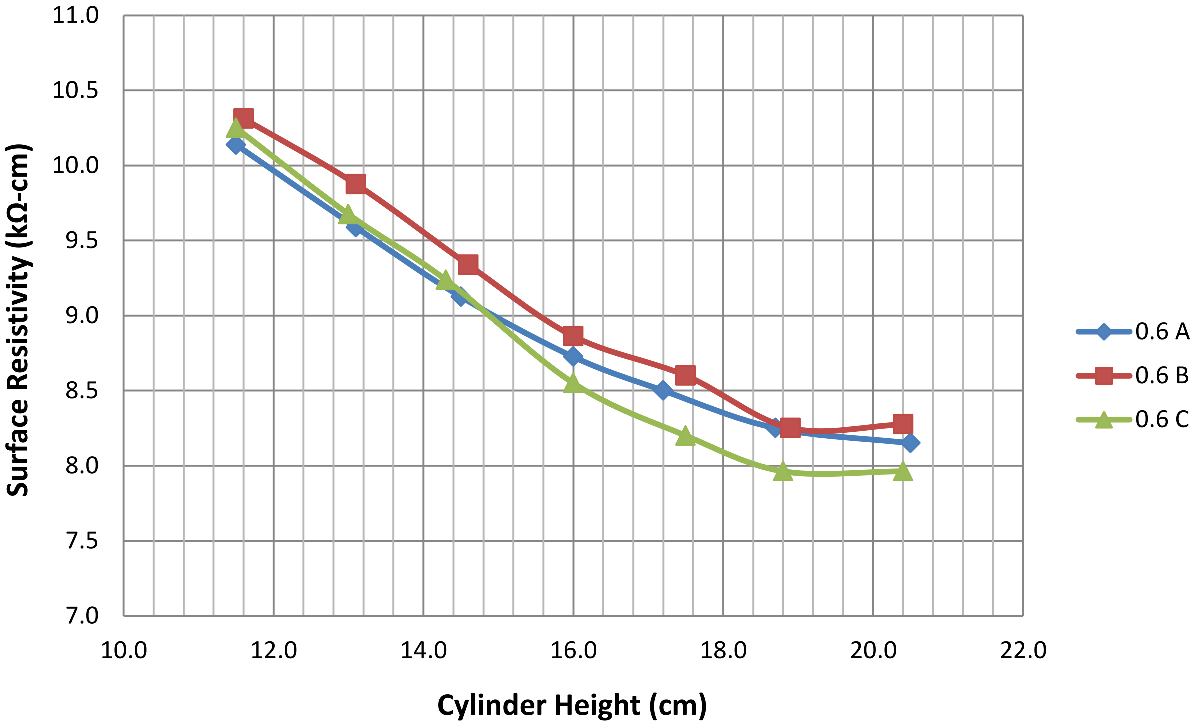

Figure 11: Change in surface resistivity as cylinder height is reduced (0.6 w/c)

Table 3: Trend-line equations and R^2 for 0.6 w/c specimens

Specimen	Trend-line Equation	Coefficient of Determination (R^2)
A	$y = -0.226x + 12.5$	0.944
B	$y = -0.247x + 13.0$	0.951
C	$y = -0.273x + 13.2$	0.941

Similarly, for concrete cylinders having a water-to-cement ratio of 0.6, the surface resistivity measured increased as the cylinder height decreased (Figure 11). The percentage increase in surface resistivity experienced by specimens A, B and C were 24.4%, 24.6% and 28.7% respectively as the height was reduced from approximately 20.4 to 11.5 cm. The rates at which the surface resistivity of specimens A, B and C increased were 0.226, 0.247 and 0.273 kΩ·cm/cm respectively (Table 3).

As shown in both Figure 10 and Figure 11, the rate of increase in surface resistivity was initially gradual but increased quickly as it approached the final height of 11.5 cm. Reducing the height of the cylinder decreases its volume and brings the edge of the cylinder closer to the outer probes of the surface resistivity device. As discussed in Section 1.2.2.2, both of these factors concentrate the current density formed by the device causing the resistivity measurement to be overestimated.

3.1.2 Water to Cement Ratio

To study the effect water-to-cement ratio has on surface resistivity, data from several different experiments performed for the purpose of this thesis were used. Data from the “Change in Height” experiment (Section 3.1.1), when the specimens were at their full length, was used for water-to-cement ratios 0.4 and 0.6. While data from the “Increasing Chloride/Sulfate Concentration” (Sections 3.1.3 and 3.1.4) when the specimens had 0 ppm or 0% concentration were used for water-to-cement ratios 0.4, 0.5 and 0.6 (Table 4).

Table 4: Surface resistivity at different w/c

W/C	Average Surface Resistivity (kΩ-cm)	From test
0.4	16.1	3.1.1 Change in Height
	16.6	3.1.3 Increasing Chloride Concentration
	16.5	3.1.4 Increasing Sulfate Concentration
0.5	11.1	3.1.3 Increasing Chloride Concentration
	11.1	3.1.4 Increasing Sulfate Concentration
0.6	8.1	3.1.1 Change in Height
	8.6	3.1.3 Increasing Chloride Concentration
	8.6	3.1.4 Increasing Sulfate Concentration

For the same water-to-cement ratio the highest differential in average surface resistivity was 0.5 kΩ-cm which is relatively low considering that the device has an error margin of ± 0.2 kΩ-cm. This indicates how accurate the surface resistivity measurements can be when factors that can cause variability are controlled.

The average surface resistivity of the concrete cylinders decreased as the water-to-cement ratio increased. An increase of water-to-cement ratio from 0.4 to 0.5 reduced average surface resistivity by 32.3%, whereas an increase of water-to-cement ratio from 0.5 to 0.6 reduced the average surface resistivity by 24.0%. A higher water-to-cement ratio will produce concrete with a higher porosity. This resulting higher porosity will allow the current to flow easier through the concrete as pore connectivity increases which will consequently lower the surface resistivity measured.

3.1.3 Increasing Chloride Concentration

The effect of increasing the chloride concentration of the concrete's mixing water on the measured surface resistivity was studied. The chloride concentrations ranged from 0 ppm to 30,000 ppm with increments of 5000 ppm. Concrete cylinders of water-to-cement ratios 0.4, 0.5 and 0.6 were used for the experimentation.

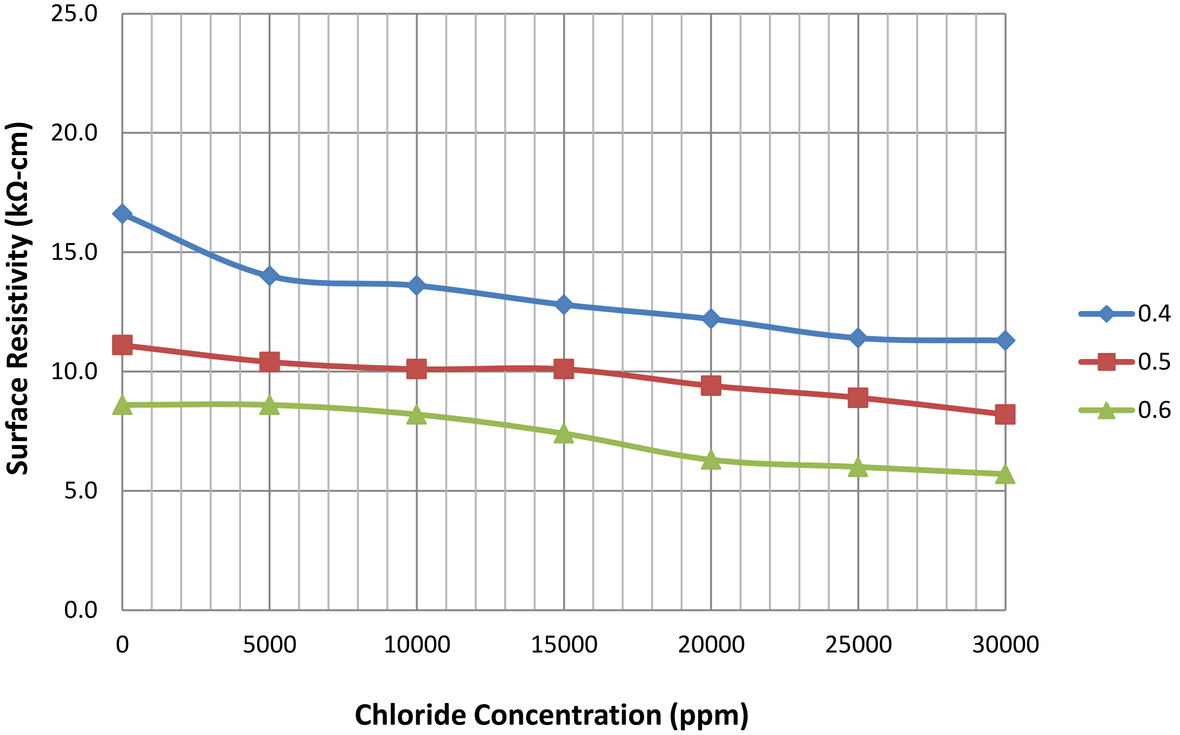

Figure 12: Change in surface resistivity with increasing chloride concentration

Table 5: Trend-line equations and R^2 for Figure 12

W/C	Trend-line Equation	Coefficient of Determination (R^2)
0.4	y = -0.000161x + 15.5	0.889
0.5	y = -0.0000886x + 11.1	0.957
0.6	y = -0.000113x + 8.95	0.945

As the chloride concentration within the concrete cylinder increased, the surface resistivity decreased. This trend was seen for all three water-to-cement ratios tested (Figure 12). An increase in chloride concentration from 0 to 30,000 ppm reduced the surface resistivity of the 0.4 water-to-cement ratio specimens from 16.6 to 11.3 kΩ-cm (31.9%), the 0.5 water-to-cement ratio specimens from 11.1 to 8.2 kΩ-cm (26.1%), and the 0.6 water-to-cement ratio specimens from 8.6 to 5.7 kΩ-cm (33.7%). The surface resistivity of the 0.4, 0.5 and 0.6 water-to-cement ratio specimens decreased at a rate of 0.805 kΩ-cm/5000 ppm, 0.443 kΩ-cm/5000 ppm, and 0.565 kΩ-cm/5000 ppm (Table 5).

The chlorides added to the concrete’s mixing water will end up, in the hardened concrete, as crystals locked up in the hydrated cement paste or as ions in the pore water solution. The resulting increase in chloride concentration of the pore water solution will improve the conduction of the current from the surface resistivity device. This improved conduction is reflected in the lower surface resistivity measured.

3.1.4 Increasing Sulfate Concentration

The effect of increasing the sulfate concentration of the concrete’s mixing water on surface resistivity was also studied. This time, the sulfate concentrations ranged from 0% to 10% by mass of the mixing water, increasing by increments of 2%. Concrete cylinders with 5% sulfate concentration were also tested as this is a concentration used by many sulfate resistance standards, such as the ASTM C1012. The specimens used for the experimentation had water-to-cement ratios of 0.4, 0.5 and 0.6.

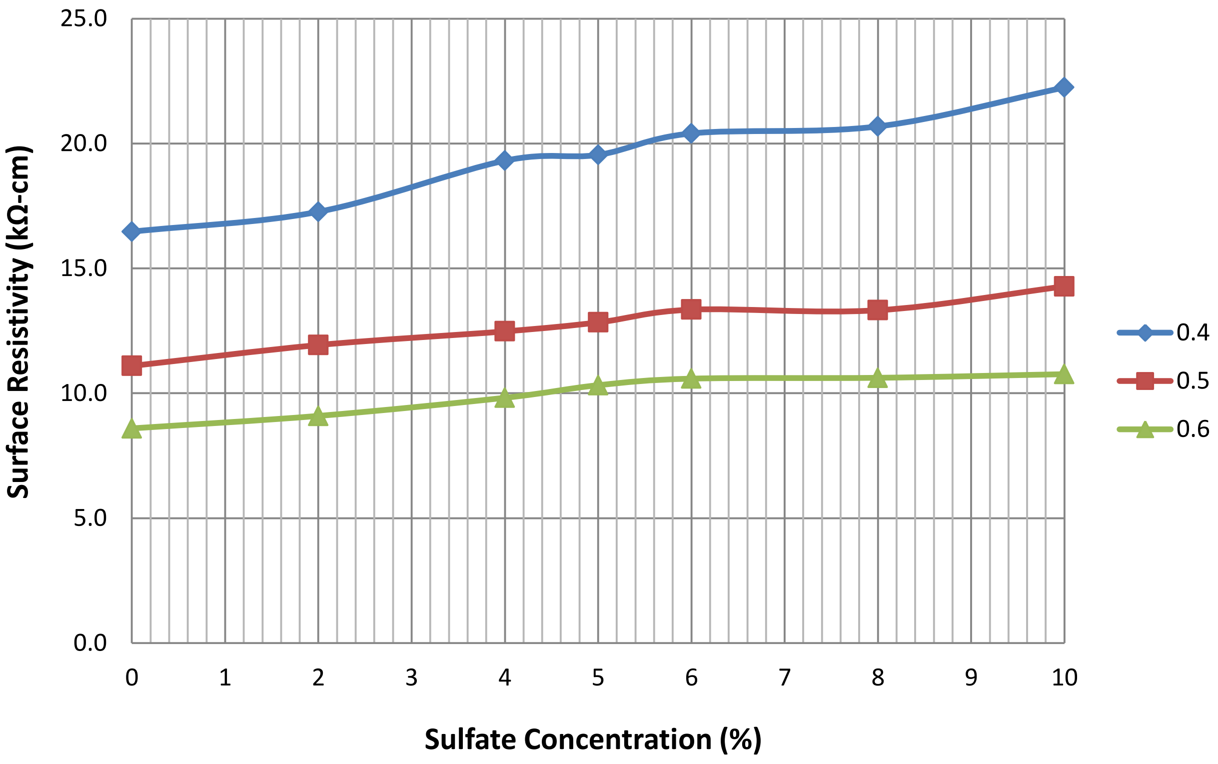

Figure 13: Change in surface resistivity with increasing sulfate concentration

Table 6: Trend-line equations and R^2 for Figure 13

W/C	Trend-line Equation	Coefficient of Determination (R^2)
0.4	$y = 0.574x + 16.5$	0.966
0.5	$y = 0.300x + 11.3$	0.964
0.6	$y = 0.231x + 8.82$	0.884

Contrary to the effect seen with chlorides, as the sulfate concentration within the concrete cylinders increased, so did the measured surface resistivity (Figure 13). Although more prominent with the 0.4 water-to-cement ratio, this trend was consistent over all three water-to-cement ratios. An increase in sulfate concentration from 0 to 10% increased the surface resistivity of the 0.4 water-to-cement ratio from 16.5 to 22.2 kΩ-cm (34.5%), the 0.5 water-to-cement ratio from 11.1 to 14.3 kΩ-cm (28.8%), and the 0.6 water-to-cement ratio from 8.6 to

10.8 kΩ-cm (25.6%). The surface resistivity of the 0.4, 0.5 and 0.6 water-to-cement ratio specimens increased at a rate of 0.574 kΩ-cm/%, 0.300 kΩ-cm/%, and 0.231 kΩ-cm/% (Table 6).

Unlike chloride ions, the sulfate ions introduced into the concrete's mixing water will cause sulfate attack as it reacts with components of the hydrated cement paste to form ettringite and gypsum. The concrete's porosity decreases as the ettringite and gypsum form within its pore spaces. In the process, calcium hydroxide is consumed followed by decalcification and disintegration of the **CSH** phase. As a result, the concentration of hydroxyl ions in the pore water solution decreases. Both of these factors play a role in the increase in surface resistivity measured.

3.1.5 Chloride Concentration Gradient

Chlorides, or a solution thereof, usually forms a concentration gradient as it penetrates exposed concrete in the field. The concentration is highest at the surface in contact with the solution and decreases with distance away from the surface. To represent that, two different chloride concentration gradients were tested to see their effect on surface resistivity. The first concentration gradient ranged from 0 – 30,000 ppm of chlorides while the second ranged from 7500 – 22,500 ppm. Three specimens per concentration gradient at a 0.5 water-to-cement ratio were utilized during testing.

Table 7: Average surface resistivity for two different chloride concentration gradients.

0 - 30,000 ppm			7500 - 22,500 ppm		
Specimen	Average Surface Resistivity (kΩ·cm)		Specimen	Average Surface Resistivity (kΩ·cm)	
A	9.2	9.2	A	9.3	9.2
B	9.4		B	9.0	
C	9.0		C	9.3	

The surface resistivity of both concentration gradients, averaged over three specimens, was equivalent at 9.2 kΩ·cm (Table 7). When compared to the average surface resistivity of the constant concentration samples at the same water-to-cement ratio of 0.5, it would be similar to having 20,000 ppm of chlorides in the concrete's mixing water which was shown to have an average surface resistivity of 9.4 kΩ·cm.

Upon further inspection, it would seem as though the surface resistivity is more influenced by the quantity of chlorides present in the cylinder than the concentration gradient it forms. For the 0 – 30,000 ppm concentration gradient, the mass of chlorides present per cylinder was 8.86 g, while for the 7500 – 22,500 ppm gradient the mass of chlorides per cylinder was 9.02 g. When compared again to the constant concentration samples at the same water-to-cement ratio, it would be close to the 11.24 g of chlorides present in the 20,000 ppm specimens but closer to the 15,000 ppm specimens which contained 8.43 g of chlorides. However, the average surface resistivity of the 15,000 ppm specimens was 10.1 kΩ·cm, which was higher than that of the 20,000 ppm specimens and both the chloride concentration gradients.

As shown above, surface resistivity can be used as a rough estimate of the quantity of chlorides present in a 100 x 200 mm (4" x 8") cylinder. With a larger data sample and further experimentation, the results could be refined which would lead to a more accurate estimation.

3.1.6 Sulfate Concentration Gradient

A concrete member in the field that is in contact with soil or water contaminated with sulfates usually develops a concentration gradient of sulfates as they penetrate inward. The concrete's surface in contact with the soil or water will have the highest concentration of sulfates, but then the concentration decreases with distance away from the surface. Similar to the experimentation done with the chlorides, 2 different concentration gradients were investigated. The first concentration gradient ranged from 0 – 10%, while the second ranged from 2.5 – 7.5%. For each concentration gradient, three specimens were prepared as per the standard.

Table 8: Average surface resistivity for two different sulfate concentration gradients.

0 – 10%			2.5 – 7.5%		
Specimen	Average Surface Resistivity (kΩ·cm)		Specimen	Average Surface Resistivity (kΩ·cm)	
A	11.0	11.4	A	12.3	12.2
B	11.6		B	12.2	
C	11.6		C	12.4	

For the sulfate concentration gradient of 0 – 10%, the average surface resistivity of the three specimens was 11.4 kΩ·cm (Table 8). When the average surface resistivity of the 0 – 10% concentration gradient was compared to that of the constant concentration samples at the same water-to-cement ratio of 0.5, it fell almost halfway between the 11.1 kΩ·cm average surface resistivity of the 0% specimens and he 11.9 kΩ·cm average surface resistivity of the 2% specimens. On the other hand, the 2.5 – 7.5% sulfate concentration gradient had an average surface resistivity of 12.2 kΩ·cm (Table 8). Comparing this value with the constant concentration samples, the average surface resistivity of the 2.5 – 7.5% concentration gradient fell halfway between the 2% and 4% specimens, which had an average surface resistivity of 11.9 kΩ·cm and 12.5 kΩ·cm, respectively.

Unlike what was seen with the chloride concentration gradient, there did not seem to be a connection between the quantity of sulfates present per cylinder in the concentration gradient specimens and the average surface resistivity of the constant concentration specimens. The 0 – 10% concentration gradient specimens had 17.92 g of sulfates per cylinder while the 2.5 – 7.5% specimens had 18.24 g of sulfates. Comparing that to the 0.5 water-to-cement ratio constant concentration specimens for which the average surface resistivity of both concentration gradients fell between, the 0%, 2%, and 4% had 0 g, 6.82 g, and 13.64 g of sulfates per cylinder, respectively. While chloride ions do not affect the concrete, sulfate ions cause sulfate attack as they react with components of the hydrated cement paste to form ettringite and gypsum. This could explain why, unlike the chlorides, no obvious connection existed between the quantity of sulfates and the average surface resistivity measured.

3.2 Effect on Bulk Resistivity

3.2.1 Water to Cement Ratio

In order to study the effect of water-to-cement ratio on bulk resistivity, data from several different experiments previously discussed in this thesis were utilized. Specifically, the chloride and sulfate constant concentration data from Sections 3.2.2 and 3.2.3 for all three water-to-cement ratios where the specimens had 0 ppm or 0% concentration were evaluated.

Table 9: Bulk resistivity at different w/c.

W/C	Bulk Resistivity (kΩ-cm)	From test
0.4	9.64	3.2.2 Increasing Chloride Concentration
	9.56	3.2.3 Increasing Sulfate Concentration
0.5	7.90	3.2.2 Increasing Chloride Concentration
	7.69	3.2.3 Increasing Sulfate Concentration
0.6	6.95	3.2.2 Increasing Chloride Concentration
	6.83	3.2.3 Increasing Sulfate Concentration

As shown in Table 9, the bulk resistivity decreased as the water-to-cement ratio of the concrete cylinders increased, which is similar to the effect water-to-cement ratio had on surface resistivity. Increasing the water-to-cement ratio of concrete from 0.4 to 0.5 reduced the average bulk resistivity by 18.8%, whereas an increase in water-to-cement ratio from 0.5 to 0.6 reduced the average bulk resistivity by 11.6%. The largest differential between measurements of bulk resistivity was 0.21 kΩ·cm. When compared to the results of surface resistivity (Section 3.1.2), which had 0.5 kΩ·cm as the largest differential, it seems that bulk resistivity measurements were more accurate.

The porosity of concrete is affected by the design water-to-cement ratio. As water-to-cement ratio increases, so does the concrete's porosity and the pore's interconnectivity. The electrical current from the bulk resistivity device travels through the ionic pore water solution through the interconnected pores of the concrete cylinder from one electrode to the other. Therefore, a higher porosity will allow the current to flow through the concrete cylinder with more ease, lowering the bulk resistivity measured.

3.2.2 Increasing Chloride Concentration

The effect of increasing chloride concentration on the measured bulk resistivity was studied. The standard 100 x 200 mm (4” x 8”) concrete cylinders were cast with increasing chloride concentrations in the mixing water. Three cylinders were utilized per concentration for repeatability. The chloride concentration of the mixing water ranged from 0 to 30,000 ppm, increasing at increments of 5,000 ppm. The chlorides were added to the mixing water to achieve a constant concentration throughout the concrete cylinder.

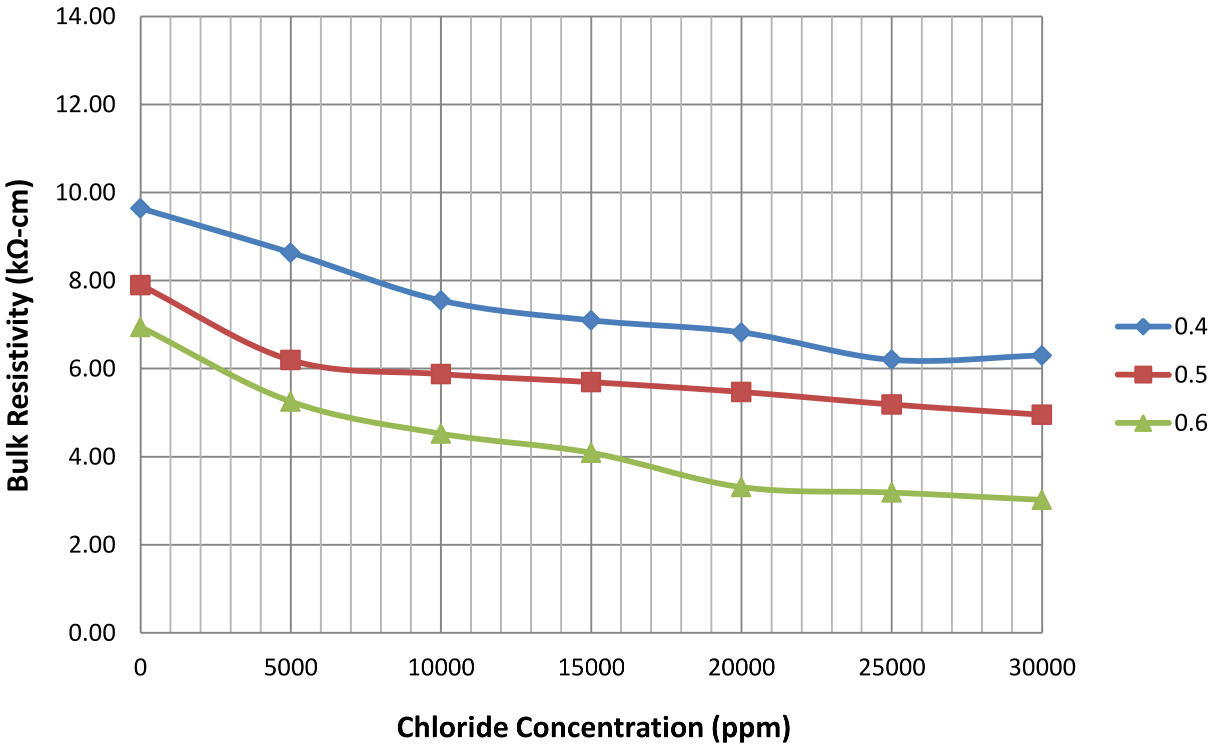

Figure 14: Change in bulk resistivity with increasing chloride concentration

Table 10: Trend-line equations and R^2 for Figure 14

W/C	Trend-line Equation	Coefficient of Determination (R^2)
0.4	$y = -0.000112x + 9.14$	0.906
0.5	$y = -0.0000804x + 7.10$	0.792
0.6	$y = -0.000122x + 6.17$	0.883

Regardless of the water-to-cement ratio, the measured bulk resistivity decreased as the chloride concentration within the concrete cylinder increased (Figure 14). As the chloride concentration increased from 0 to 30,000 ppm, the bulk resistivity of the 0.4 water-to-cement ratio specimens decreased from 9.64 to 6.30 kΩ·cm (34.7%), the 0.5 water-to-cement ratio specimens from 7.90 to 4.95 kΩ·cm (37.3%), and the 0.6 water-to-cement ratio specimens from 6.95 to 3.02 kΩ·cm (56.6%). The bulk resistivity of the 0.4, 0.5 and 0.6 water-to-cement ratio specimens decreased at a rate of 0.560 kΩ-cm/5000 ppm, 0.402 kΩ-cm/5000 ppm, and 0.610 kΩ-cm/5000 ppm, respectively (Table 10).

Chlorides have no known reaction with components of the hydrated cement paste. The chlorides that were added to the mixing water remain within the concrete cylinder as crystals trapped in the hydrated cement paste or dissolved as ions in the pore water solution. Increasing the chloride concentration of the mixing water will inevitably increase the chloride concentration of the concrete's pore water solution. A higher concentration of chloride ions in the pore water solution will improve the conduction of electrical current from the bulk resistivity device's electrodes, and consequently lower the bulk resistivity measured.

3.2.3 Increasing Sulfate Concentration

To study the effect of sulfates on the bulk resistivity measured, concrete cylinders were cast with increasing concentrations of sulfates in their mixing water. The sulfate concentration ranged from 0 to 10% by mass, increasing in increments of 2%. The halfway 5% sulfate concentration was also included in the testing. Three cylinders were utilized per concentration. The effect was studied across water-to-cement ratios of 0.4, 0.5, and 0.6 to cover the range typically used in the field.

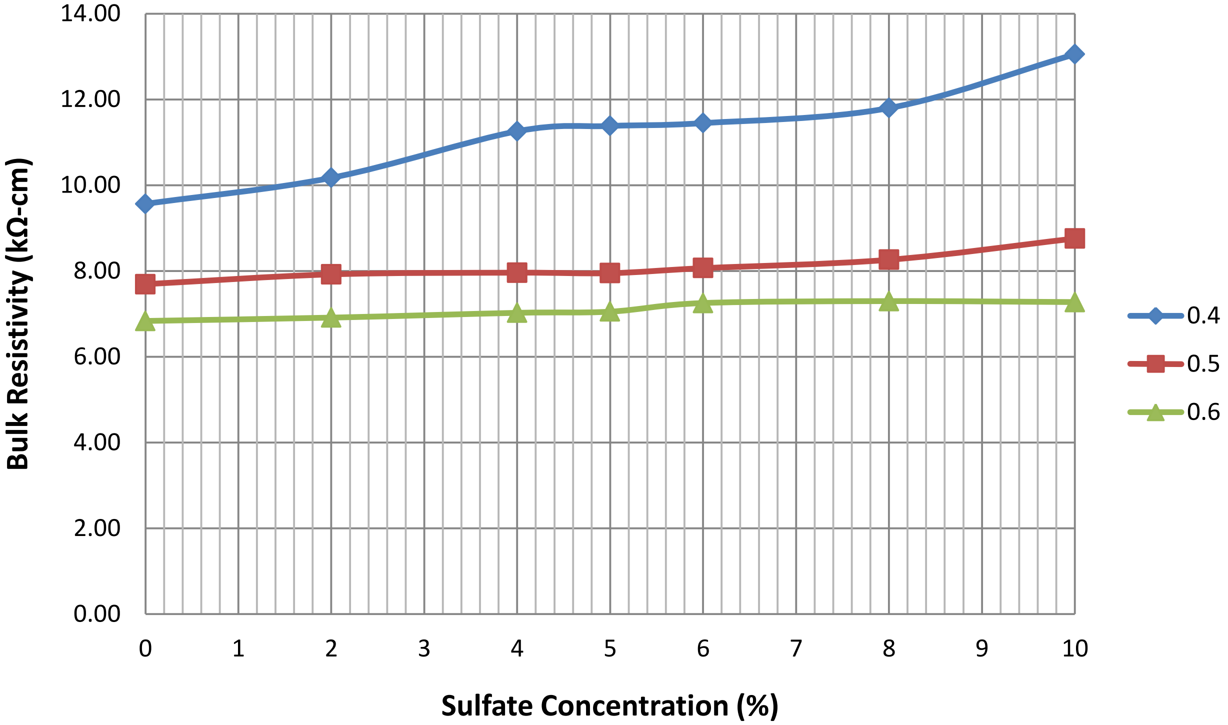

Figure 15: Change in bulk resistivity with increasing sulfate concentration

Table 11: Trend-line equations and R^2 for Figure 15

W/C	Trend-line Equation	Coefficient of Determination (R^2)
0.4	$y = 0.322x + 9.63$	0.951
0.5	$y = 0.0921x + 7.63$	0.851
0.6	$y = 0.0512x + 6.84$	0.891

As shown in Figure 15, the measured bulk resistivity increased as the sulfate concentration increased, which is similar to the effect sulfate concentration had on the surface resistivity. Although more prominent with the 0.4 water-to-cement ratio, this trend is seen for all three water-to-cement ratios. An increase in sulfate concentration from 0 to 10% increased the bulk resistivity of the 0.4 water-to-cement ratio from 9.56 to 13.05 kΩ-cm (36.5%), the 0.5 water-to-cement ratio from 7.69 to 8.76 kΩ-cm (13.8%), and the 0.6 water-to-cement ratio from 6.83 to

7.27 kΩ-cm (6.44%). The bulk resistivity of the 0.4, 0.5 and 0.6 water-to-cement ratio specimens increased at a rate of 0.322 kΩ-cm/%, 0.0921 kΩ-cm/%, and 0.0512 kΩ-cm/% (Table 11).

In the presence of sulfate ions, concrete undergoes sulfate attack where the sulfate ions react with calcium hydroxide and **C-S-H** in the hydrated cement paste to form ettringite and gypsum. Increasing the concentration of sulfates in the mixing water will increase the amounts of ettringite and gypsum formed. During the initial stages of sulfate attack, ettringite and gypsum form in the empty pore spaces, lowering the concrete's porosity and temporarily increasing its compressive strength. Lowering concrete's porosity will also increase the measured bulk resistivity since the electrical current must flow through the ionic solution of the interconnected pores. The calcium required for the sulfate attack reaction is obtained from the calcium hydroxide in the hydrated cement paste, and once that has been depleted then decalcification of the C-S-H phase begins. This leads to a substantial decrease in calcium cations available in the pore water solution which consequently lowers the electrical conductivity of the concrete. The lower conductivity is reflected in the higher bulk resistivity measured.

3.2.4 Chloride Concentration Gradient

When chlorides contaminate concrete structures in the field, they usually form a concentration gradient. A concentration gradient forms with the surface in contact having the highest concentration, which then decreases with depth as the chlorides penetrate inward. In order to see the effect a chloride concentration gradient has on the bulk resistivity, two different gradients were studied: 0 – 30,000 ppm and 7,500 – 22,500 ppm. Three concrete cylinders were utilized per concentration gradient all of which had a water-to-cement ratio of 0.5.

Table 12: Average bulk resistivity for two different chloride concentration gradients

0 - 30,000 ppm			7,500 - 22,500 ppm		
Specimen	Bulk Resistivity (kΩ·cm)	Average Bulk Resistivity (kΩ·cm)	Specimen	Bulk Resistivity (kΩ·cm)	Average Bulk Resistivity (kΩ·cm)
A	7.87	7.52	A	4.88	4.87
B	7.05		B	4.88	
C	7.64		C	4.85	

Although the results for surface resistivity of both chloride concentration gradients were equal at 9.2 kΩ·cm, the results for bulk resistivity were not. The average bulk resistivity of the 0 – 30,000 ppm concentration gradient was 7.52 kΩ·cm, while that of the 7,500 – 22,500 ppm was lower at 4.87 kΩ·cm (Table 12). When compared to the bulk resistivity results of the constant concentration samples at the same water-to-cement ratio of 0.5, the 0 – 30,000 ppm concentration gradient fell between the 0 and 5,000 ppm specimens having a bulk resistivity of 7.90 and 6.19 kΩ·cm respectively, while the 7,500 – 22,500 ppm concentration gradient had a bulk resistivity that was lower than the 4.95 kΩ·cm of the 30,000 ppm specimens. The relationship between the quantity of chlorides and the measured surface resistivity did not seem to apply to the bulk resistivity. The 0 – 30,000 ppm specimens each contained 8.86 g of chlorides, while the 7,500 – 22,500 ppm specimens contained 9.02 g. Although they contained similar quantities of chlorides, their respective bulk resistivities were on opposite ends of the range attained by the constant concentration specimens.

3.2.5 Sulfate Concentration Gradient

The effect that a sulfate concentration gradient has on the bulk resistivity was studied. This was done to mimic what is typically encountered in the field. The surface of a concrete member in contact with a source of sulfates will have the highest concentration, which then decreases with depth as the sulfates slowly penetrate inward. The two sulfate concentration gradients studied were 0 – 10% and 2.5 – 7.5%. Each concentration gradient utilized three specimens at a water-to-cement ratio of 0.5.

Table 13: Average bulk resistivity for two different sulfate concentration gradients

0 – 10%			2.5 – 7.5%		
Specimen	Bulk Resistivity (kΩ·cm)	Average Bulk Resistivity (kΩ·cm)	Specimen	Bulk Resistivity (kΩ·cm)	Average Bulk Resistivity (kΩ·cm)
A	6.35	6.39	A	6.85	6.73
B	6.27		B	6.65	
C	6.57		C	6.70	

As shown in Table 13, the average bulk resistivity of both sulfate concentration gradients were similar, where the 0 – 10% gradient had an average bulk resistivity of 6.39 kΩ·cm, while the 2.5 – 7.5% gradient had an average bulk resistivity of 6.73 kΩ·cm. When compared to the bulk resistivity of the constant concentration specimens at the same water-to-cement ratio of 0.5, the bulk resistivity of both concentration gradients fell below the 0% specimen's average bulk resistivity of 7.69 kΩ·cm.

3.3 Effect on Surface Resistivity of Split Faces

The results of this section should not be compared to that of surface resistivity performed on the concrete cylinders as a whole outlined in Section 3.1. This is due to the surface resistivity being performed on samples with different geometries. The concrete cylinders were tested under splitting tension to obtain the two halves on which the inner surface resistivity was measured.

3.3.1 Water to Cement Ratio

The effect of water-to-cement ratio on the surface resistivity of the split faces of a concrete cylinder was studied. For that, data for all three water-to-cement ratios of the chloride and sulfate constant concentration specimens where the concentration was 0 ppm or 0% were used.

Table 14: Surface resistivity of split faces at different w/c

W/C	Surface Resistivity of Split Faces (kΩ-cm)	From test
0.4	23.0	3.3.2 Increasing Chloride Concentration
	22.8	3.3.3 Increasing Sulfate Concentration
0.5	15.2	3.3.2 Increasing Chloride Concentration
	15.0	3.3.3 Increasing Sulfate Concentration
0.6	12.6	3.3.2 Increasing Chloride Concentration
	13.2	3.3.3 Increasing Sulfate Concentration

As shown in Table 14, the surface resistivity of the split faces decreased as the water-to-cement ratio of the concrete cylinder increased. This trend was seen in the surface resistivity data of the whole cylinder as well as the bulk resistivity. Increasing the water-to-cement ratio of concrete from 0.4 to 0.5 reduced the average surface resistivity of the split faces by 34.1%, whereas an increase in water-to-cement ratio from 0.5 to 0.6 reduced the average surface resistivity of the split faces by 13.6%.

The porosity of concrete is related to the water-to-cement ratio chosen during mixture design. Increasing the water-to-cement ratio will consequently increase the number of pores as well the interconnectivity of the pores. The electrical current from the surface resistivity device travels through the ionic pore water solution contained within the interconnected pores. The higher the porosity, the easier the current travels through the concrete's pore network and the lower the measured electrical resistivity.

3.3.2 Increasing Chloride Concentration

The effect of increasing chloride concentration on the surface resistivity of the split faces was studied. To achieve a constant concentration, concrete cylinders were cast with increasing concentration of chlorides in their mixing water. The chloride concentration of the mixing water ranged from 0 to 30,000 ppm increasing in increments of 5,000 ppm. Three cylinders were utilized per concentration. Water-to-cement ratios of 0.4, 0.6 and 0.6 were included in the study to cover the typical range used in construction.

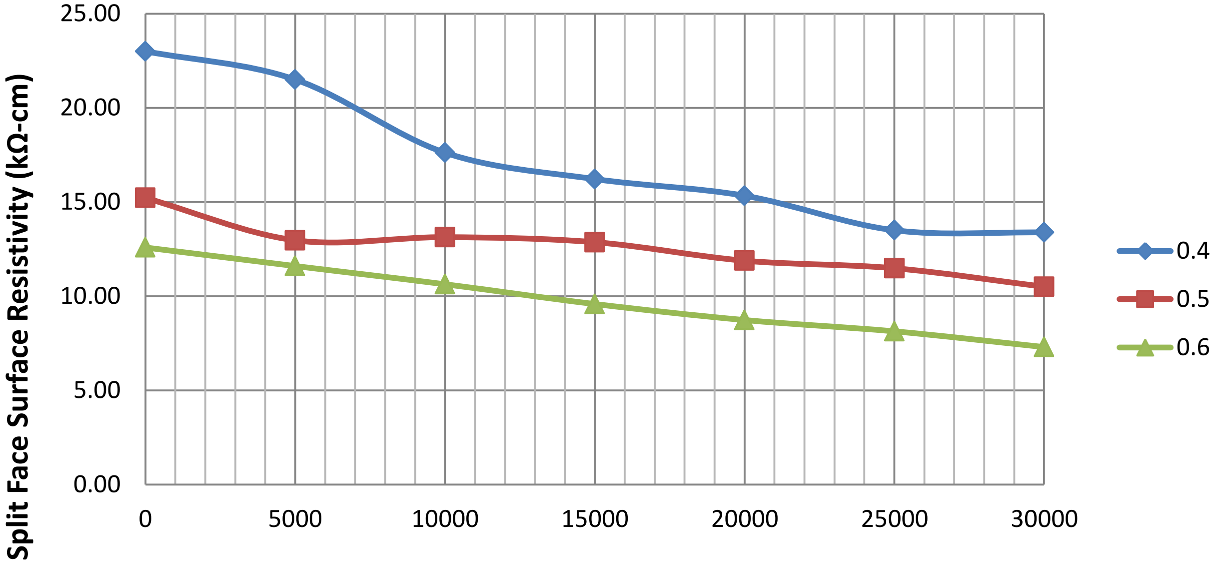

Figure 16: Change in surface resistivity of split faces with increasing chloride concentration

Table 15: Trend-line equations and R^2 for Figure 16

W/C	Trend-line Equation	Coefficient of Determination (R^2)
0.4	y = -0.000337x + 22.3	0.933
0.5	y = -0.000131x + 14.5	0.892
0.6	y = -0.000176x + 12.4	0.993

The surface resistivity of the split faces decreased as the chloride concentration of the mixing water increased (Figure 16). This trend was also seen in the surface resistivity of the whole cylinder (Section 3.1.3) as well as in the bulk resistivity (Section 3.2.2). As the chloride concentration increased from 0 to 30,000 ppm, the surface resistivity of the split faces of the 0.4 water-to-cement ratio specimens decreased from 16.6 to 11.3 kΩ·cm (31.9%), the 0.5 water-to-cement ratio specimens from 11.1 to 8.2 kΩ·cm (26.1%), and the 0.6 water-to-cement ratio specimens from 8.6 to 5.7 kΩ·cm (33.7%). The split face surface resistivity of the 0.4, 0.5 and 0.6 water-to-cement ratio specimens decreased at rates of 1.69 kΩ-cm/5000 ppm, 0.655 kΩ-cm/5000 ppm, and 0.880 kΩ-cm/5000 ppm, respectively (Table 15).

Increasing the chloride concentration of the mixing water will increase the concentration of chlorides present in the pore water solution. Since the electrical current from the surface resistivity device travels through the ionic pore water solution, increasing the concentration of chlorides in the pore water solution will improve the conduction of current. The improved electrical conduction is reflected in the lower surface resistivity measured, as these properties have an inversely proportional relationship.

3.3.3 Increasing Sulfate Concentration

The effect of increasing the sulfate concentration on the measured surface resistivity of the split faces was studied. Concrete cylinders were cast with increasing concentration of sulfates in their mixing water to achieve a constant concentration throughout. Three cylinders were cast per concentration. The sulfate concentration of the mixing water ranged from 0 to 10% by weight, increasing in increments of 2%. The halfway concentration of 5% was also included. The experiment was performed on concrete with a water-to-cement ratio of 0.4, 0.5 and 0.6.

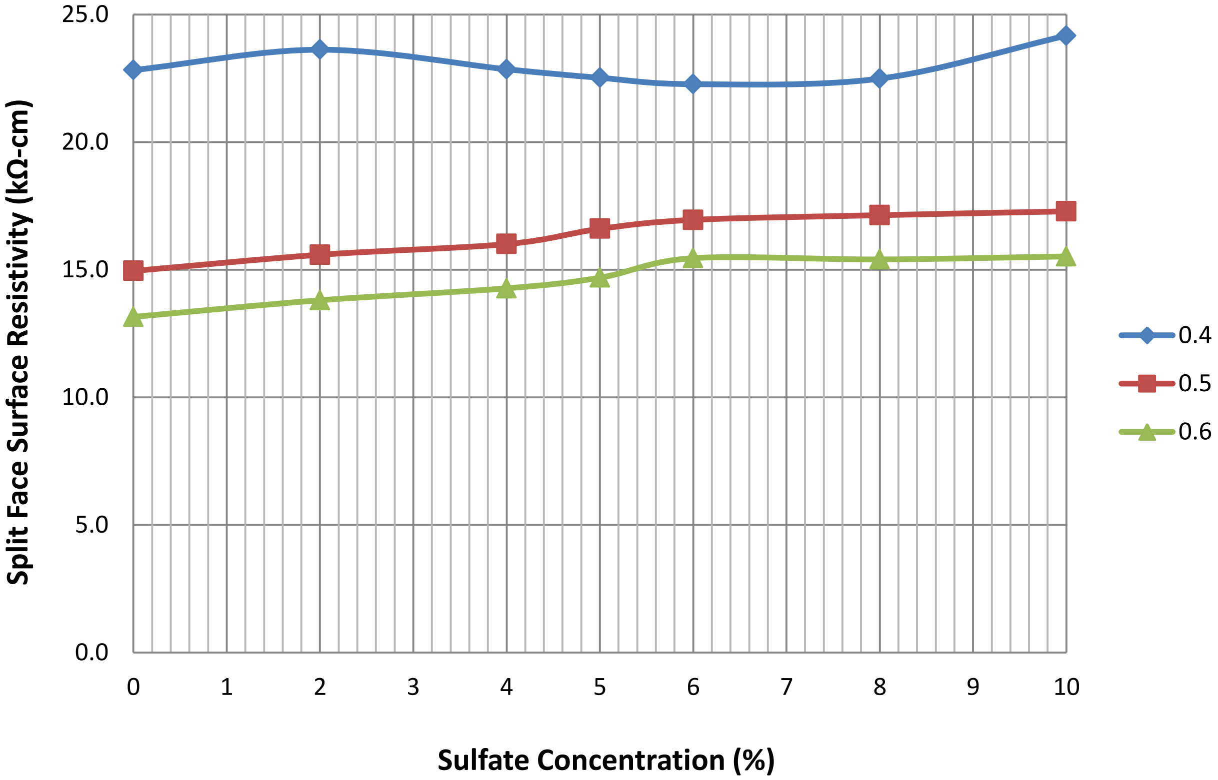

Figure 17: Change in surface resistivity of split faces with increasing sulfate concentration

Table 16: Trend-line equations and R^2 for Figure 17

W/C	Trend-line Equation	Coefficient of Determination (R^2)
0.4	$y = 0.0395x + 22.8$	0.0387
0.5	$y = 0.247x + 15.1$	0.931
0.6	$y = 0.255x + 13.3$	0.896

Increasing the sulfate concentration of the mixing water had a similar effect on the surface resistivity of the split faces as it did with the surface resistivity of the whole cylinder and bulk resistivity. The surface resistivity of the split faces increased as the concentration of the sulfates increased (Figure 17). An increase in sulfate concentration from 0 to 10% increased the surface resistivity of the split faces of the 0.4 water-to-cement ratio from 22.8 to 24.2 kΩ-cm (5.92%), the 0.5 water-to-cement ratio from 15.0 to 17.3 kΩ-cm (15.6%), and the 0.6 water-to-cement ratio from 13.2 to 15.5 kΩ-cm (18.0%). The surface resistivity of the split faces for the 0.5 and 0.6 water-to-cement ratio specimens increased at a rate of 0.247 kΩ-cm/% and 0.255 kΩ-cm/%, respectively (Table 16). The rate for the 0.4 water-to-cement ratio specimens was not representative as the coefficient of determination was extremely low.

Sulfate ions cause sulfate attack in concrete as they react with components of the hydrated cement paste, specifically calcium hydroxide and **C-S-H**, to form ettringite and gypsum. In the chemical reactions of sulfate attack, calcium cations are consumed from the calcium hydroxide until it is depleted, then decalcification of the **C-S-H** phase occurs. Reducing the concentration of calcium in the pore water solution will impede the flow of electrical current through the concrete sample lowering the surface resistivity of the split faces. In addition, the ettringite and gypsum that form as a byproduct of the sulfate attack reactions fill the empty pore spaces, thus reducing the concrete’s porosity. Since the current flows through the pore network, a decrease in porosity will also impede the flow of current, lowering the surface resistivity of the split faces.

3.3.4 Chloride Concentration Gradient

The effect a chloride concentration gradient has on the surface resistivity of the split faces of a concrete cylinder was studied. This was done to replicate the condition of chloride contaminated concrete in the field. The concrete surface in contact with the source of chlorides will have the highest concentration, equal to that of the source, which decreases with depth as the chlorides slowly penetrate within. The first concentration gradient studied ranged from 0 – 30,000 ppm while the other ranged from 7,500 – 22,500 ppm. Three cylinders were utilized per concentration gradient, all at a water-to-cement ratio of 0.5.

Table 17: Average surface resistivity of split faces for two different chloride concentration gradients.

0 - 30,000 ppm			7,500 - 22,500 ppm		
Specimen	Split Face Surface Resistivity (kΩ·cm)	Average Split Face Surface Resistivity (kΩ·cm)	Specimen	Split Face Surface Resistivity (kΩ·cm)	Average Split Face Surface Resistivity (kΩ·cm)
A	10.8	11.2	A	8.5	9.8
B	10.7		B	11.5	
C	12.2		C	9.6	

Although the results for the surface resistivity of the whole cylinder for both concentration gradients were equal, the surface resistivity of the split faces were not. For the 0 – 30,000 ppm gradient the average surface resistivity of the split faces was 11.2 kΩ·cm while for the 7,500 – 22,500 ppm gradient it was 9.8 kΩ·cm (Table 17).

3.3.5 Sulfate Concentration Gradient

The effect a sulfate concentration gradient has on the surface resistivity of the split faces of a concrete cylinder was also studied. When soil or water containing sulfate ions contaminate concrete, it forms a concentration gradient as it slowly penetrates inwards. The highest concentration will be found at the surface in contact with the source of sulfates and then decrease with distance away from the surface. The first concentration gradient studied ranged from 0 – 10% while the second ranged from 2.5 – 7.5%. Three cylinders were utilized per concentration gradient with a water-to-cement ratio of 0.5.

Table 18: Average surface resistivity of split faces for two different sulfate concentration gradients.

0 – 10%			2.5 – 7.5%		
Specimen	Split Face Surface Resistivity (kΩ·cm)	Average Split Face Surface Resistivity (kΩ·cm)	Specimen	Split Face Surface Resistivity (kΩ·cm)	Average Split Face Surface Resistivity (kΩ·cm)
A	13.9	14.2	A	14.1	14.1
B	14.4		B	14.3	
C	14.4		C	14.1	

The average surface resistivity of the split faces for both concentration gradients were similar, where the 0 – 10% gradient had an average surface resistivity of 14.2 kΩ·cm, while the 2.5 – 7.5% gradient had an average surface resistivity of 14.1 kΩ·cm (Table 18). Both sulfate concentration gradients seem to have the same effect on the electrical resistivity of concrete. The surface resistivity of the whole cylinder had a differential of 0.80 kΩ·cm between the two gradients and the bulk resistivity had a differential of 0.34 kΩ·cm.

3.4 Splitting Tension

Splitting tensile strength testing indirectly determines the tensile strength of a concrete cylinder. A compression load is applied along the length of the cylinder until the concrete cylinder fails by splitting along the vertical axis. The concrete cylinder fails in indirect tension which acts along the horizontal axis due to the Poisson effect. Tensile loading in concrete is more sensitive to flaws and cracks than compression loading. Splitting tensile strength testing was done in accordance with the ASTM C 496 standard.

3.4.1 Chloride Specimens

3.4.1.1 Constant Concentration

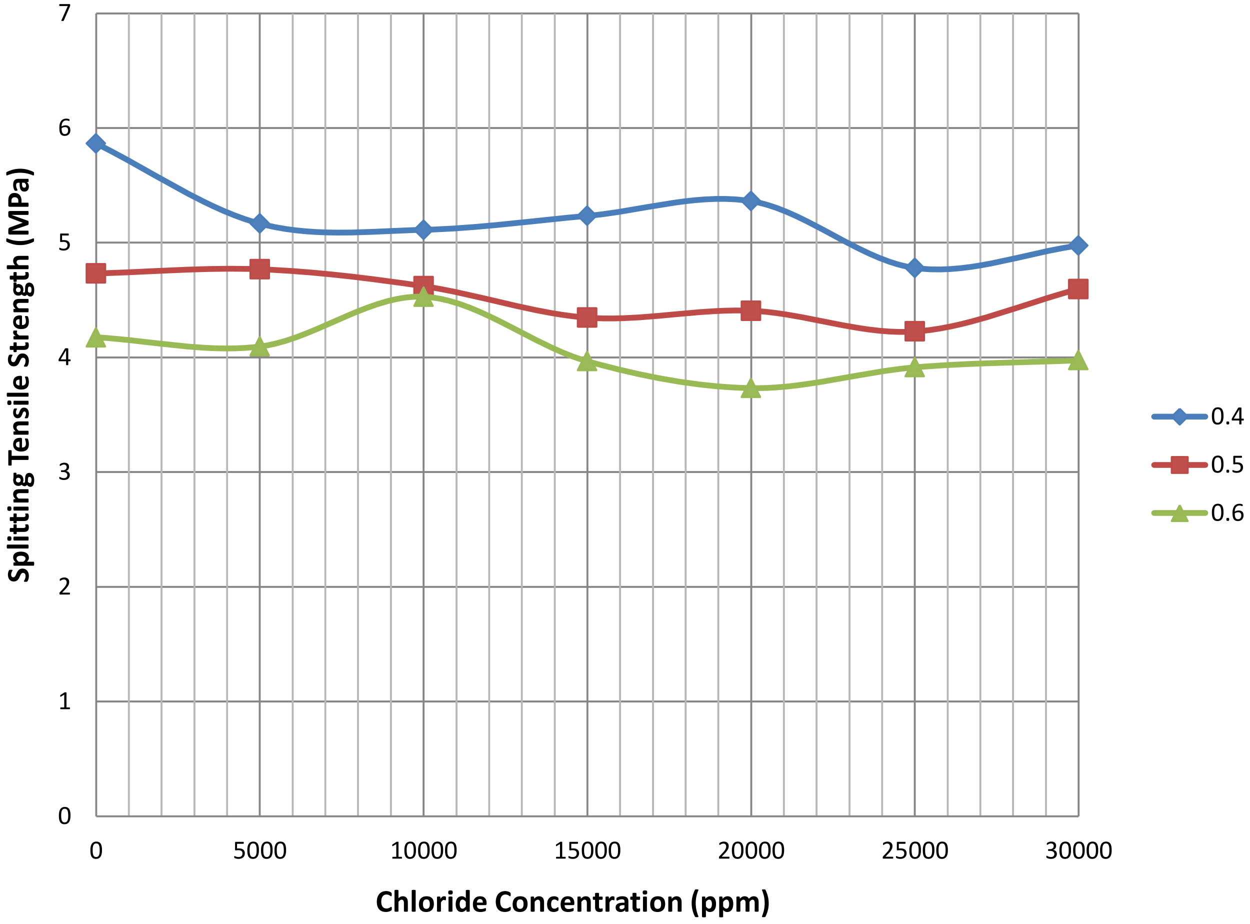

Figure 18: Change in splitting tensile strength with increasing chloride concentration

Increasing the chloride concentration within the concrete specimens seemed to decrease its splitting tensile strength slightly (Figure 18). The within-batch coefficient of variation was 6.57% for the 0.4 water-to-cement ratio specimens, 4.52% for the 0.5 water-to-cement ratio specimens, and 6.20% for the 0.6 water-to-cement ratio specimens. The maximum and minimum values for splitting tensile strength differed from the average by 20.4% for the 0.4 water-to-cement ratio specimens, 12.1% for the 0.5 water-to-cement ratio specimens, and 19.3% for the 0.6 water-to-cement ratio specimens. The 0.4 and 0.6 water-to-cement ratio specimens exceeded the 5% within-batch coefficient of variation and the 14% difference-from-average limit for two properly conducted tests on the same material set by the ASTM C 496 standard.

Chlorides have no known reaction with the components of the hydrated cement paste. However, as the water is being used up by the cement hydration reactions, the chloride concentration within the pores eventually reaches saturation and begins to crystalize into sodium, potassium and calcium chloride. Excessive expansive crystal growth can form a flaw within the concrete to which splitting tensile testing is sensitive. The flaw acts as a crack and under tensile loading it takes far less energy to propagate a crack than to initiate it.

3.4.1.2 Concentration Gradient

Table 19: Tensile splitting strength for two different chloride concentration gradients

Concentration Gradient (ppm)	Average Ultimate Load (kN)	Splitting Tensile Strength (MPa)
0 – 30,000	137.1	4.23
7,500 – 22,500	151.1	4.66

A chloride concentration gradient of 0 – 30,000 ppm or 7,500 – 22,500 ppm within the concrete cylinder did not have a significant effect on the splitting tensile strength (Table 19). The within-batch coefficient of variation was 4.84% for the 0 – 30,000 ppm specimens and 4.30% for 7,500 – 22,500 ppm specimens when compared with the 0.5 constant concentration specimens. The greatest difference from the splitting tensile strength of the 0.5 water-to-cement ratio constant concentration specimens was 12.0% for the 0 – 30,000 ppm specimens and 9.78% for the 7,500 – 22,500 specimens. Both concentration gradients were below the 5% within-batch coefficient of variation and the 14% difference-from-average limit for two properly conducted tests on the same material set by the ASTM C 496 standard.

3.4.2 Sulfate Specimens

3.4.2.1 Constant Concentration

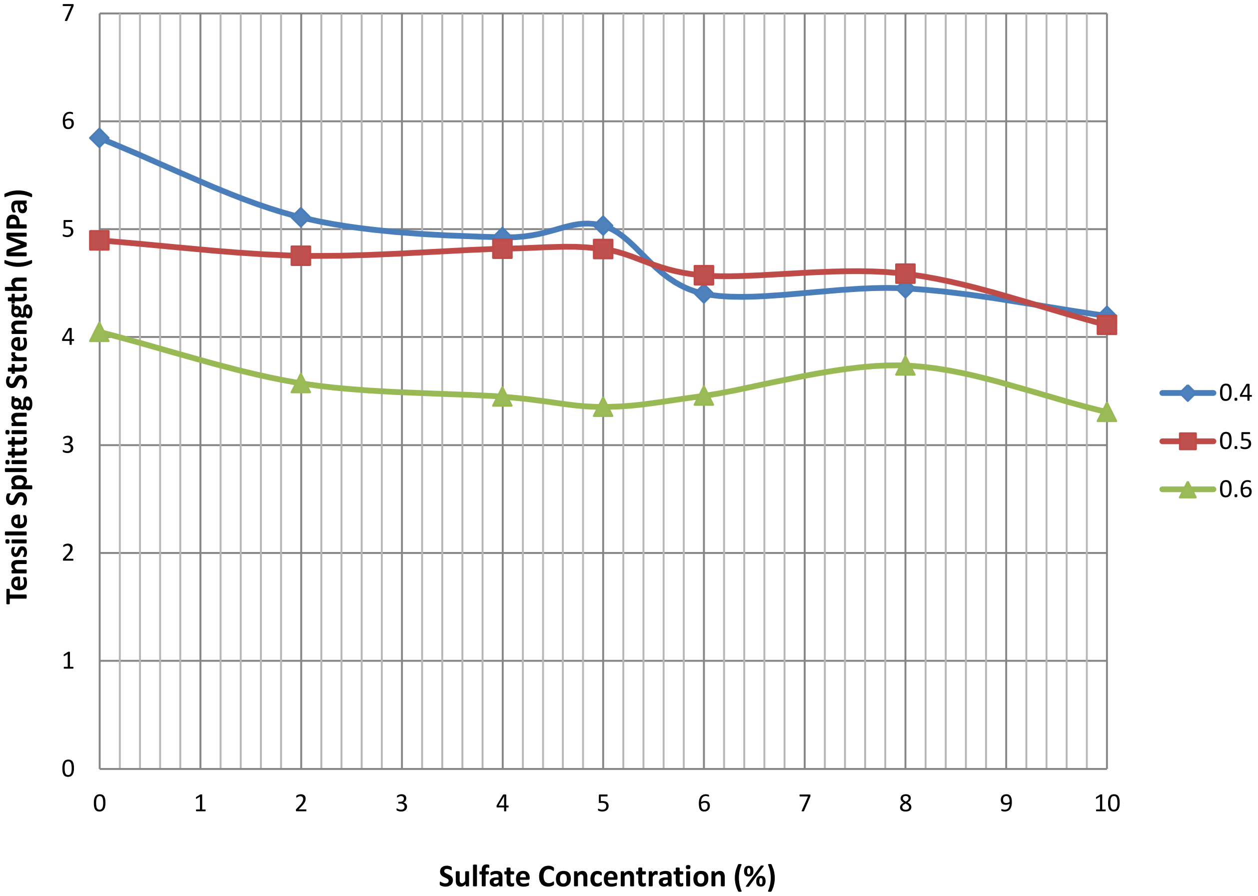

Figure 19: Change in splitting tensile strength with increasing sulfate concentration

Increasing the sulfate concentration within the concrete specimens seemed to decrease their splitting tensile strength. The decrease was most evident with the 0.4 water-to-cement ratio specimens (Figure 19). The within-batch coefficient of variation was 11.5% for the 0.4 water-to-cement ratio specimens, 5.73% for the 0.5 water-to-cement ratio specimens, and 7.25% for the 0.6 water-to-cement ratio specimens. The maximum and minimum values for splitting tensile strength differed from the average by 32.8% for the 0.4 water-to-cement ratio specimens, 16.9% for the 0.5 water-to-cement ratio specimens, and 20.8% for the 0.6 water-to-cement ratio specimens. All three water-to-cement ratio specimens exceed the 5% within-batch coefficient of variation and the 14% difference-from-average limit for two properly conducted tests on the same material set by the ASTM C 496 standard.

The sulfates introduced into the mixing water will cause sulfate attack of the concrete as it chemically reacts with components of the hydrated cement paste to form gypsum and ettringite. The formation of ettringite is expansive and will induce cracks within the concrete, to which tensile loading is sensitive, as it takes much less energy to propagate a crack than to initiate one. In addition, the consumption of calcium hydroxide and the decalcification of the **C-S-H** phase weakens the mechanical properties of the paste. The drop in splitting tensile strength was more prominent with the 0.4 water-to-cement ratio specimens due to the abundance of hydration products with which the sulfates react.

When concrete in the field experiences sulfate attack, usually the source of sulfates is external and has to permeate through the concrete to cause damage. For that reason, concrete with a lower water-to-cement ratio would have better sulfate resistance as it would have a lower permeability. However, the 0.4 water-to-cement ratio specimens experienced the largest drop in splitting tensile strength due to the sulfates being added to the mixing water. That circumvents the need for the sulfate ions to penetrate. Since the lowest water-to-cement ratio specimens have the highest concentration of hydration products required by the sulfate attack chemical reactions, and the least amount of porosity in which early crystal growth can take place safely, it experienced the most damage as evident by the drop in tensile splitting strength.

3.4.2.2 Concentration Gradient

Table 20: Tensile splitting strength for two different sulfate concentration gradients

Concentration Gradient	Average Ultimate Load (kN)	Splitting Tensile Strength (MPa)
0 – 150%	143.4	4.42
37.5 – 112.5%	148.0	4.56

A sulfate concentration gradient of 0 – 10% or 2.5 – 7.5% by weight had a minor effect on the splitting tensile strength of concrete (Table 20). The within-batch coefficient of variation was 5.62% for the 0 – 10% specimens and 5.36% for 2.5 – 7.5% specimens when compared with the 0.5 constant concentration specimens. The greatest difference from the splitting tensile strength of the 0.5 water-to-cement ratio constant concentration specimens is 10.2% for the 0 – 10% specimens and 10.4% for the 2.5 – 7.5% specimens. Both concentration gradients exceed the 5% within-batch coefficient of variation but not the 14% difference-from-average limit for two properly conducted tests on the same material set by the ASTM C 496 standard.

4 Summary and Conclusions

Electrical resistivity measurement has proven to be a quick, easy and reliable method for durability assessment. There are many factors that affect resistivity measurements, the most important of which are temperature and moisture content. The effect of both factors on resistivity measurements has been studied and well documented. However, due to the electrical nature of resistivity measurements, the presence of ions within the section of concrete to be tested will affect the results. The two ions that cause the greatest durability concerns are chlorides and sulfates. Chlorides cause no damage to concrete but will initiate corrosion of the steel reinforcement once they penetrate through the cover concrete. Sulfates, on the other hand, cause sulfate attack of concrete.

The main focus of the experimental section of this thesis was to study the effect of sulfate and chloride ions on the electrical resistivity of concrete. The two different resistivity methods utilized in the study were surface resistivity using a Wenner four probe assembly and bulk resistivity. Surface resistivity was performed on the concrete cylinder as a whole as well as on the split faces after the cylinder has undergone a splitting tensile strength test. To achieve a constant concentration within the concrete cylinder, the required amount of sodium chloride (NaCl) or anhydrous sodium sulfate ($\mathrm{Na_2SO_4}$) was added to the mixing water. To achieve a concentration gradient, the cylinder was cast in layers where each subsequent layer had an increasing amount of NaCl or $\mathrm{Na_2SO_4}$.

The resistivity device used for the experimental section of this thesis, the Proceq Resipod, was designed to be used on concrete cylinders with 100 x 200 mm (4” x 8”) or 150 x 300 mm (6” x 12”) dimensions. The measured surface resistivity decreased as the height of the100 x 200 mm cylinder was reduced. That was observed for both 0.4 and 0.6 water-to-cement ratios tested. As the height is reduced, the edge of the cylinder moves closer to the outer electrodes. That leads to a concentration of the current density as the volume is being reduced, which overestimates the resistivity.

Increasing the concentration of chlorides within the concrete cylinder had the same effect on the surface resistivity of the cylinder as a whole, the bulk resistivity, and the surface resistivity of the split faces. The resistivity decreased with increasing chloride concentration, following a linear regression. Most of the chlorides added to the mixing water will remain in the pore water solution of the hardened concrete as chlorides and concrete do not react. Therefore, increasing the chloride concentration of the mixing water will increase the chloride concentration of the pore water solution. Since the device measures resistivity by applying a current through the concrete and measuring the potential difference, increasing the chloride concentration of the pore water solution will improve the current conduction as ions help carry the current. This is reflected in the lower resistivity measured. Increasing the chloride concentration had a minor effect on the splitting tensile strength. The results of the 0.4 and 0.6 water-to-cement ratio specimens exceeded the 5% within-batch coefficient of variation and the 14% difference-from-average limit for two properly conducted tests (using the maximum and minimum splitting tensile strengths) on the same material set by the ASTM C 496 standard. The results of the 0.5 water-to-cement ratio specimens were below both limits

Increasing the sulfate concentration within the concrete cylinder had an opposing effect on the measured resistivity. The surface resistivity of the cylinder as a whole, the bulk resistivity, and the surface resistivity of the split faces increased with increasing sulfate concentration, also following a linear regression. The sulfates added to the mixing water will cause sulfate attack of the hardened concrete as they chemically react with certain components of the hydrated cement paste to form ettringite and gypsum. The ettringite and gypsum form within the available pore space, reducing the overall porosity of the concrete. The current from the electrical resistivity device flows through the interconnected pores so reducing the porosity will lower the measured resistivity. In addition, the consumption of calcium hydroxide followed by the decalcification of the **C-S-H** phase reduces the calcium concentration in the pore water solution which will also lower the resistivity. The results of all three water-to-cement ratios exceeded the 5% within-batch coefficient of variation and the 14% difference-from-average limit (also using the maximum and minimum splitting tensile strengths).

The resistivity results for both the chloride and sulfate concentration gradients were inconclusive. The concentration gradients tested were 0 – 30,000 ppm and 7,500 – 22,500 ppm for the chlorides and 0 – 10% and 2.5 – 7.5% by weight for the sulfates. Although the surface resistivity results for both chloride concentration gradients were equal and closest to the 20,000 ppm constant concentration samples, the results for the bulk resistivity were on the opposite sides of the 0 – 30,000 ppm range. The resistivity results for both sulfate concentration gradients mostly fell at or below the results for the 0% constant concentration. Both chloride concentration gradients had no effect on the splitting tensile strength as the coefficient of variation was below the 5% limit and difference-from-average was below the 14% limit. The results of the sulfate concentration gradients, however, were inconclusive as the coefficient of variation exceeded the 5% limit even though the difference-from-average was below the 14% limit.

Comparing the results of the 0 ppm chloride samples with the 0% sulfate samples at the same water-to-cement ratio showed that with increasing water-to-cement ratio the resistivity of concrete decreases. A higher water-to-cement ratio will produce concrete that is more porous with a greater degree of pore interconnectivity. That will lower the resistivity measured as the current from the resistivity device travels through the ionic solution contained within the interconnected pores. The 0% concentration specimens also served as a test for the variation of the data. For the same water-to-cement ratio, the largest difference between data of the surface resistivity, the bulk resistivity, and the surface resistivity of the split faces was 0.1 kΩ·cm, 0.21 kΩ·cm, and 0.6 kΩ·cm, respectively.

Electrical resistivity measurement can be particularly useful for the durability assessment of concrete. Interconnected pores are the key that contributor to concrete transfer properties through which deleterious substances ingress and cause damage. Resistivity measurement can be used as an indicator for many of the factors that affect concrete by controlling the other factors or keeping them constant. Its uses include quality assurance, indicating sections of concrete with higher moisture content, and even detecting cracks using resistivity tomography. One of its main uses is to assess the potential for reinforcement corrosion due to its ability to detect moisture and chloride ingress, two of the three factors required for corrosion. There are charts and tables, made available through research, which can estimate the likelihood of corrosion or even the corrosion rate using resistivity measurements. Additional research is needed to better understand the effect of sulfates on resistivity. The extent of damage caused by sulfate attack can be monitored through periodic measurements of resistivity.

References

AASHTO T 277, Standard Method of Test for Electrical Indication of Concrete's Ability to Resist Chloride Ion Penetration, American Association of State and Highway Transportation Officials. 2007.

AASHTO TP 95, Standard Method of Test for Surface Resistivity Indication of Concrete's Ability to Resist Chloride Ion Penetration, American Association of State and Highway Transportation Officials. 2014.

ASTM C496 / C496M-11, Standard Test Method for Splitting Tensile Strength of Cylindrical Concrete Specimens, ASTM International. West Conshohocken, PA, 2004.

ASTM C1202-12, Standard Test Method for Electrical Indication of Concrete's Ability to Resist Chloride Ion Penetration, ASTM International. West Conshohocken, PA, 2012a.

ASTM C1760-12, Standard Test Method for Bulk Electrical Conductivity of Hardened Concrete, ASTM International. West Conshohocken, PA, 2012b.

Alexander, M.; Bertron, A.; De Belie, N., *Performance of Cement-Based Materials in Aggressive Aqueous Environments: State-of-the-Art Report, RILEM TC 211 - PAE*. Springer: 2012.

Andrade, C., Electrical resistivity as microstructural parameter for the calculation of reinforcement service life. *Mari Carmen Andrade* 2009, 1.

Barron, J. J.; Ashton, C., The effect of temperature on conductivity measurement. *TSP* 2005, *7*.

Bellmann, F.; Möser, B.; Stark, J., Influence of sulfate solution concentration on the formation of gypsum in sulfate resistance test specimen. *Cement and Concrete Research* 2006, *36* (2), 358-363.

Bonen, D.; Cohen, M. D., Magnesium sulfate attack on portland cement paste-I. Microstructural analysis. *Cement and Concrete Research* 1992, *22* (1), 169-180.

Boyd, A. J.; Mindess, S., The use of tension testing to investigate the effect of W/C ratio and cement type on the resistance of concrete to sulfate attack. *Cement and Concrete Research* 2004, *34* (3), 373-377.

Brandt, A. M., *Cement-Based Composites: Materials, Mechanical Properties and Performance, Second Edition*. Taylor & Francis: 2009.

Breysse, D., *Non-Destructive Assessment of Concrete Structures: Reliability and Limits of Single and Combined Techniques: State-of-the-Art Report of the RILEM Technical Committee 207-INR*. Springer: 2012.

Broomfield, J. P., *Corrosion of Steel in Concrete: Understanding, investigation and repair*. Taylor & Francis: 2002.

Bye, G. C., *Portland Cement: Composition, Production and Properties*. Thomas Telford: 1999.

Chatterji, S.; Jensen, A., Efflorescence and breakdown of building materials. *Nordic concrete research* 1989, (8), 56-61.

Claisse, P. A.; El-Sayad, H. I.; Shaaban, I. G., Permeability and pore volume of carbonated concrete. *ACI Materials Journal* 1999, *96* (3).

Collepardi, M., A state-of-the-art review on delayed ettringite attack on concrete. *Cement and Concrete Composites* 2003, *25* (4–5), 401-407.

Diamond, S., Delayed ettringite formation — Processes and problems. *Cement and Concrete Composites* 1996, *18* (3), 205-215.

Flatt, R. J., Salt damage in porous materials: how high supersaturations are generated. *Journal of Crystal Growth* 2002, *242* (3–4), 435-454.

Folliard, K.; Sandberg, P., Mechanisms of concrete deterioration by sodium sulfate crystallization. *ACI Special Publication* 1994, *145*.

Fu, Y.; Ding, J.; Beaudoin, J. J., Expansion of portland cement mortar due to internal sulfate attack. *Cement and Concrete Research* 1997, *27* (9), 1299-1306.

Gjørv, O. E.; Vennesland, Ø. E.; El-Busaidy, A. In *Electrical resistivity of concrete in the oceans*, Offshore Technology Conference, Offshore Technology Conference: 1977.

González, M. A.; Irassar, E. F., ETTRINGITE FORMATION IN LOW C3A PORTLAND CEMENT EXPOSED TO SODIUM SULFATE SOLUTION. *Cement and Concrete Research* 1997, *27* (7), 1061-1072.

Hartell, J. A.; Boyd, A. J.; Ferraro, C. C., Sulfate attack on concrete: effect of partial immersion. *Journal of Materials in Civil Engineering* 2010, *23* (5), 572-579.

Hobbs, D., Expansion and cracking in concrete associated with delayed ettringite formation. *ACI Special Publication* 1999, *177*.

Hooton, R. D., Permeability and pore structure of cement pastes containing fly ash, slag, and silica fume. *Blended Cements, ASTM STP* 1986, *897*, 128-143.

Hussain, S. E.; Rasheeduzzafar, Corrosion resistance performance of fly ash blended cement concrete. *ACI Materials Journal* 1994, *91* (3).

Johansen, V.; Thaulow, N.; Skalny, J., Simultaneous presence of alkali—silica gel and ettringite in concrete. *Advances in Cement Research* 1993, *5* (17), 23-29.

Lacasse, M. A.; Vanier, D. J., *Durability of Building Materials and Components 8: Service life and durability of materials and components*. NRC Research Press: 1999.

Lataste, J. F.; Sirieix, C.; Breysse, D.; Frappa, M., Electrical resistivity measurement applied to cracking assessment on reinforced concrete structures in civil engineering. *NDT & E International* 2003, *36* (6), 383-394.

Liu, Z.; Deng, D.; De Schutter, G.; Yu, Z., *" Salt Weathering" Distress on Concrete by Sulfates?* INTECH Open Access Publisher: 2012.

Maierhofer, C.; Reinhardt, H. W.; Dobmann, G., *Non-Destructive Evaluation of Reinforced Concrete Structures: Non-Destructive Testing Methods*. Elsevier Science: 2010.

Marchand, J.; Bentz, D. P.; Samson, E.; Maltais, Y., Influence of calcium hydroxide dissolution on the transport properties of hydrated cement systems. 2001.

Marchand, J.; Odler, I.; Skalny, J. P., *Sulfate Attack on Concrete*. Taylor & Francis: 2003.

Mbessa, M.; Péra, J., Durability of high-strength concrete in ammonium sulfate solution. *Cement and Concrete Research* 2001, *31* (8), 1227-1231.

McCarter, W. J.; Brousseau, R., The A.C. response of hardened cement paste. *Cement and Concrete Research* 1990, *20* (6), 891-900.

Mehta, P. K., Mechanism of expansion associated with ettringite formation. *Cement and Concrete Research* 1973, *3* (1), 1-6.

Mehta, P. K., Mechanism of sulfate attack on portland cement concrete — Another look. *Cement and Concrete Research* 1983, *13* (3), 401-406.

Mehta, P. K., Scanning electron micrographic studies of ettringite formation. *Cement and Concrete Research* 1976, *6* (2), 169-182.

Mehta, P. K.; Hu, F., Further evidence for expansion of ettringite by water adsorption. *Journal of the American ceramic Society* 1978, *61* (3-4), 179-181.

Mehta, P. K.; Monteiro, P. J. M., *Concrete: Microstructure, Properties, and Materials*. McGraw-Hill Education: 2013.

Mehta, P. K.; Pirtz, D.; Polivka, M., Properties of alite cements. *Cement and Concrete Research* 1979, *9* (4), 439-450.

Miletić, S.; Ilić, M. In *Effect of ammonium-sulphate corrosion on the strength of concrete*, Proceedings of the 10th ICCC, 1997.

Millard, S. G., Reinforced Concrete Resistivity Measurement Techniques. *ICE Proceedings* 1991, *91*, 71-88.

Min, D.; Mingshu, T., Formation and expansion of ettringite crystals. *Cement and Concrete Research* 1994, *24* (1), 119-126.

Mindess, S.; Young, J. F.; Darwin, D., *Concrete*. Prentice Hall: 2003.

Monfore, G. E., *The Electrical Resistivity of Concrete*. Portland Cement Association, Research and Development Laboratories: 1968.

Morris, W.; Moreno, E. I.; Sagüés, A. A., Practical evaluation of resistivity of concrete in test cylinders using a Wenner array probe. *Cement and Concrete Research* 1996, *26* (12), 1779-1787.

Newlands, M.; Jones, M. R.; Kandasami, S.; Harrison, T., Sensitivity of electrode contact solutions and contact pressure in assessing electrical resistivity of concrete. *Mat. Struct.* 2008, *41* (4), 621-632.

Odler, I.; Colán-Subauste, J., Investigations on cement expansion associated with ettringite formation. *Cement and Concrete Research* 1999, *29* (5), 731-735.

Pettifer, K.; Nixon, P. J., Alkali metal sulphate — a factor common to both alkali aggregate reaction and sulphate attack on concrete. *Cement and Concrete Research* 1980, *10* (2), 173-181.

Polder, R.; Andrade, C.; Elsener, B.; Vennesland, Ø.; Gulikers, J.; Weidert, R.; Raupach, M., Test methods for on site measurement of resistivity of concrete. *Mat. Struct.* 2000, *33* (10), 603-611.

Rasheeduzzafar; Al-Amoudi, O. S. B.; Abduljauwad, S. N.; Maslehuddin, M., Magnesium-sodium sulfate attack in plain and blended cements. *Journal of Materials in Civil Engineering* 1994, *6* (2), 201-222.

Rodriguez-Navarro, C.; Doehne, E., Salt weathering: influence of evaporation rate, supersaturation and crystallization pattern. *Earth Surface Processes and Landforms* 1999, *24*, 191-209.

Saleem, M.; Shameem, M.; Hussain, S.; Maslehuddin, M., Effect of moisture, chloride and sulphate contamination on the electrical resistivity of Portland cement concrete. *Construction and Building Materials* 1996, *10* (3), 209-214.

Santhanam, M.; Cohen, M.; Olek, J., Differentiating seawater and groundwater sulfate attack in Portland cement mortars. *Cement and Concrete Research* 2006, *36* (12), 2132-2137.

Santhanam, M.; Cohen, M. D.; Olek, J., Effects of gypsum formation on the performance of cement mortars during external sulfate attack. *Cement and Concrete Research* 2003, *33* (3), 325-332.

Santhanam, M.; Cohen, M. D.; Olek, J., Sulfate attack research — whither now? *Cement and Concrete Research* 2001, *31* (6), 845-851.

Scherer, G. W., Stress from crystallization of salt. *Cement and Concrete Research* 2004, *34* (9), 1613-1624.

Sengul, O., Factors Affecting the Electrical Resistivity of Concrete. In *Nondestructive Testing of Materials and Structures*, Güneş, O.; Akkaya, Y., Eds. Springer Netherlands: 2013; Vol. 6, pp 263-269.

Shayan, A.; Ivanusec, I., An experimental clarification of the association of delayed ettringite formation with alkali-aggregate reaction. *Cement and Concrete Composites* 1996, *18* (3), 161-170.

Steiger, M.; Asmussen, S., Crystallization of sodium sulfate phases in porous materials: The phase diagram Na2SO4–H2O and the generation of stress. *Geochimica et Cosmochimica Acta* 2008, *72* (17), 4291-4306.

Stutzman, P. E., Scanning electron microscopy in concrete petrography. *Materials Science of Concrete Special Volume: Calcium Hydroxide in Concrete, Proceedings-Anna Maria Island-FL* 2000, 59-72.

Taylor, H. F. W.; Famy, C.; Scrivener, K. L., Delayed ettringite formation. *Cement and Concrete Research* 2001, *31* (5), 683-693.

Thaulow, N.; Sahu, S., Mechanism of concrete deterioration due to salt crystallization. *Materials Characterization* 2004, *53* (2–4), 123-127.

Tian, B.; Cohen, M. D., Does gypsum formation during sulfate attack on concrete lead to expansion? *Cement and Concrete Research* 2000, *30* (1), 117-123.

Tsui, N.; Flatt, R. J.; Scherer, G. W., Crystallization damage by sodium sulfate. *Journal of Cultural Heritage* 2003, *4* (2), 109-115.

Wei, X.; Xiao, L., Influence of the aggregate volume on the electrical resistivity and properties of portland cement concretes. *J. Wuhan Univ. Technol.-Mat. Sci. Edit.* 2011, *26* (5), 965-971.

Whiting, D. A.; Nagi, M. A., Electrical resistivity of concrete-a literature review. *R&D Serial* 2003, (2457).

Winkler, E. M.; Singer, P. C., Crystallization pressure of salts in stone and concrete. *Geological society of America bulletin* 1972, *83* (11), 3509-3514.

Wolsiefer, J. T., Silica fume concrete: a solution to steel reinforcement corrosion in concrete. *ACI Special Publication* 1991, *126*.

Xiong, C.; Jiang, L.; Song, Z.; Liu, R.; You, L.; Chu, H., Influence of cation type on deterioration process of cement paste in sulfate environment. *Construction and Building Materials* 2014, *71* (0), 158-166.

Yang, R.; Lawrence, C. D.; Lynsdale, C. J.; Sharp, J. H., Delayed ettringite formation in heat-cured Portland cement mortars. *Cement and Concrete Research* 1999, *29* (1), 17-25.

Yu, P.; Kirkpatrick, R. J.; Poe, B.; McMillan, P. F.; Cong, X., Structure of calcium silicate hydrate (C-S-H): Near-, Mid-, and Far-infrared spectroscopy. *Journal of the American ceramic Society* 1999, *82* (3), 742-748.

Appendices

Appendix A: Change in Height Results

Specimens 0.4 w/c

	Length (cm)	Surface Resistivity Reading (kΩ·cm)								
		0°	90°	180°	270°	0°	90°	180°	270°	Average
Specimen A	20.4	16.5	16.2	15.9	16.2	16.4	16.2	16.0	16.4	16.2
	18.8	17.4	17.0	16.7	16.9	17.5	17.0	16.5	17.0	17.0
	17.4	17.9	17.3	17.1	17.4	18.1	17.4	17.0	17.6	17.5
	16.0	18.3	17.7	17.5	17.7	18.4	17.9	17.3	17.9	17.8
	14.3	19.0	18.6	18.2	18.5	19.2	18.4	18.2	18.6	18.6
	12.8	19.9	19.4	19.1	19.5	20.1	19.5	18.9	19.9	19.5
	11.5	21.8	21.3	21.2	21.6	21.9	21.0	21.1	21.5	21.4

	Length (cm)	Surface Resistivity Reading (kΩ·cm)								
		0°	90°	180°	270°	0°	90°	180°	270°	Average
Specimen B	20.5	16.3	15.5	16.8	16.0	16.2	15.8	16.5	15.9	16.1
	19.0	16.9	16.3	17.2	16.8	17.0	16.5	17.2	16.7	16.8
	17.4	17.3	16.8	17.7	17.0	17.2	17.0	18.0	17.5	17.3
	16.1	17.8	17.2	18.3	17.5	18.0	17.3	18.2	17.5	17.7
	14.6	18.3	17.9	18.7	18.2	18.2	18.2	18.7	18.2	18.3
	13.1	19.1	18.7	20.0	18.9	19.0	18.7	19.7	19.2	19.2
	11.5	21.1	20.7	22.0	20.9	21.3	20.8	22.0	20.9	21.2

	Length (cm)	Surface Resistivity Reading (kΩ·cm)								
		0°	90°	180°	270°	0°	90°	180°	270°	Average
Specimen C	20.4	15.7	15.7	16.1	15.8	15.7	15.8	16.1	15.8	15.8
	18.9	16.4	16.3	16.7	16.5	16.4	16.3	16.9	16.5	16.5
	17.5	17.3	17.2	17.6	17.1	17.0	17.2	17.5	16.9	17.2
	16.0	17.7	17.5	18.0	17.6	17.7	17.4	17.9	17.7	17.7
	14.8	18.2	18.1	18.5	18.1	18.4	18.1	18.4	17.9	18.2
	13.3	18.9	19.0	19.4	19.2	18.8	19.0	19.4	18.8	19.1
	11.6	21.1	20.7	21.4	21.4	20.9	20.8	21.3	21.2	21.1

Specimens 0.6 w/c

	Length (cm)	Surface Resistivity Reading (kΩ·cm)								
		0°	90°	180°	270°	0°	90°	180°	270°	Average
Specimen A	20.5	8.0	8.5	8.2	7.9	8.0	8.6	8.2	7.8	8.2
	18.7	7.9	8.5	8.4	8.0	8.0	8.6	8.5	8.1	8.3
	17.2	8.0	8.7	8.9	8.2	8.0	9.0	8.9	8.3	8.5
	16.0	8.5	8.9	9.2	8.5	8.3	8.9	9.0	8.5	8.7
	14.5	9.0	9.3	9.5	8.9	8.9	9.3	9.4	8.7	9.1
	13.1	9.4	9.5	10.2	9.2	9.3	9.5	10.0	9.6	9.6
	11.5	10.0	9.9	10.7	9.9	9.9	9.9	10.7	10.1	10.1

	Length (cm)	Surface Resistivity Reading (kΩ·cm)								
		0°	90°	180°	270°	0°	90°	180°	270°	Average
Specimen B	20.4	8.2	8.2	8.3	8.6	8.1	8.0	8.3	8.5	8.3
	18.9	8.2	8.0	8.4	8.4	8.2	7.9	8.3	8.6	8.3
	17.5	8.2	8.3	8.7	8.9	8.5	8.4	8.8	9.0	8.6
	16.0	8.6	8.5	9.0	9.5	8.4	8.5	9.1	9.3	8.9
	14.6	8.8	9.0	9.6	10.1	8.7	8.8	9.6	10.1	9.3
	13.1	9.3	9.6	9.9	10.6	9.4	9.3	9.9	11.0	9.9
	11.6	9.8	10.1	10.4	10.9	9.8	10.2	10.5	10.8	10.3

	Length (cm)	Surface Resistivity Reading (kΩ·cm)								
		0°	90°	180°	270°	0°	90°	180°	270°	Average
Specimen C	20.4	8.2	7.9	7.7	8.0	8.2	8.0	7.7	8.0	8.0
	18.8	8.2	8.0	7.6	8.2	8.1	8.0	7.5	8.1	8.0
	17.5	8.5	8.2	7.9	8.3	8.3	8.2	8.0	8.2	8.2
	16.0	9.0	8.5	8.2	8.4	9.1	8.7	8.2	8.3	8.6
	14.3	9.9	9.2	8.9	9.0	9.7	9.3	8.7	9.2	9.2
	13.0	10.3	9.6	9.3	9.3	10.5	9.7	9.3	9.4	9.7
	11.5	10.8	10.3	9.9	10.0	10.7	10.2	10.0	10.1	10.3

Appendix B: Increasing Chloride Concentration (0.4 w/c)

Surface Resistivity Results

Concentration (ppm)	Specimen	Surface Resistivity Reading (kΩ·cm)								Average (kΩ·cm)
		0°	90°	180°	270°	0°	90°	180°	270°	
0	A	16.0	16.5	16.0	17.1	16.1	16.6	15.9	17.2	16.6
	B	16.8	16.3	16.6	16.6	16.7	16.3	16.5	16.6	
	C	16.4	17.3	17.0	16.1	16.4	17.0	17.0	16.3	
5000	A	13.7	13.9	14.4	14.2	13.7	14.1	14.3	14.0	14.0
	B	13.4	14.7	14.1	13.4	13.3	14.6	14.2	13.4	
	C	14.3	14.1	14.5	13.5	14.3	14.0	14.6	13.3	
10000	A	14.9	13.6	13.0	13.8	15.0	13.2	12.7	13.6	13.6
	B	14.2	14.6	13.5	13.9	14.0	14.2	13.5	13.4	
	C	13.7	13.2	13.0	13.0	13.7	13.3	12.8	13.0	
15000	A	12.8	12.3	13.2	13.2	13.0	12.5	13.1	12.9	12.8
	B	12.4	12.2	12.9	13.0	12.5	12.6	12.7	13.2	
	C	12.6	12.8	13.2	13.0	12.4	12.9	12.9	12.6	
20000	A	11.4	11.3	11.7	12.4	11.5	11.4	11.7	12.3	12.2
	B	12.6	13.0	12.8	12.9	12.6	13.0	12.9	13.0	
	C	11.6	12.0	12.6	11.8	11.7	11.6	12.5	11.8	
25000	A	10.8	11.4	11.8	11.4	10.9	11.5	12.0	11.6	11.4
	B	11.2	11.5	10.9	11.1	11.2	11.4	10.8	11.5	
	C	11.2	11.6	11.5	11.4	11.3	11.6	11.8	11.4	
30000	A	11.4	10.8	11.7	11.6	11.4	10.8	11.6	11.6	11.3
	B	11.3	11.3	10.7	11.3	11.0	11.4	10.9	11.4	
	C	11.0	11.6	10.8	11.7	11.3	11.6	10.6	11.7	

Bulk Resistivity Results

Concentration (ppm)	Specimen	Resistivty Readings (kΩ·cm)			R_{actual} (kΩ·cm)	Average R_{actual} (kΩ·cm)	Bulk Resistivity (kΩ·cm)
		R_{upper}	R_{lower}	$R_{measured}$			
0	A	1.6	0.0	59.6	58.0	57.7	9.64
	B	1.4	0.0	59.3	57.9		
	C	1.3	0.0	58.5	57.2		
5000	A	1.5	0.0	52.7	51.2	51.7	8.63
	B	1.6	0.0	53.2	51.6		
	C	1.8	0.0	54.0	52.2		
10000	A	1.8	0.0	46.7	44.9	45.2	7.55
	B	1.6	0.0	47.6	46.0		
	C	1.4	0.0	46.0	44.6		
15000	A	1.2	0.0	43.5	42.3	42.5	7.10
	B	1.4	0.0	43.9	42.5		
	C	1.1	0.0	43.7	42.6		
20000	A	1.3	0.0	42.0	40.7	40.8	6.82
	B	1.3	0.0	42.9	41.6		
	C	1.1	0.0	41.3	40.2		
25000	A	1.0	0.0	39.1	38.1	37.1	6.20
	B	1.3	0.0	38.2	36.9		
	C	1.2	0.0	37.5	36.3		
30000	A	1.4	0.0	39.2	37.8	37.7	6.30
	B	1.1	0.0	37.9	36.8		
	C	1.0	0.0	39.5	38.5		

Surface Resistivity of Split Faces Results

Concentration (ppm)	Specimen	Surface Resistivity Readings (kΩ·cm)		Average (kΩ·cm)
		Face 1	Face 2	
0	A	22.3	23.3	23.0
	B	24.0	23.2	
	C	21.7	23.5	
5000	A	22.1	25.6	21.5
	B	20.3	22.4	
	C	19.4	19.2	
10000	A	16.5	18.4	17.6
	B	17.5	19.1	
	C	17.8	16.4	
15000	A	15.5	16.2	16.2
	B	15.8	16.0	
	C	16.7	17.1	
20000	A	15.4	14.8	15.3
	B	14.5	15.8	
	C	16.0	15.5	
25000	A	12.5	13.3	13.5
	B	13.6	14.2	
	C	13.0	14.4	
30000	A	13.8	13.5	13.4
	B	13.1	12.6	
	C	13.9	13.4	

Appendix C: Increasing Chloride Concentration (0.5 w/c)

Surface Resistivity Results

Concentration (ppm)	Specimen	Surface Resistivity Reading (kΩ·cm)								Average (kΩ·cm)
		0°	90°	180°	270°	0°	90°	180°	270°	
0	A	11.4	11.6	10.4	11.1	11.2	11.4	10.4	11.0	11.1
	B	10.7	11.4	11.1	11.0	10.9	11.5	11.1	10.9	
	C	11.4	11.0	11.4	10.7	11.4	11.0	11.3	10.9	
5000	A	11.0	11.1	10.9	10.7	11.1	11.0	11.0	10.9	10.4
	B	9.8	10.4	9.8	10.1	9.8	10.2	9.9	10.2	
	C	10.6	10.2	9.7	10.0	10.6	10.4	9.5	9.9	
10000	A	10.5	10.0	10.2	10.3	10.5	10.0	10.1	10.5	10.1
	B	9.6	10.1	9.9	10.0	9.5	9.8	9.9	9.8	
	C	10.5	10.6	9.8	9.8	10.3	10.4	9.8	10.0	
15000	A	10.0	10.2	10.9	10.6	10.1	10.0	10.8	10.6	10.1
	B	10.5	10.7	9.6	10.1	10.2	10.5	9.5	9.8	
	C	10.4	10.2	10.4	8.8	10.2	10.0	10.1	9.1	
20000	A	9.5	9.0	9.7	10.0	9.2	9.1	9.4	9.7	9.4
	B	9.2	9.0	9.0	9.2	9.3	8.8	8.9	9.2	
	C	9.5	9.3	10.1	9.8	9.4	9.3	9.8	9.5	
25000	A	8.9	9.1	9.2	8.2	9.0	8.9	9.2	8.3	8.9
	B	9.8	8.6	8.8	8.3	9.5	8.6	8.7	8.5	
	C	9.9	8.5	8.3	8.2	9.6	9.1	8.8	8.8	
30000	A	8.6	8.4	8.0	8.1	8.4	8.2	8.0	8.2	8.2
	B	7.6	7.8	7.8	8.1	7.7	8.0	7.8	7.9	
	C	8.6	7.9	8.3	9.0	8.3	8.0	8.4	9.0	

Bulk Resistivity Results

Concentration (ppm)	Specimen	Resistivty Reading (kΩ·cm)			R_{actual} (kΩ·cm)	Average R_{actual} (kΩ·cm)	Bulk Resistivity (kΩ·cm)
		R_{upper}	R_{lower}	$R_{measured}$			
0	A	1.2	0.0	45.6	44.4	47.3	7.90
	B	1.6	0.0	50.1	48.5		
	C	1.4	0.0	50.3	48.9		
5000	A	1.5	0.0	38.7	37.2	37.1	6.19
	B	1.6	0.0	38.1	36.5		
	C	1.3	0.0	38.8	37.5		
10000	A	1.4	0.0	37.2	35.8	35.2	5.88
	B	1.1	0.0	36.3	35.2		
	C	1.2	0.0	35.7	34.5		
15000	A	1.3	0.0	35.2	33.9	34.1	5.69
	B	1.6	0.0	35.5	33.9		
	C	1.3	0.0	35.7	34.4		
20000	A	1.4	0.0	34.1	32.7	32.7	5.47
	B	1.1	0.0	33.3	32.2		
	C	1.4	0.0	34.7	33.3		
25000	A	1.5	0.0	32.2	30.7	31.0	5.19
	B	1.5	0.0	32.1	30.6		
	C	1.4	0.0	33.2	31.8		
30000	A	1.3	0.0	30.3	29.0	29.6	4.95
	B	1.2	0.0	30.0	28.8		
	C	1.4	0.0	32.5	31.1		

Surface Resistivity of Split Faces Results

Concentration (ppm)	Specimen	Surface Resistivity Readings (kΩ·cm)		Average (kΩ·cm)
		Face 1	Face 2	
0	A	15.0	17.1	15.2
	B	16.9	14.5	
	C	14.0	13.8	
5000	A	13.5	13.0	13.0
	B	11.3	13.6	
	C	11.5	14.9	
10000	A	14.7	13.5	13.1
	B	11.4	13.2	
	C	11.9	14.1	
15000	A	12.0	13.5	12.9
	B	13.9	12.7	
	C	12.2	12.9	
20000	A	11.7	12.4	11.9
	B	11.2	10.7	
	C	11.7	13.6	
25000	A	10.6	11.8	11.5
	B	11.5	12.6	
	C	10.9	11.5	
30000	A	11.2	10.6	10.5
	B	10.9	9.3	
	C	9.9	11.1	

Appendix D: Increasing Chloride Concentration (0.6 w/c)

Surface Resistivity Results

Concentration (ppm)	Specimen	Surface Resistivity Reading (kΩ·cm)								Average (kΩ·cm)
		0°	90°	180°	270°	0°	90°	180°	270°	
0	A	8.7	8.7	8.7	8.8	8.6	8.9	8.7	8.5	8.6
	B	8.6	8.4	8.4	8.9	8.6	8.1	8.5	8.8	
	C	8.1	8.0	9.0	8.4	8.6	8.1	9.1	8.3	
5000	A	9.1	8.6	8.5	8.3	9.0	8.6	8.7	8.6	8.6
	B	8.6	8.5	8.3	8.5	8.6	8.5	8.2	8.5	
	C	8.7	8.8	8.6	8.6	8.7	8.7	8.8	8.6	
10000	A	8.1	8.1	7.9	8.1	8.2	8.0	7.9	8.0	8.2
	B	8.4	8.4	7.9	8.3	8.5	8.4	7.9	8.2	
	C	8.6	8.3	8.1	8.2	8.6	8.2	8.1	8.3	
15000	A	7.5	7.2	7.7	7.5	7.6	7.4	7.6	7.4	7.4
	B	6.8	7.8	7.4	7.4	6.9	7.8	7.5	7.5	
	C	7.1	7.4	7.8	7.6	7.1	7.4	7.8	7.4	
20000	A	6.7	6.7	6.7	6.9	6.6	6.8	6.6	6.9	6.3
	B	6.4	6.0	6.3	6.3	6.3	5.9	6.3	6.4	
	C	6.0	6.2	5.8	5.8	6.1	6.2	5.7	5.8	
25000	A	6.1	6.3	6.1	6.2	6.0	6.3	6.1	6.3	6.0
	B	6.3	5.8	6.1	5.7	6.2	5.8	6.0	5.8	
	C	6.3	5.8	5.6	6.1	6.1	5.7	5.6	6.2	
30000	A	5.7	6.0	5.8	5.3	5.8	6.0	5.8	5.4	5.7
	B	5.6	5.7	5.6	5.6	5.5	5.6	5.7	5.6	
	C	5.8	5.7	5.5	5.9	5.4	5.7	5.5	5.8	

Bulk Resistivity Results

Concentration (ppm)	Specimen	Resistivty Reading (kΩ·cm)			R_{actual} (kΩ·cm)	Average R_{actual} (kΩ·cm)	Bulk Resistivity (kΩ·cm)
		R_{upper}	R_{lower}	$R_{measured}$			
0	A	1.4	0.0	42.9	41.5	41.6	6.95
	B	1.1	0.0	41.7	40.6		
	C	1.2	0.0	43.8	42.6		
5000	A	1.2	0.0	34.5	33.3	31.4	5.25
	B	1.1	0.0	31.5	30.4		
	C	0.0	0.0	30.6	30.6		
10000	A	1.4	0.0	27.3	25.9	27.1	4.52
	B	1.5	0.0	28.7	27.2		
	C	1.2	0.0	29.3	28.1		
15000	A	1.0	0.0	26.1	25.1	24.5	4.09
	B	0.0	0.0	24.9	24.9		
	C	1.3	0.0	24.7	23.4		
20000	A	1.1	0.0	21.6	20.5	19.8	3.31
	B	1.3	0.0	20.8	19.5		
	C	0.0	0.0	19.4	19.4		
25000	A	0.0	0.0	19.6	19.6	19.1	3.19
	B	1.0	0.0	19.7	18.7		
	C	1.1	0.0	20.0	18.9		
30000	A	1.2	0.0	19.7	18.5	18.1	3.02
	B	1.3	0.0	19.2	17.9		
	C	1.0	0.0	18.8	17.8		

Surface Resistivity of Split Faces Results

Concentration (ppm)	Specimen	Surface Resistivity Readings (kΩ·cm)		Average (kΩ·cm)
		Face 1	Face 2	
0	A	13.0	11.1	12.6
	B	13.5	12.7	
	C	12.8	12.4	
5000	A	11.5	11.7	11.6
	B	10.7	11.5	
	C	12.4	11.8	
10000	A	10.8	10.1	10.6
	B	10.3	10.7	
	C	10.6	11.3	
15000	A	10.2	8.9	9.6
	B	9.1	9.5	
	C	9.7	10.1	
20000	A	8.5	9.1	8.7
	B	8.9	8.2	
	C	8.3	9.4	
25000	A	9.0	8.6	8.1
	B	7.7	8.2	
	C	7.4	7.9	
30000	A	6.5	6.2	7.3
	B	8.6	8.0	
	C	7.6	6.9	

Appendix E: Increasing Sulfate Concentration (0.4 w/c)

Surface Resistivity Results

Concentration (%)	Specimen	Surface Resistivity Reading (kΩ·cm)								Average (kΩ·cm)
		0°	90°	180°	270°	0°	90°	180°	270°	
0	A	16.8	16.9	17.1	16.6	16.6	16.5	17.2	16.6	16.5
	B	16.6	16.8	15.8	16.0	16.5	16.8	16.0	15.9	
	C	16.8	16.1	15.8	16.4	16.8	16.4	16.1	16.2	
2	A	17.7	17.8	17.0	17.5	17.6	17.9	17.2	17.2	17.3
	B	17.6	17.9	17.2	16.9	17.6	17.3	17.4	16.7	
	C	17.1	16.7	16.7	17.0	17.3	17.1	17.0	17.0	
4	A	20.1	17.8	18.2	19.1	19.4	18.8	18.8	18.7	19.3
	B	19.9	19.1	20.1	19.7	19.7	19.0	20.4	19.7	
	C	19.5	18.7	20.0	19.4	19.3	19.2	19.3	19.6	
5	A	20.0	19.6	19.6	19.9	20.2	19.5	19.8	20.2	19.5
	B	18.6	18.5	18.9	19.1	18.5	20.0	19.3	19.8	
	C	20.0	19.9	19.4	19.5	19.8	20.3	19.2	19.5	
6	A	21.0	20.5	20.2	20.1	20.7	20.1	19.8	20.5	20.4
	B	20.7	20.6	20.9	19.7	20.3	20.6	19.9	20.2	
	C	19.4	20.7	19.6	21.8	20.3	20.9	19.9	21.3	
8	A	21.7	20.9	21.6	21.7	21.6	20.8	21.3	20.9	20.7
	B	21.0	20.6	19.8	21.3	21.6	19.8	20.3	21.6	
	C	21.3	20.2	18.8	20.2	20.4	20.4	20.1	18.5	
10	A	22.7	22.6	22.9	22.5	22.3	22.4	23.3	21.5	22.2
	B	22.5	23.1	21.4	22.6	22.4	23.2	20.8	23.0	
	C	22.6	21.2	21.0	22.3	22.0	21.3	21.6	22.6	

Bulk Resistivity Results

Concentration (%)	Specimen	Resistivty Reading (kΩ·cm)			R_{actual} (kΩ·cm)	Average R_{actual} (kΩ·cm)	Bulk Resistivity (kΩ·cm)
		R_{upper}	R_{lower}	$R_{measured}$			
0	A	1.4	0.0	60.2	58.8	57.2	9.56
	B	1.2	0.0	57.9	56.7		
	C	1.4	0.0	57.6	56.2		
2	A	1.6	0.0	62.0	60.4	60.9	10.17
	B	1.7	0.0	62.8	61.1		
	C	1.2	0.0	62.3	61.1		
4	A	1.1	0.0	69.0	67.9	67.4	11.26
	B	1.2	0.0	68.2	67.0		
	C	1.3	0.0	68.5	67.2		
5	A	1.1	0.0	70.4	69.3	68.1	11.38
	B	1.0	0.0	69.4	68.4		
	C	1.1	0.0	67.7	66.6		
6	A	1.2	0.0	68.3	67.1	68.5	11.45
	B	1.1	0.0	71.6	70.5		
	C	1.2	0.0	69.1	67.9		
8	A	1.2	0.0	74.1	72.9	70.6	11.80
	B	1.4	0.0	71.5	70.1		
	C	1.2	0.0	70.0	68.8		
10	A	1.4	0.0	78.4	77.0	78.1	13.05
	B	1.3	0.0	81.8	80.5		
	C	1.0	0.0	77.8	76.8		

Surface Resistivity of Split Faces Results

Concentration (%)	Specimen	Surface Resistivity Readings (kΩ·cm)		Average (kΩ·cm)
		Face 1	Face 2	
0	A	22.1	24.3	22.8
	B	23.2	22.2	
	C	21.2	23.9	
2	A	24.4	25.2	23.6
	B	25.0	22.1	
	C	23.6	21.4	
4	A	20.8	22.0	22.9
	B	22.5	24.1	
	C	22.4	25.3	
5	A	24.8	21.3	22.5
	B	24.4	20.9	
	C	20.1	23.6	
6	A	22.4	21.5	22.3
	B	22.1	22.0	
	C	23.4	22.2	
8	A	22.5	20.6	22.5
	B	23.7	24.4	
	C	21.4	22.3	
10	A	24.3	25.6	24.2
	B	23.0	24.7	
	C	22.5	24.9	

Appendix F: Increasing Sulfate Concentration (0.5 w/c)

Surface Resistivity Results

Concentration (%)	Specimen	Surface Resistivity Reading (kΩ·cm)								Average (kΩ·cm)
		0°	90°	180°	270°	0°	90°	180°	270°	
0	A	11.3	11.1	10.8	11.1	11.4	11.2	10.8	11.0	11.1
	B	10.5	11.0	11.1	11.5	10.7	11.0	11.1	11.5	
	C	11.1	11.4	11.1	11.0	11.2	11.4	11.0	11.0	
2	A	11.4	12.0	12.0	11.7	11.5	11.6	12.2	11.9	11.9
	B	11.4	12.2	12.3	12.6	12.1	11.8	12.3	12.5	
	C	11.8	11.5	12.1	11.9	12.0	11.6	11.9	12.1	
4	A	13.4	12.3	12.1	13.1	13.1	12.0	11.9	12.9	12.5
	B	12.4	12.1	13.3	12.7	12.5	12.0	12.9	13.0	
	C	12.3	12.4	12.8	11.5	12.0	12.3	12.7	11.8	
5	A	13.0	13.1	12.7	12.6	12.7	13.0	12.8	12.5	12.8
	B	12.8	11.5	13.2	13.2	12.8	11.4	13.4	13.5	
	C	13.1	13.1	13.0	12.8	13.2	13.1	13.0	12.6	
6	A	13.7	13.7	13.6	13.0	13.5	13.7	13.5	12.7	13.4
	B	13.0	13.2	13.9	13.5	13.2	13.4	13.5	13.5	
	C	12.6	13.5	13.7	13.4	12.3	13.4	13.5	13.4	
8	A	13.2	13.8	13.7	13.2	12.9	13.3	13.7	13.3	13.3
	B	13.9	13.5	13.5	13.8	13.9	13.6	13.5	13.6	
	C	12.3	13.8	13.1	12.7	12.3	13.6	13.0	12.6	
10	A	14.6	14.4	14.3	13.5	14.6	14.4	14.4	13.3	14.3
	B	14.3	13.7	14.6	14.8	14.4	13.7	14.6	14.7	
	C	14.0	14.2	15.1	14.3	13.6	13.9	14.9	14.4	

Bulk Resistivity Results

Concentration (%)	Specimen	Resistivty Reading (kΩ·cm)			R_{actual} (kΩ·cm)	Average R_{actual} (kΩ·cm)	Bulk Resistivity (kΩ·cm)
		R_{upper}	R_{lower}	$R_{measured}$			
0	A	1.0	0.0	46.6	45.6	46.0	7.69
	B	1.4	0.0	47.9	46.5		
	C	1.2	0.0	47.2	46.0		
2	A	1.7	0.0	48.2	46.5	47.4	7.92
	B	1.5	0.0	49.5	48.0		
	C	1.3	0.0	49.0	47.7		
4	A	1.5	0.0	48.9	47.4	47.6	7.96
	B	1.4	0.0	48.7	47.3		
	C	1.4	0.0	49.6	48.2		
5	A	1.6	0.0	49.2	47.6	47.6	7.95
	B	1.3	0.0	47.5	46.2		
	C	1.0	0.0	49.9	48.9		
6	A	1.4	0.0	48.2	46.8	48.3	8.07
	B	1.3	0.0	51.0	49.7		
	C	1.4	0.0	49.7	48.3		
8	A	1.4	0.0	51.5	50.1	49.4	8.26
	B	1.6	0.0	52.3	50.7		
	C	1.6	0.0	49.1	47.5		
10	A	1.4	0.0	54.4	53.0	52.4	8.76
	B	1.2	0.0	53.2	52.0		
	C	1.4	0.0	53.6	52.2		

Surface Resistivity of Split Faces Results

Concentration (%)	Specimen	Surface Resistivity Readings (kΩ·cm)		Average (kΩ·cm)
		Face 1	Face 2	
0	A	14.3	14.6	15.0
	B	15.3	14.9	
	C	15.4	15.2	
2	A	14.4	15.5	15.6
	B	16.5	15.3	
	C	15.8	16.0	
4	A	16.0	16.3	16.0
	B	16.3	16.8	
	C	15.4	15.2	
5	A	16.4	16.4	16.6
	B	17.2	16.7	
	C	15.7	17.2	
6	A	18.5	16.8	17.0
	B	17.8	15.2	
	C	17.5	15.9	
8	A	18.4	16.1	17.1
	B	17.9	17.4	
	C	17.2	15.8	
10	A	16.7	17.4	17.3
	B	18.4	15.7	
	C	16.6	18.9	

Appendix G: Increasing Sulfate Concentration (0.6 w/c)

Surface Resistivity Results

Concentration (%)	Specimen	Surface Resistivity Reading (kΩ·cm)								Average (kΩ·cm)
		0°	90°	180°	270°	0°	90°	180°	270°	
0	A	8.4	9.0	8.7	9.1	8.5	8.8	8.5	8.9	8.6
	B	8.5	7.9	8.4	8.7	8.3	8.0	8.4	8.8	
	C	8.7	9.0	8.7	8.3	8.6	9.1	8.9	8.1	
2	A	8.5	9.1	9.3	9.0	8.6	9.1	9.5	8.9	9.1
	B	9.4	9.2	8.8	8.9	9.3	9.2	8.8	9.1	
	C	9.0	9.5	9.3	8.9	8.9	9.5	9.4	9.1	
4	A	9.6	9.6	9.9	9.7	9.6	9.5	10.0	9.9	9.8
	B	10.0	9.6	9.5	9.7	10.1	9.5	9.5	9.8	
	C	9.9	10.2	9.9	10.1	10.0	10.1	9.9	10.1	
5	A	10.2	10.4	10.5	10.2	10.3	10.2	10.4	10.2	10.3
	B	10.6	10.2	10.8	10.7	10.5	10.3	10.6	10.6	
	C	9.7	10.3	10.5	9.9	9.9	10.3	10.6	9.9	
6	A	10.8	10.5	10.6	10.5	10.6	10.5	10.7	10.3	10.6
	B	10.5	10.3	10.9	10.4	10.5	10.4	10.8	10.4	
	C	10.7	10.4	10.8	10.8	10.7	10.5	10.8	10.7	
8	A	10.6	10.9	10.6	10.3	10.7	11.0	10.6	10.5	10.6
	B	10.2	10.3	10.6	10.7	10.4	10.4	10.9	10.8	
	C	10.5	10.6	10.8	10.6	10.5	10.7	11.0	10.7	
10	A	10.4	10.7	11.0	10.9	10.5	10.5	10.9	11.0	10.8
	B	10.6	11.2	10.9	10.6	10.6	11.1	10.7	10.5	
	C	10.7	11.0	10.8	10.8	10.5	11.0	10.8	10.7	

Bulk Resistivity Results

Concentration (%)	Specimen	Resistivty Reading (kΩ·cm)			R_{actual} (kΩ·cm)	Average R_{actual} (kΩ·cm)	Bulk Resistivity (kΩ·cm)
		R_{upper}	R_{lower}	$R_{measured}$			
0	A	1.0	0.0	43.5	42.5	40.9	6.83
	B	1.4	0.0	41.0	39.6		
	C	1.2	0.0	41.8	40.6		
2	A	1.9	0.0	42.2	40.3	41.4	6.91
	B	1.6	0.0	42.8	41.2		
	C	1.4	0.0	44.0	42.6		
4	A	1.5	0.0	43.1	41.6	42.0	7.02
	B	1.3	0.0	43.4	42.1		
	C	1.5	0.0	43.9	42.4		
5	A	1.5	0.0	42.7	41.2	42.2	7.05
	B	1.8	0.0	45.2	43.4		
	C	1.3	0.0	43.3	42.0		
6	A	1.6	0.0	46.0	44.4	43.4	7.25
	B	1.5	0.0	44.5	43.0		
	C	1.4	0.0	44.2	42.8		
8	A	1.2	0.0	44.7	43.5	43.7	7.30
	B	1.4	0.0	45.1	43.7		
	C	1.1	0.0	44.9	43.8		
10	A	1.3	0.0	44.8	43.5	43.5	7.27
	B	1.2	0.0	45.3	44.1		
	C	1.5	0.0	44.5	43.0		

Surface Resistivity of Split Faces

Concentration (%)	Specimen	Surface Resistivity Readings (kΩ·cm)		Average (kΩ·cm)
		Face 1	Face 2	
0	A	12.9	14.3	13.2
	B	14.0	12.2	
	C	12.2	13.3	
2	A	13.2	14.1	13.8
	B	14.9	12.7	
	C	14.3	13.6	
4	A	14.5	15.1	14.3
	B	13.9	14.1	
	C	13.4	14.6	
5	A	14.8	15.3	14.7
	B	15.5	13.0	
	C	14.6	14.9	
6	A	16.3	15.4	15.5
	B	14.5	15.4	
	C	16.0	15.1	
8	A	15.3	15.6	15.4
	B	15.7	16.2	
	C	14.7	14.9	
10	A	17.3	14.2	15.5
	B	14.5	15.7	
	C	15.4	16.0	

Appendix H: Chloride Concentration Gradient (0 – 30,000 ppm)

Surface Resistivity Results

Specimen	Surface Resistivity Reading (kΩ·cm)								Average (kΩ·cm)	
	0°	90°	180°	270°	0°	90°	180°	270°		
A	9.4	9.1	8.8	9.5	9.5	9.3	8.8	9.4	9.2	9.2
B	9.8	9.6	9.2	9.3	9.5	9.4	9.2	9.3	9.4	
C	9.4	9.0	8.8	8.8	9.1	8.7	9.0	8.8	9.0	

Bulk Resistivity Results

Specimen	Resistivty Reading (kΩ·cm)			R_{actual} (kΩ·cm)	Average R_{actual} (kΩ·cm)	Bulk Resistivity (ρ)	Average Bulk Resistivity (ρ)
	R_{upper}	R_{lower}	$R_{measured}$				
A	1.4	0.0	48.5	47.1	45.0	7.87	7.52
B	1.0	0.0	43.2	42.2		7.05	
C	1.4	0.0	47.1	45.7		7.64	

Surface Resistivity of Split Faces Results

Specimen	Surface Resistivity Readings (kΩ·cm)		Average (kΩ·cm)
	Face 1	Face 2	
A	9.3	12.2	11.2
B	11.8	9.6	
C	8.8	15.6	

Appendix I: Chloride Concentration Gradient (7,500 – 22,500 ppm)

Surface Resistivity Results

Specimen	Surface Resistivity Reading (kΩ·cm)								Average (kΩ·cm)	
	0°	90°	180°	270°	0°	90°	180°	270°		
A	9.1	9.5	9.3	9.3	8.9	9.3	9.4	9.2	9.3	9.2
B	9.0	8.7	9.2	9.0	8.9	8.8	9.2	9.1	9.0	
C	9.6	9.2	9.1	9.4	9.6	9.4	9.1	9.2	9.3	

Bulk Resistivity Results

Specimen	Resistivty Reading (kΩ·cm)			R_{actual} (kΩ·cm)	Average R_{actual} (kΩ·cm)	Bulk Resistivity (ρ)	Bulk Resistivity (ρ)
	R_{upper}	R_{lower}	$R_{measured}$				
A	1.6	0.0	30.8	29.2	29.1	4.88	4.87
B	1.4	0.0	30.6	29.2		4.88	
C	1.4	0.0	30.4	29.0		4.85	

Surface Resistivity of Split Faces Results

Specimen	Surface Resistivity Readings (kΩ·cm)		Average (kΩ·cm)
	Face 1	Face 2	
A	10.4	6.5	9.8
B	11.2	11.7	
C	12.1	7.0	

Appendix J: Sulfate Concentration Gradient (0 – 10%)

Surface Resistivity Results

Specimen	Surface Resistivity Reading (kΩ·cm)								Average (kΩ·cm)	
	0°	90°	180°	270°	0°	90°	180°	270°		
A	11.5	11.4	10.4	10.9	11.5	11.4	10.1	10.6	11.0	11.4
B	11.8	11.4	11.3	11.7	11.9	11.7	11.5	11.7	11.6	
C	12.0	11.7	11.3	11.5	11.9	11.8	11.1	11.2	11.6	

Bulk Resistivity Results

Specimen	Resistivty Reading (kΩ·cm)			R_{actual} (kΩ·cm)	Average R_{actual} (kΩ·cm)	Bulk Resistivity (ρ)	Bulk Resistivity (ρ)
	R_{upper}	R_{lower}	$R_{measured}$				
A	1.8	0.0	36.1	34.3	36.1	5.73	6.04
B	2.0	0.0	38.7	36.7		6.13	
C	1.6	0.0	39.0	37.4		6.25	

Surface Resistivity of Split Faces Results

Specimen	Surface Resistivity Readings (kΩ·cm)		Average (kΩ·cm)
	Face 1	Face 2	
A	12.3	15.5	14.2
B	14.7	14.1	
C	15.0	13.8	

Appendix K: Sulfate Concentration Gradien (2.5 – 7.5%)

Surface Resistivity Results

Specimen	Surface Resistivity Reading (kΩ·cm)								Average (kΩ·cm)	
	0°	90°	180°	270°	0°	90°	180°	270°		
A	12.3	11.8	12.9	12.4	12.8	12.2	13.0	12.5	12.5	12.2
B	12.7	12.2	11.8	11.7	12.5	12.1	11.8	11.9	12.1	
C	11.5	12.2	12.4	12.3	11.6	12.3	12.6	12.4	12.2	

Bulk Resistivity Results

Specimen	Resistivty Reading (kΩ·cm)			R_{actual} (kΩ·cm)	Average R_{actual} (kΩ·cm)	Bulk Resistivity (ρ)	Bulk Resistivity (ρ)
	R_{upper}	R_{lower}	$R_{measured}$				
A	1.2	0.0	42.2	41.0	40.3	6.85	6.73
B	1.7	0.0	41.5	39.8		6.65	
C	1.5	0.0	41.6	40.1		6.70	

Surface Resistivity of Split Faces

Specimen	Surface Resistivity Readings (kΩ·cm)		Average (kΩ·cm)
	Face 1	Face 2	
A	14.5	13.6	14.1
B	16.4	12.1	
C	12.9	15.3	

Appendix L: Splitting Tension Results for Increasing Chloride Concentration

Specimens 0.4 w/c

Chloride Concentration (ppm)	Specimen	Ultimate Load (kN)	Average Ultimate Load (kN)	Tensile Splitting Strength (MPa)
0	A	185.4	190.2	5.86
	B	191.6		
	C	193.6		
5000	A	168.0	167.5	5.17
	B	163.9		
	C	170.7		
10000	A	170.7	165.8	5.11
	B	165.3		
	C	161.4		
15000	A	174.0	169.7	5.23
	B	168.8		
	C	166.4		
20000	A	162.5	173.9	5.36
	B	184.4		
	C	174.8		
25000	A	149.5	155.0	4.78
	B	156.6		
	C	158.9		
30000	A	160.1	161.3	4.98
	B	162.9		
	C	161.1		

Specimens 0.5 w/c

Chloride Concentration (ppm)	Specimen	Ultimate Load (kN)	Average Ultimate Load (kN)	Tensile Splitting Strength (MPa)
0	A	151.0	153.5	4.73
	B	158.4		
	C	151.0		
5000	A	158.7	154.6	4.77
	B	149.3		
	C	155.9		
10000	A	153.5	149.9	4.62
	B	157.7		
	C	138.3		
15000	A	131.4	141.0	4.35
	B	153.7		
	C	137.8		
20000	A	135.5	142.9	4.41
	B	145.5		
	C	147.7		
25000	A	128.9	137.0	4.23
	B	141.6		
	C	140.6		
30000	A	161.5	149.0	4.60
	B	143.7		
	C	142.0		

Specimens 0.6 w/c

Chloride Concentration (ppm)	Specimen	Ultimate Load (kN)	Average Ultimate Load (kN)	Tensile Splitting Strength (MPa)
0	A	148.2	135.4	4.18
	B	110.7		
	C	147.3		
5000	A	116.7	132.8	4.09
	B	135.6		
	C	146.1		
10000	A	140.2	146.9	4.53
	B	147.6		
	C	152.8		
15000	A	127.0	128.6	3.97
	B	137.9		
	C	121.0		
20000	A	124.3	121.0	3.73
	B	125.0		
	C	113.7		
25000	A	124.7	126.9	3.91
	B	129.2		
	C	126.8		
30000	A	127.5	128.9	3.97
	B	117.7		
	C	141.5		

Appendix M: Splitting Tension Results for Increasing Sulfate Concentration

Specimens 0.4 w/c

Sulfate Concentration (%)	Specimen	Ultimate Load (kN)	Average Ultimate Load (kN)	Tensile Splitting Stength (MPa)
0	A	198.1	189.5	5.84
	B	174.7		
	C	195.6		
2	A	170.4	165.7	5.11
	B	171.9		
	C	154.8		
4	A	158.7	159.7	4.92
	B	159.2		
	C	161.2		
5	A	167.3	163.1	5.03
	B	158.4		
	C	163.7		
6	A	139.5	142.7	4.40
	B	143.1		
	C	145.6		
8	A	142.4	144.4	4.45
	B	153.4		
	C	137.3		
10	A	125.9	136.1	4.20
	B	138.0		
	C	144.4		

Specimens 0.5 w/c

Sulfate Concentration (%)	Specimen	Ultimate Load (kN)	Average Ultimate Load (kN)	Tensile Splitting Stength (MPa)
0	A	163.0	158.8	4.90
	B	157.4		
	C	156.0		
2	A	155.8	154.2	4.75
	B	145.5		
	C	161.2		
4	A	148.5	156.3	4.82
	B	160.8		
	C	159.6		
5	A	161.4	156.2	4.82
	B	150.7		
	C	156.4		
6	A	146.1	148.2	4.57
	B	152.6		
	C	146.0		
8	A	148.6	148.7	4.59
	B	148.2		
	C	149.4		
10	A	126.5	133.4	4.11
	B	132.5		
	C	141.1		

Specimens 0.6 w/c

Sulfate Concentration (%)	Specimen	Ultimate Load (kN)	Average Ultimate Load (kN)	Tensile Splitting Stength (MPa)
0	A	133.6	131.3	4.05
	B	117.7		
	C	142.5		
2	A	117.8	115.8	3.57
	B	106.3		
	C	123.5		
4	A	102.3	111.8	3.45
	B	115.5		
	C	117.6		
5	A	100.3	108.8	3.35
	B	112.8		
	C	113.2		
6	A	101.1	112.1	3.46
	B	121.2		
	C	114.0		
8	A	123.9	121.2	3.74
	B	115.2		
	C	124.4		
10	A	116.1	107.2	3.31
	B	83.5		
	C	122.0		

Appendix N: Splitting Tension Results for Chloride Concentration Gradient

Concentration Gradient (ppm)	Specimen	Ultimate Load (kN)	Average Ultimate Load (kN)	Tensile Splitting Strength (MPa)
0 - 30,000	A	129.9	137.1	4.23
	B	137.8		
	C	143.7		
7,500 - 22,500	A	139.7	151.1	4.66
	B	160.2		
	C	153.4		

Appendix O: Splitting Tension Results for Sulfate Concentration Gradient

Concentration Gradient	Specimen	Ultimate Load (kN)	Average Ultimate Load (kN)	Tensile Splitting Strength (MPa)
0% - 10%	A	129.9	137.1	4.23
	B	137.8		
	C	143.7		
2.5% - 7.5%	A	139.7	151.1	4.66
	B	160.2		
	C	153.4		